Multiple-Model Robust Adaptive Vehicle Motion Control

by

Halit Zengin

A thesis
presented to the University of Waterloo
in fulfillment of the
thesis requirement for the degree of
Doctor of Philosophy
in
Mechanical and Mechatronics Engineering

Waterloo, Ontario, Canada, 2019

Examining Committee Membership

The following served on the Examining Committee for this thesis. The decision of the Examining Committee is by majority vote.

External Examiner	NAME: Fengjun Yan Title: Associate Professor
Supervisor	NAME: Baris Fidan Title: Associate Professor
Supervisor	NAME: Amir Khajepour Title: Professor
Internal Member	NAME: William Melek Title: Professor
Internal Member	NAME: Soo Jeon Title: Associate Professor
Internal-external Member	NAME: Daniel Miller Title: Professor

I hereby declare that I am the sole author of this thesis. This is a true copy of the thesis, including any required final revisions, as accepted by my examiners.

I understand that my thesis may be made electronically available to the public.

Abstract

An improvement in active safety control systems has become necessary to assist drivers in unfavorable driving conditions. In these conditions, the dynamic of the vehicle shows rather different respond to driver command. Since available sensor technologies and estimation methods are insufficient, uncertain nonlinear tire characteristics and road condition may not be correctly figured out. Thus, the controller cannot provide the appropriate feedback input to vehicle, which may result in deterioration of controller performance and even in loss of vehicle control. These problems have led many researchers to new active vehicle stability controllers which make vehicle robust against critical driving conditions like harsh maneuvers in which tires show uncertain nonlinear behaviour and/or the tire-road friction coefficient is uncertain and low.

In this research, the studied vehicle has active front steering system for driver steer correction and in-wheel electric motors in all wheels to generate torque vector at vehicle center of gravity. To address robustness against uncertain nonlinear characteristics of tire and road condition, new blending based multiple-model adaptive schemes utilizing gradient and recursive least squares (RLS) methods are proposed for a faster system identification. To this end, the uncertain nonlinear dynamics of vehicle motion is addressed as a multiple-input multiple-output (MIMO) linear system with polytopic parameter uncertainties. These polytopic uncertainties denote uncertain variation in tire longitudinal and lateral force capacity due to nonlinear tire characteristics and road condition. In the proposed multiple-model approach, a set of fixed linear parametric identification models are designed in advance, based on the known bounds of polytopic parameter set. The proposed adaptive schemes continuously generates a weighting vector for blending the identification model to achieve the true model (operation condition) of the vehicle. Furthermore, the proposed adaptive schemes are generalized for MIMO systems with polytopic parameter uncertainties. The asymptotic stability of the proposed adaptive identification schemes for linear MIMO systems is studied in detail.

Later, the proposed blending based adaptive identification schemes are used to develop Linear Quadratic (LQ) based multiple-model adaptive control (MMAC) scheme for MIMO systems with polytopic parameter uncertainties. To this end, for each identification model, an optimal LQ controller is computed off-line for the corresponding model in advance, which saves computation power during operation. The generated control inputs from the set of LQ controllers is being blended on-line using weighting vector continuously updated by the proposed adaptive identification schemes. The stability analysis of the proposed LQ based optimal MMAC scheme is provided. The developed LQ based optimal MMAC scheme has been applied to motion control of the vehicle. The simulation application

to uncertain lateral single-track vehicle dynamics is presented in Simulink environment. The performances of the proposed LQ based MMAC utilizing RLS and gradient based methods have been compared to each other and an LQ controller which is designed using the same performance matrices and fixed nominal values of the uncertain parameters. The results validated the stability and effectiveness of the proposed LQ based MMAC algorithm and demonstrate that the proposed adaptive LQ control schemes outperform over the LQ control scheme for tracking tasks.

In the next step, we addressed the constraints on actuation systems for a model predictive control (MPC) based MMAC design. To determine the constraints on torque vectoring at vehicle center of gravity (CG), we have used the min/max values of torque and torque rate at each corner, and the vehicle kinematic structure information. The MPC problem has been redefined as a constrained quadratic programming (QP) problem which is solved in real-time via interior-point algorithm by an embedded QP solver using MATLAB each time step. The solution of the designed MPC based MMAC provides total steering angle and desired torque vector at vehicle CG which is optimally distributed to each corner based on holistic corner control (HCC) principle. For validation of the designed MPC based MMAC scheme, several critical driving scenarios has been simulated using a high-fidelity vehicle simulation environment CarSim/Simulink. The performance of the proposed MPC based MMAC has been compared to an MPC controller which is designed for a wet road condition using the same tuning parameters in objective function design. The results validated the stability and effectiveness of the proposed MPC based MMAC algorithm and demonstrate that the proposed adaptive control scheme outperform over an MPC controller with fixed parameter values for tracking tasks.

Acknowledgements

Firstly, I would like to express my sincere gratitude to my advisors Prof. Baris Fidan and Prof. Amir Khajepour for their continuous support of my Ph.D study and related research, for their patience, motivation, and immense knowledge.

Besides my advisors, I would like to thank my committee: Prof. Daniel Miller, Prof. Soo Jeon, Prof. William Melek, and Prof. Fengjun Yan for their insightful comments and encouragement, but also for the hard questions which incented me to widen my research from various perspectives.

I would also thank to all staff in University of Waterloo and General Motors who have supported me throughout the process. I will always appreciate all they have done.

I would like to acknowledge the financial support of Ontario Research Fund (ORF), Natural Sciences and Engineering Research Council of Canada (NSERC), and General Motors in this work.

Last but not least, I would like to thank my family: to my wife, to my parents for their support and encouragement during this journey. I appreciate their sacrifices and I would not have been able to get to this stage without them.

Dedication

To my love and my parents.

Table of Contents

List of Tables

List of Figures

Nomenclature

ABS Antilock Braking System

CG Center of Gravity

DOF Degree of Freedom

DYC Direct Yaw Control

EV Electric Vehicle

GPC Generalized Predictive Control

GPS Global Positioning System

HCC Holistic Corner Control

IMU Inertia Measurement Unit

LMI Liear Matrix Inequality

LPV Linear Parameter Varying

LQ Linear Quadratic

LSD Limited Slip Differentials

LTI Linear Time Invariant

LTV Linear Time Variant

MIMO Multiple Input Multiple Output

MMAC Multiple-Model Adaptive Control

MPC Model Predictive Control

PE Persistency of Existence

PLDI Polytopic Linear Differential Inclusion

QP Quadratic Programming

RHC Receding Horizon Control

SISO Single Input Single Output

Chapter 1

Introduction

1.1 Motivation and Objective

Traffic accidents are one of the main cause of many deaths and unrecoverable injuries. These accidents generally take place in critical driving conditions such as high speed, low surface friction, sudden changes in road surface and vehicle conditions. Under these critical conditions, the response of a vehicle to the driver command is resulting in potential instability of the vehicle or large deviations from the trajectory that the driver requests. Since vehicles move by means of contact forces between tire-road surface, uncertain road condition and nonlinear tire characteristics have significant effects on tire force capacity in longitudinal/lateral direction, and thus considerably affect stability and tracking performance of the motion controller. These uncertainties are also affected by changes in tire-road friction coefficient and tire longitudinal/lateral force capacities in front/rear axles due to combined slip effect during vehicle manoeuvre. Therefore a vehicle motion controller should guarantee to generate forces such that the vehicle track the requested trajectory while maintaining the vehicle stability considering uncertain road condition and nonlinear tire characteristics. In this regard, extensive number of studies have been conducted for robust control of vehicle stability in recent years. However, robustness to fast and wide range of changes in road conditions and tire longitudinal/lateral force capacities in normal and critical driving conditions are still open problems for design of a robust motion controller.

The main problem in robustness of a vehicle to the road surface and nonlinear tire characteristics is that current controllers are highly dependent on estimators. Present estimation algorithms are not capable of detecting the road conditions and changing tire

longitudinal/lateral force capacity accurately and fast enough during manoeuvre. In this case, driver's misinterpretation of these uncertainties could be finalized with the loss of vehicle control or stability. In such a critical situation, the controller requires to avoid any large deviation from trajectory requested by driver and instability issue by taking an appropriate action.

Based on the above discussion, a system identifier must exist to detect any sudden changes in vehicle dynamic using all measured data efficiently. This data is generally used to identify the parameters of a system by a single model, but this process requires more time than the designer wish to use on-line for control purposes. Instead of this slow process, the identification can be accelerated using multiple models. To this end, the identifier should know all possible cases(i.e, models) in advance. After identification of the vehicle dynamics, the control needs to compute the optimal control input and implement it to the vehicle system. The required computation power of the optimum control input can be saved if all possible models are already known and controller gain for each known possible model can be computed off-line in advance. Thus, the control system would be ready to directly implement the proper and optimum input based on the changing situation in the dynamic.

This thesis aimed at an improvement in the vehicle handling performance by making the vehicle dynamic robust to uncertain non-linear tire characteristic and wide range of changes in road condition without any estimation and additional sensor usage. The studied vehicle was equipped with active front steering system and direct yaw control system that uses independent in-wheel motor at corners to generate torque at vehicle center of gravity (CG).

This thesis focused on multiple-model based adaptive optimal control schemes. The idea of multiple-model in control systems has been put forward to achieve more comprehensive description and control of time-varying and/or uncertain systems. The intuitive idea is the utilisation of different models to identify the system for various operational conditions instead of a single model with a wide range of uncertainty in its dynamic equation. Thus, the conservativeness of a single model with large uncertainties is decreased and more realistic approach for the real systems is obtained.

In literature, there are two main approaches for multiple-model based system identification, including switching and blending based approaches. The switching based approaches have two major challenges. First, since at least one of the fixed models is required to be sufficiently close to the original plant in the system parameter space at any time instant, the corresponding number of fixed models may be large and grows exponentially with the dimension of the unknown parameter vector [64]. Second, the models other than best

matching one do not contribute to the estimation of the unknown parameters. Particularly, the performance indices of the fixed models or any other data from all models are not used efficiently to achieve a closer model. Thus, our objective was to utilize blending based multiple-model system identification scheme for uncertain lateral vehicle dynamics.

For adaptive optimal control of the lateral vehicle motion, this thesis focused on two different types of control scheme, including linear quadratic (LQ) and model predictive control (MPC) based schemes. For the former, we could compute an LQ controller gain off-line for each corresponding identification model in multiple-model system identifier before operation, which saves computation power to generate control law in real-time implementation. The control law could be adapted to the operation condition of the vehicle based on the blending based multiple-model system identifier. For the latter, constraints on the actuation systems of the vehicle could be addressed to guarantee that the requested control input by the controller is feasible.

1.2 Contributions

Contributions of this thesis are outlined as follows.

• New blending multiple-model parameter identification schemes, utilizing gradient and RLS methods, have been proposed for uncertain lateral dynamics of ground vehicles equipped with active front steering system and in-wheel electric motor at each corner which can generate torque vector at vehicle CG. The proposed multiple-model identification schemes have been generalized for multiple-input multiple-output (MIMO) systems with polytopic parameter uncertainties. In the proposed identification schemes, the uncertain system is expressed in terms of polytopic linear differential inclusions (PLDIs). For each vertex of such a polytopic inclusion, a fixed model is selected. Based on the inputs and outputs of the system and designed models, the weights are generated by the developed multiple-model adaptive laws utilizing convexity property of PLDIs. The developed identification schemes have been proven to be asymptotically stable for uncertain linear time-invariant MIMO systems, and is shown to provide fast adaptation for even uncertain linear time-varying (LTV) systems. The stability of the proposed scheme has been studied and its effectiveness has been validated via simulations. Furthermore, the proposed identification scheme is able to combined any model based control scheme. The proposed identification schemes require much less number of models than other multiple-model parameter identification approaches in literature to cover all uncertain parameter space.

• The proposed multiple-model parameter identification schemes have been utilized to develop LQ based multiple-model adaptive control (MMAC) scheme for MIMO systems with polytopic parameter uncertainties. In this scheme, for each identification model, there is an optimal LQ controller gain which is computed off-line before the operation, which saves the computation power in real-time. The generated control inputs from the designed LQ controllers are blended on-line to adapt the control input to operation condition of the system using proposed adaptive scheme. The stability analysis of the proposed optimal MMAC scheme is provided. Furthermore, the developed LQ based MMAC scheme has been implemented to vehicle motion control and tested via simulations. The results verified the stability and demonstrated better tracking performance of the developed control scheme compared to a non-adaptive LQ based optimal control scheme.

• The constraints on actuation systems of the vehicle are addressed to design an MPC based MMAC. To determine the constraint of torque vectoring at vehicle CG, we utilized the maximum and minimum torque and torque rate for each corner in addition to vehicle kinematic structure. To have system matrices which is used for the prediction model of MPC scheme, we provide a method to directly estimate uncertain system matrices on-line via the proposed gradient based multiple-model parameter identification scheme. The developed MPC based MMAC scheme has been simulated using a high-fidelity vehicle model in CarSim/Simulink environment. The results verified the stability and demonstrated superior tracking performance of the developed control scheme over a non-adaptive MPC scheme. Furthermore the developed MPC based MMAC scheme could be applied to any MIMO system with polytopic parameter uncertainties.

1.3 Organization

Chapter 2 is dedicated to background and the literature review of lateral vehicle motion dynamics and control. In this regard, the importance of the vehicle handling enhancement and stability control in critical operation conditions is discussed. The literature review focused on available control vehicle control systems and optimal vehicle motion control schemes, especially MPC schemes, and MMAC approaches. For background information, MPC theory and formulation, holistic corner control strategy, and MMAC approaches are given.

In Chapter 3, the proposed blending based multiple-model on-line parameter identification schemes for MIMO systems with polytopic uncertain parameters are presented. Stability of the proposed schemes are studied in detail. Parameter projection are applied to the proposed adaptive identification schemes to guarantee that the convexity condition

is satisfied during adaptation especially for fast transients in system parameters. Lastly, the proposed adaptive schemes are used to design an LQ based optimal MMAC scheme for polytopic uncertain linear systems. The stability analysis of the proposed optimal MMAC scheme is studied.

In Chapter 4, the proposed LQ based optimal MMAC scheme in Chapter 3 is applied to vehicle motion control. The objective is to improve vehicle handling performance and to maintain stability during cornering manoeuvres. The studied vehicle is equipped with active front steering system and direct yaw control system that uses independent in-wheel motor at corners to generate torque at vehicle CG. The simulation application to uncertain lateral vehicle dynamics of the proposed adaptive control scheme using the propose RLS and gradient based identification methods, is presented in Simulink environments comparing with nonadaptive optimal LQ controller for the system states with/without measurement noise.

Chapter 5 addressed the constraints on actuation systems, including active front steering system and torque vectoring, for an MPC based MMAC design. The proposed control scheme has been combined with a low level controller HCC to optimally distribute the required CG torque to the corners. In order to validate our control algorithm, several critical driving scenarios were simulated using a high-fidelity vehicle simulation environment CarSim/Simulink. Performance comparison of the proposed adaptive MPC controller with nonadaptive MPC control scheme has been provided.

Finally, the conclusions of this thesis and a few future works to carry on this research were presented in Chapter 6.

Chapter 2

Background and Literature Review

This chapter presents a review on the literature of the lateral vehicle motion stability analysis and of various motion control approaches at first. The main focus of control scheme is on multiple-model adaptive control approaches. Subsequent to literature review, the required background information on multiple-model adaptive control schemes is investigated to be referred in the following chapters.

2.1 Lateral Vehicle Motion Dynamics and Stability

Stability analysis is mainly performed to find the conditions for stability of a vehicle and stability margin. Many research have been conducted for stability analysis of vehicles. A precise stability of vehicle dynamics was analysed in [33]. This study proposed phase plane analysis for a 2-Degree of Freedom (DOF) bicycle model with Pacejka tire model considering sideslip angle β and its rate $\dot{\beta}$ as the state variables since the saddle and equilibrium points move along a horizontal axis, $\dot{\beta}$ vanishes. These phase plots provide very comprehensive information for system dynamic response and stability analysis. The authors concluded from the phase portraits that as the vehicle is steered in one direction, the stability margin reduces in the steered direction and increases in the opposite direction.

The phase plane $\beta - \dot{\beta}$ cannot be directly obtained in practice since commercial vehicles have no hardware to measure both states. Thus, many researchers have considered vehicle yaw rate instead of vehicle side slip angle rate in phase plane stability analysis since yaw rate should be measured via stock sensors available in today's vehicles. Furthermore, yaw rate can be directly affected by current actuation systems.

[30] considered a 2-DOF bicycle model for the stability analysis of directional behaviour according to different steering angles and forward velocities. They used phase portrait of yaw rate r - lateral velocity v_y to observe the vehicle response. Tire lateral forces were estimated by Pacejka tire model. The study concluded that as vehicle forward velocity increases, the stability margin shrinks. Moreover, if the steering angel is applied, the equilibrium point moves along the yaw rate axis till the equilibrium point disappears, which implies that when the steering angle crossed a certain limit, the vehicle system becomes unstable. A similar study [68] used a 2-DOF bicycle model using the phase plane portrait β-r analysis. The authors observed that an increase in the front wheel steering angle reduces the stability margin since the equilibrium point moves in the steered direction.

[74] introduced a nonlinear analysis of the steady-state vehicle dynamics called β-method. The method produces the stabilizing yaw moment and lateral force for different vehicle speeds, side-slip angles and front wheel steering angles. It is observed that the front wheel steering angle has little effect on the yaw moment (reduced steerability) at high slip angles. The study mainly focused on analysis of the effect of acceleration and deceleration during steady-state cornering and development of a simple Direct Yaw Control (DYC) scheme to attenuate the adverse effect of vehicle acceleration. The results showed that torque vectoring based control algorithm could improve the limits of the vehicle manoeuvrability.

[71, 39, 73] performed similar stability analysis using a nonlinear tire model. They simulated the open loop behavior of vehicle at different forward speeds and front/rear steering angles. For these operation conditions, they defined stable and unstable regions. These definitions are widely used in controller design for vehicle stability.

2.2 Vehicle Dynamic Model

For vehicle lateral stability and handling control, the vehicle sideslip angle β and the yaw rate r are critical as stated in Section 2.1. In this section the lateral dynamics of a ground vehicles with the capability of generating differential torque as shown in Fig. 2.1 is presented

Consider the dynamics of vehicle with in-wheel electric motors in Fig. 2.1,

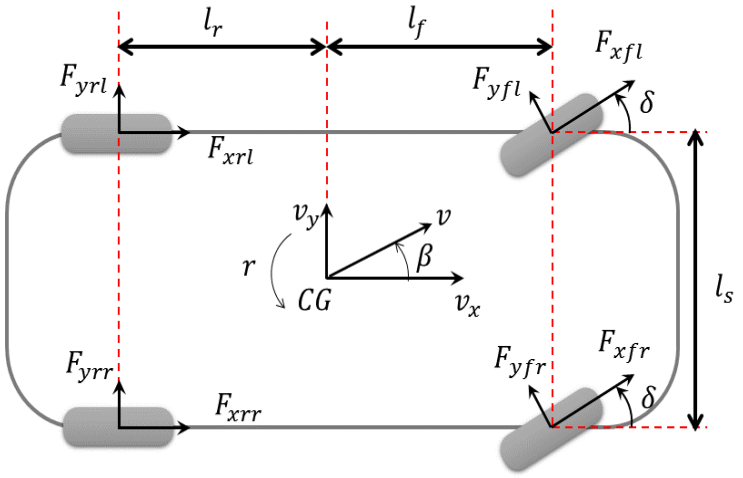

Figure 2.1: Vehicle model with one electric motor on each axle.

$$
\begin{aligned}
\dot{v}_y =& - v_x r + \frac{1}{m}[(F_{yfl} + F_{yfr})\cos\delta + F_{yrl} + F_{yrr} \\
&+ (F_{xfl} + F_{xflr})\sin\delta] \\
\dot{r} =& \frac{1}{I_z}[l_f(F_{yfl} + F_{yfr})\cos\delta - l_r(F_{yrl} + F_{yrr}) \\
&+ l_f(F_{xfl} + F_{xfr})\sin\delta], \\
&+ \frac{l_s}{2I_z}[(F_{xfl}\cos\delta + F_{xrl}) - (F_{xfr}\cos\delta + F_{xrr})] \\
&- \frac{l_s}{2I_z}(F_{yfl} - F_{yfr})\sin\delta,
\end{aligned}
\tag{2.1}
$$

where m, I_z, v_y, v_x, r are the vehicle mass, the vehicle moment of inertia about yaw axis, lateral velocity, longitudinal velocity, yaw rate, respectively; δ, and the lengths l_f, l_r, l_s refer to the steering angle of the front wheels, the distance from front axle to CG, the distance from rear axle to CG, and the lateral distance between the left and right

wheels, respectively; F_{xi} and $F_{yi}(\alpha_i, F_{zi}, C_{\alpha_i}, \xi_i, \mu_i)$ for $(i = fl, fr, rl, rr)$ are longitudinal and nonlinear lateral forces generated at each corner, respectively. F_{yi} is calculated for each corner by using fiala tire model

$$\begin{aligned} F_{y_i} &= \begin{cases} -C_{\alpha_i} z + \frac{C_{\alpha_i}^2}{3\xi_i \mu_i F_{z_i}} |z_i| z_i - \frac{C_{\alpha_i}^3}{27 \xi_i^2 \mu_i^2 F_{z_i}^2} z_i^3 & |\alpha_i| < \alpha_{sl_i}, \\ -\mu_i F_{z_i} sgn \alpha_i & |\alpha_i| \geq \alpha_{sl_i}, \end{cases} \\ z_i &= \tan \alpha_i, \\ \alpha_{sl_i} &= \arctan \frac{3\xi_i \mu_i F_{z_i}}{C_{\alpha_i}}, \end{aligned} \tag{2.2}$$

where C_{α_i} is the tire cornering stiffness; F_{z_i} is the normal load on the tire; α_i is slip angle and calculated for the front and rear tires as follows

$$\begin{aligned} \alpha_f &= \arctan\left(\beta + \frac{l_f r}{v_x}\right) - \delta, \\ \alpha_r &= \arctan\left(\beta - \frac{l_r r}{v_x}\right), \end{aligned} \tag{2.3}$$

respectively; α_{sl_i} is the saturation limit of slip angle. ξ_i is a derating factor representing the reduced lateral force capacity due to the applied longitudinal force at the tire based on "friction circle", which is called combined-slip effect:

$$\xi_i = \frac{\sqrt{(\mu_i F_{z_i})^2 - F_{x_i}^2}}{\mu_i F_{z_i}}, \tag{2.4}$$

The rotational dynamics of each wheel can be used to achieve the longitudinal tire force at each tire

$$F_{xi} = \frac{Q_i - I_w \dot{\omega}_i}{R_{eff}}, \tag{2.5}$$

where I_w is the wheel moment of inertia, R_{eff} is the tire rolling radius, and Q_i is the applied torques on tires.

2.3 Lateral Vehicle Motion Control

This section is dedicated to the literature of lateral vehicle motion control. First, the lateral vehicle motion control problem and the control systems are introduced. Then, the optimum control strategies used in vehicle motion control are reviewed. Lastly, the conventional multiple-model adaptive control methods are reviewed, and two of these strategies are examined in detail as a background.

2.3.1 Lateral Vehicle Motion Control Problem and Systems

In the lateral vehicle motion control, the controller continuously has command on the response of the vehicle to follow the desired vehicle states which are generally defined in terms of the desired yaw rate and/or desired sideslip angle.

An important review in the lateral vehicle stability control can be found in [51]. The main focus of this review was to improve desired yaw rate trajectory tracking in non-critical driving conditions. The control goal was classified into three categories: yaw rate control, sideslip angle control and yaw rate-sideslip angle control. The controllers utilize different actuator systems, including differential braking [84, 23], active steering [16, 23], and active torque distribution systems [38, 1]. The functionality of these control systems can be categorized as:

• **Differential Braking Systems:** Using the Anti-Lock Braking System (ABS) on the vehicle to apply differential braking between the right and left wheels.

• **Active Steering Systems:** Providing additional steering angle to the driver's wheel steering angle to improve handling performance.

• **Active Torque Distribution Systems:** Generating required torque at each wheel through torque distributor devices.

Stability Control by Differential Braking System

In differential braking systems, ABS technology on the vehicle is utilized to apply differential torque between the right and left wheels in order to generate the required yaw moment at vehicle CG for its stability. Differential torque at CG is generated by applying more brake pressure at one side than the other side, generally using hydraulic modulators.

Differential braking system in current commercial cars mostly utilizes four-wheel speeds, yaw rate, steering angle, accelerometer, and brake pressure sensors. Researchers and automotive industry has interested in differential braking for vehicle stability control in last decade. Due to simplicity, some research studies have focused on only the control of one wheel to generate desired yaw moment torque at vehicle CG. On the other hand, there are many works in literature which utilized multiple wheels control for differential braking considering it as an optimization problem.

[17] designed a Linear Parametric Varying (LPV) robust yaw control algorithm using a rear active differential braking system. The study proposed a cost-effective approach for an active control of lateral dynamics of a four-wheel vehicle during braking considering the effect of load changes. The proposed model and approach has been validated by experiment.

[85] developed a fuzzy logic-based yaw control algorithm using a brake-by-wire differential braking system. This study presented a nonlinear vehicle model in which wheel dynamics has been considered for lateral vehicle dynamics. The results of this approach showed that yaw rate is within reasonable range of tire capacity when the driver is assumed to have enough quick response to the yaw rate disturbances to avoid instability.

[7] designed an ABS control scheme to maintain the tire slip ratios within the desired range using an on/off control strategy for integrated vehicle stability control. The proposed reconfigurable model for the vehicle and the braking system with variable parameters provided a prototype and design platform.

[3] developed a Generalized Predictive Control (GPC) to predict the future yaw rate and use control actions to minimize the yaw rate error utilizing a brake-by-wire system. The dynamic model employed a simple linear tire model without tire saturation. The effectiveness of the proposed control algorithm and actuation system is experimentally tested for over-/under-steer conditions in mild maneuvers on packed snow.

Stability Control by Active Steering System

Active steering system assists to generate required lateral forces at front tires for vehicle stability and desired yaw-rate. In this system, an electric motor in the joint adjusts the front wheel's angle for different driving conditions.

Some of the studies listed below use active steering systems in their works to obtain desired values. [77] designed a Lyapunov based control allocation scheme for vehicle stabilization using active steering and adaptive braking systems. The control structure included three levels, high, intermediate, and low. The high-level module is used to generate desired

yaw rate based on driver commands. The intermediate-level generates the desired longitudinal tire slips and adjusts steering angle commanded by driver to achieve the desired yaw rate. The low-level module control the longitudinal slip and estimate maximal tire-road friction such that tire forces are distributed in a desirable way while satisfying actuator constraints.

[69] developed an LMI based LPV controller utilizing active steering and braking systems. The control scheme used mainly differential braking, and if the braking system exceeded its limits, the active steering helped to generate additional torque at vehicle CG required for stability and tracking. Competency and robustness of the controller are validated by with a high fidelity full vehicle simulation model.

[10] designed an integrated vehicle stability control with a state feedback linearization technique using active steering and braking systems. The control scheme mainly corrects steering, and if necessary, it applies differential braking. Experiment results shows that a globally smooth and stable vehicle response was achieved.

Stability Control by Active Torque Distribution System

Even though differential braking and steering systems improve vehicle safety and performance, they a couple of drawbacks. Introduction of braking during maneuver to regain the vehicle stability cause a significant decrease in vehicle speed and thus loss of energy. Furthermore, the decrease in speed might conflict with driver intention which could be an acceleration scenario for emergency.

On the other hand, active steering system could not generate additional lateral tire forces in the case of tire saturation and not respond to driver command given in [40]. Thus, active torque distribution is an efficient and reliable solution for tracking and stability problems. Active torque distribution systems used to distribute the required torque at vehicle CG to vehicle corners. The system utilizes electric motors in Electric Vehicles (EVs) and active differentials in conventional vehicles for torque distribution.

[21] developed a generalized mathematical model of an active differential dynamics using a bond graph modeling technique. The paper considered different levels of model complexity for an auto Limited Slip Differentials (LSD) with single clutch mechanisms. The main superiority of LSD over conventional open differentials is the restriction of the independency between the wheels on an axle. In the open differentials, the engine torque is transmitted to a planetary gear set via drive shaft, and it is distributed between the right and left wheels. However, in limited slip differentials, the engine power follows the path of the least resistance. The independency design between the axle wheels can be achieved

with a number of mechanical, electrical, and hydraulic systems given by [22]. In addition, some patents and technical reports can be found in [72, 57] that were oriented to achieving outstanding differential design features for active torque distribution.

Another actuation configuration for torque vectoring is to have independently actuated electric in-wheel motor at the vehicle corners. For this system, the lateral stability control system is usually consisting of two layers, including higher-level controller that computes the required torque vector at vehicle CG to track desired states while maintaining lateral stability, and lower-level controller that allocates the required torque vector at vehicle CG to vehicle corners considering physical constraints [78].

Unlike other control approaches, optimization based control schemes have the advantage of considering specific constraints on the dynamical system and on the control actions. Model Predictive Control (MPC) and Holistic Corner Control (HCC) are discussed in the following sections.

2.3.2 Model Predictive Control

This control approach is also known as Receding Horizon Control (RHC) and one of the most popular optimal control strategies used in vehicle stability control. The method utilizes a mathematical description (dynamic model) of a vehicle to predict the behavior of the vehicle over a finite/infinite horizon of time [9]. MPC algorithm provides solution for the optimal tracking control such that tracking error, discrepancies between predicted and reference signals, can be minimized over a future horizon possibly imposing some constraints [13].

MPC also considers the physical constraints while searching the optimal solution, which has drawn the attention of many researchers not just in vehicle stability control but also in vehicle cruise control to improve comfort and safety of a drive, fuel efficiency and path following performance [46, 49, 20, 37]. Furthermore, the ability of making prediction of MPC makes the controller robust against delays due to measurement and action process [18, 45, 44, 50].

The prediction model used in MPC needs to be accurate enough to represent the significant dynamics of the vehicle and simple enough for real-time implementation. Thus, linear prediction models have been more preferable than complicated nonlinear models for the industrial applications due to the limitation of computational hardware resources.

Linear Model Predictive Control

The stability control of a vehicle dynamics is often required in the nonlinear range. However, nonlinear models hugely increases the computational cost, which has led many researchers to use a successive linearization of a nonlinear model, and thus searches a sub-optimal control solution with less computational effort.

[24] designed a sub-optimal linear MPC controller for autonomous path tracking problem through successive linearization around the current operating point of the nonlinear vehicle dynamics. By the active steering system, the controller applied front steering angles to track the desired trajectory on slippery roads. The effectiveness of designed control scheme was demonstrated via simulation and experiments for up to 21 m/s on icy roads. For the same control problem, [25] proposed a Linear Time Varying (LTV) MPC controller for an active steering system of an autonomous vehicle. The paper provided a sufficient stability condition for the closed loop system. The stability condition was derived for nonlinear discrete time systems and is added as an additional convex constraint to LTV MPC design. The stability was examined for double lane change maneuvers at high longitudinal speeds.

To avoid computational complexities of a nonlinear MPC, [13] proposed another linearization method based on Set Membership. The performance of this approximation based controller was investigated with software-in-the-loop simulations and compared with the original nonlinear model. Although the controller performance results for the both models are very similar, the approximated linear model MPC is more feasible than nonlinear one for real-time implementation.

Robust Model Predictive Control

Robustness of MPC controllers against model uncertainties and noise is a crucial issue to be solved. MPC performance may be adversely affected by unmodelled dynamics or parameter uncertainties of prediction model. Therefore, [53, 82, 67, 19, 86, 41] presented various approaches to guarantee the stability of controlled system in presence of model uncertainties. These methods requires an appropriate description of the uncertainties in model. A review study [6] was performed on robust MPC techniques in the literature, and the conclusion was drawn that there were two different approaches for robust MPC stability, indirect vs. direct.

In indirect method the performance objective and uncertainty description are specified. Direct method introduces a kind of robust contraction constraint to guarantee shrinking

of the state for all plants in an uncertainty set. However, the study also emphasized that due to extensive computational effort the both techniques were unsuitable for real-time implementation except for a few cases. Thus, only a few applications have been reported in vehicle stability [13], although robust MPC has been studied excessively in the theory.

Several studies have been done recently that improved the robust MPC algorithms. [8] proposed an explicit robust MPC for LPV systems and guarantee the stability and optimality by a suitable selection of the terminal state constraint and terminal cost. The optimal control problem was solved backward by Dynamic Programming. [80] proposed a parameter dependent control law and solved a convex optimization problem using LMI technique. The same problem has been solved for asymmetric constraints in [81].

Model Predictive Control Theory and Formulation

An observer estimates the system state vector $\hat{x}_p$ utilizing the plant input vector u and measurement vector y_p and feed the estimated state vector to optimizer. The optimizer generates the optimal control input signal u such that the error between the estimated state signal $\hat{x}_p$ and reference signal r are minimized over a future horizon. For prediction of future behavior of the system over a finite prediction time horizon N_p, its dynamic model and the manipulated inputs changing over a finite control time horizon N_c are utilized.

A prediction model for a system, assuming all system states are measurable, is expressed in the following standard continuous state space model

$$\dot{x}_p(t) = A_p(t)x_p(t) + B_p(t)u(t) + D_p(t), \tag{2.6}$$

where $A_p(t) \in R^{n\times n}$, $B_p(t) \in R^{n\times r}$ are system matrices, and D is known disturbance matrices at time t; $x_p(t) \in R^n$ and $u(t) \in R^r$ are the (measurable) system state, and the system input, respectively.

The prediction model (2.6) can be discretized at time t by Euler approximation with sample time T_s in the following form

$$x_p[t+1] = A_d[t]x_p[t] + B_d[t]u[t] + D_d[t], \tag{2.7}$$

where

$$\begin{aligned} A_d &= I + A_pT_s, \\ B_d &= B_pT_s, \\ D_d &= DT_s. \end{aligned} \tag{2.8}$$

The discrete system model (2.7) can be used for prediction over a finite time horizon $N_p \in Z^+$.

The optimization problem is set to find a control input series u over a control horizon $N_c \in Z^+$ to minimize the error between the actual system state vector x_p and the desired state vector x_{des} subject to some state and input constraints. To this end, the optimization problem is addressed as follows:

$$\begin{aligned} J_{MPC} = arg\min_{u} \sum_{k=1}^{N_p} (x_p[t+k|t] - x_{des}[t+k|t])^T \ Q \ (x_p[t+k|t] - x_{des}[t+k|t]) \\ + \sum_{k=0}^{N_c-1} u[t+k|t]^T \ R \ u[t+k|t] \end{aligned} \tag{2.9}$$

subject to

$$\begin{aligned} x_p[t+k+1|t] &= A_d[t+k|t]x_p[t+k|t] + B_d[t+k|t]u[t+k|t] + D_d[t+k|t], \\ x_p[t+k|t] &\in \mathcal{X}, \quad k = 1, \cdots, N_p, \\ u[t+k|t] &\in \mathcal{U}, \quad k = 1, \cdots, N_c, \end{aligned} \tag{2.10}$$

where N_p is the number of steps in the prediction horizon. In the right-hand side of (2.9), the first term is related to the tracking error; the second term is to adjust the control input for minimization of the control effort. The weighting matrices Q, R, are design matrices to tune the controller, where Q is positive semi-definite, R is positive definite. The state and control input constraints are defined with $\mathcal{X}$ and $\mathcal{U}$ symbols, respectively.

$x[t+k|t]$ denotes the predicted state trajectory at time step $t+k$ ($k = 1, \cdots, N_p$) for given current state $x[t]$ utilizing the prediction model (2.7); $u[t+k|t]$ denotes the prospective input trajectory at time step $t+k$ for $k = 1, \cdots, N_c$, and solution to minimize the cost function J_{MPC} in (2.9). Based on the MPC theory, at each time step, the first sample of the control input sequence is applied to the system and the rest are discarded.

The prediction model presented (2.7) is utilized to form (2.9) in terms of the current state and prospective control actions. Assume that the control and prediction horizons have the same length (i.e. $N_c = N_p$). By the batch approach, the future system states are

$$X = S_x x_0 + S_u U + S_D, \ x_0 = x[0], \tag{2.11}$$

where $X = \begin{bmatrix} x^T[1] & x^T[2] & \cdots & x^T[N_p] \end{bmatrix}^T$, $U = \begin{bmatrix} u^T[0] & u^T[1] & \cdots & u^T[N_p-1] \end{bmatrix}^T$, and

$$S_x = \begin{bmatrix} A_d \\ A_d^2 \\ \vdots \\ A_d^{N_p} \end{bmatrix}, \; S_u = \begin{bmatrix} B_d & 0 & \cdots & 0 \\ A_dB_d & B_d & \cdots & 0 \\ \vdots & \ddots & \ddots & \vdots \\ A_d^{N_p-1}B_d & \cdots & \cdots & B_d \end{bmatrix}, \; S_D = \begin{bmatrix} D_d & 0 & \cdots & 0 \\ A_dD_d & D_d & \cdots & 0 \\ \vdots & \ddots & \ddots & \vdots \\ A_d^{N_p-1}D_d & \cdots & \cdots & D_d \end{bmatrix}.$$

The desired states over the prediction horizon is $X_{des} = \begin{bmatrix} x_{des}^T[1] & x_{des}^T[2] & \cdots & x_{des}^T[N_p] \end{bmatrix}^T$. Thus, (2.9) can be written in the following compact form,

$$J_{MPC} = arg\min_{U} (X - X_{des})^T \; \mathbf{Q} \; (X - X_{des}) + U^T \; \mathbf{R} \; U, \tag{2.12}$$

where $\mathbf{Q} = blockdiag\{Q, Q, \cdots, Q\}$ and $\mathbf{R} = blockdiag\{R, R, \cdots, R\}$. Substituting (2.11) into (2.12), the original optimization problem (2.9),(2.10) are converted into the following constrained quadratic programming problem

$$J_{MPC} = arg\min_{U} \frac{1}{2} U^T H U + F^T U + \Upsilon, \tag{2.13}$$

subject to

$$\begin{aligned} x_p[t+k|t] &\in \mathcal{X}, \quad k = 0, \cdots, N_p, \\ u[t+k|t] &\in \mathcal{U}, \quad k = 0, \cdots, N_p - 1, \end{aligned} \tag{2.14}$$

where

$$\begin{aligned} H =& S_u^T \mathbf{Q} S_u + \mathbf{R}, \\ F =& 2\left(x_0^T S_x^T \mathbf{Q} S_u + S_D^T \mathbf{Q} S_u - X_{des}^T \mathbf{Q} S_u\right), \\ \Upsilon =& x_0^T S_x^T \mathbf{Q} S_x x_0 + 2 x_0^T S_x^T \mathbf{Q} S_D + S_D^T \mathbf{Q} S_D \\ & - 2 X_{des}^T \mathbf{Q} S_D - 2 X_{des}^T \mathbf{Q} S_x x_0 + X_{des}^T \mathbf{Q} X_{des}, \end{aligned}$$

After solving the problem (2.13), (2.14), the first input vector of the series of optimal control inputs U is applied to the system (2.6).

Considering Input Rate in MPC Design

$$U = S_{\Delta u}\Delta U + U_{-1}, \tag{2.15}$$

where $\Delta U = \begin{bmatrix}\Delta u^T[0] & \Delta u^T[1] & \cdots & \Delta u^T[N_p-1]\end{bmatrix}^T$ in which $\Delta u^T[k] = u[k] - u[k-1]$, $U_{-1} = \begin{bmatrix}u^T[-1] & u^T[-1] & \cdots & u^T[-1]\end{bmatrix}^T$ in which $u[-1]$ denotes the input applied in previous time step, and

$$S_{\Delta u} = \begin{bmatrix} I & 0 & \cdots & 0 \\ I & I & \cdots & 0 \\ \vdots & \ddots & \ddots & \vdots \\ I & \cdots & \cdots & I \end{bmatrix}.$$

Substituting (2.15) into (2.11), the following dynamic system is obtained

$$X = S_x x[0] + S_u S_{\Delta u}\Delta U + S_u U_{-1} + S_D. \tag{2.16}$$

To consider the input rate, the cost function (2.12) is adjusted as follow

$$J_{A_{MPC}} = arg\min_{\Delta U} (X - X_{des})^T \ \mathbf{Q} \ (X - X_{des}) + U^T \ \mathbf{R} \ U + \Delta U^T \ \mathbf{R_2} \ \Delta U, \tag{2.17}$$

where $\mathbf{R_2} = blockdiag\{R_2, R_2, \cdots, R_2\}$. Substituting (2.16) into (2.17), the following constrained quadratic programming problem is obtained

$$J_{A_{MPC}} = arg\min_{\Delta U} \frac{1}{2}\Delta U^T H_A \Delta U + F_A^T \Delta U + \Upsilon_A, \tag{2.18}$$

subject to

$$\begin{aligned} x_p[t+k|t] &\in \mathcal{X}, \quad k = 0, \cdots, N_p, \\ u[t+k|t] &\in \mathcal{U}, \quad k = 0, \cdots, N_p - 1, \\ u[t+k|t] - u[t+k-1|t] &\in \Delta\mathcal{U}, \quad k = 0, \cdots, N_p - 1, \end{aligned} \tag{2.19}$$

where

$$
\begin{aligned}
H_A =& S_u^T S_{\Delta u}^T \mathbf{Q} S_{\Delta u} S_u + S_{\Delta u}^T \mathbf{R} S_{\Delta u} + \mathbf{R_2}, \\
F_A =& 2(S_u U_{-1} + S_x x_0 + S_D)^T \mathbf{Q} S_u S_{\Delta u} - 2X_{des}^T \mathbf{Q} S_u S_{\Delta u} + 2U_{-1}^T \mathbf{R} S_{\Delta u}, \\
\Upsilon_A =& (S_u U_{-1} + S_x x_0 + S_D)^T \mathbf{Q} (S_u U_{-1} + S_x x_0 + S_D) + U_{-1}^T \mathbf{R} U_{-1} \\
& - 2\left(X_{des}^T \mathbf{Q} (S_u U_{-1} + S_x x_0 + S_D)\right).
\end{aligned}
$$

The solution of the QP problem in (2.18) with the constraints in (2.19) provides the series of optimal control input increments ΔU. The first input vector of ΔU is added to the control input applied in previous time step $u[-1]$. The resultant total control input is applied to system (2.6).

2.3.3 Holistic Corner Control Strategy

This approach was proposed to optimally distribute torque to each wheel (corner) to control the vehicle stability [15, 70]. The control aim is to adjust the necessary tire forces to achieve minimum path error and thus to improve the comfort of drive on various road conditions. The control algorithm is applied in real-time through explicit analytical optimum solution. The cost function structure was adopted from [28]. This novel strategy avoids a complex real-time implementation of a combined-slip tire model and results in a much more efficient computation. The controller is designed as two-layer. In first layer, the difference between the required forces and/or moments for the vehicle stabilization and actual ones are determined. Then, the longitudinal and lateral force command are generated for each wheel in the second layer. The tire ellipse constraint was imposed to the optimization problem. Since HCC scheme does not use a model in the optimal force distribution layer, it is inherently robust to model uncertainties.

HCC Formulation

The desired CG forces are determined from driver's inputs, including steering wheel angle and driving/braking torque values. These desired CG forces are denoted by

$$
F_{des} = \begin{bmatrix} F_{x_{des}} & F_{y_{des}} & M_{z_{des}} \end{bmatrix}^T, \tag{2.20}
$$

where $F_{x_{des}}, F_{y_{des}}$, and $M_{z_{des}}$ are the desired CG longitudinal force, lateral force, and yaw moment, respectively. The actual forces on CG are denoted by

$$F = \begin{bmatrix} F_x & F_y & M_z \end{bmatrix}^T, \tag{2.21}$$

where F_x, F_y, and M_z are the actual CG longitudinal force, lateral force, and yaw moment acting on the vehicle CG, respectively. The total tire force vector is defined as

$$f = \begin{bmatrix} F_{xfl} & F_{yfl} \cdots F_{xrr} & F_{yrr} \end{bmatrix}^T, \tag{2.22}$$

where F_{xi}, F_{yi} are the longitudinal and lateral tire forces for $i = fl,\ fr,\ rl,\ rr$ representing the corresponding corner of the vehicle. In this case, actual CG force F can be expressed as a function of all tire forces, i.e., $F(f)$. The corresponding adjusted CG forces that reduces the error between the desired F_{des} and the actual F is given as follows:

$$F(f + \Delta f) \approxeq F(f) + A_f \Delta f. \tag{2.23}$$

A_f is a Jacobian matrix that relates the tire-level forces to actual forces at the CG. Each entry of (2.22) can be derived using vehicle motion equations that links the relationship between tire forces and CG.

The vector of control actions required to reduce the error between (2.21) and (2.20) is defined as follows:

$$\Delta f = \begin{bmatrix} \Delta F_{xfl} & \Delta F_{yfl} \cdots \Delta F_{xrr} & \Delta F_{yrr} \end{bmatrix}^T, \tag{2.24}$$

Since it is assumed that tire lateral forces directly is not adjusted, the following relation is obtained:

$$\Delta F_{yi} = 0, \quad i = fl,\ fr,\ rl,\ rr. \tag{2.25}$$

The CG force error vector E_{CG} is defined as the difference between actual CG forces and the desired CG forces given by

$$E_{CG} = \begin{bmatrix} F_{x_{des}} - F_x(F + \Delta f) \\ F_{y_{des}} - F_y(F + \Delta f) \\ M_{zdes} - M_z(F + \Delta f) \end{bmatrix}. \tag{2.26}$$

Thus, the HCC optimization is designed to minimize the following cost function over Δf :

$$J_{HCC}(\Delta f) = \frac{1}{2}\left(E_{CG} - A_f \Delta f\right)^T W_E \left(E_{CG} - A_f \Delta f\right) + \frac{1}{2}\Delta f^T W_{\Delta f} \Delta f, \tag{2.27}$$

where $W_E, W_{\Delta f}$ are diagonal weight matrices for CG force error and control effort, respectively, and selected such that the objective function in (2.27) maintains its positive definiteness:

$$W_E = \begin{bmatrix} W_{F_x} & 0 & 0 \\ 0 & W_{F_y} & 0 \\ 0 & 0 & W_{M_z} \end{bmatrix}, \tag{2.28}$$

$$W_{\Delta f} = diag\left[W_{xfl}, W_{xfr}, W_{xrl}, W_{xrr}\right], \tag{2.29}$$

where the individual components correspond to weights on traction motor effort for individual wheels.

Assuming that the tire forces are inside the friction circle. The solution for the minimization problem is derived as follows:

$$\Delta f = \left[W_{\Delta f} + \left(A_f^T W_E\right) A_f\right]^{-1} \left[A_f^T \left(W_E E_{CG}\right)\right]^T, \tag{2.30}$$

unless the following condition is satisfied

$$det\left[W_{\Delta f} + \left(A_f^T W_E\right) A_f\right] \neq 0. \tag{2.31}$$

This solution is most commonly referred to as a closed-form solution. After calculating the unknown tire force control vector Δf , differential torque ΔQ that corresponds to this tire force control vector is calculated using the following:

$$\Delta Q_i = R_{eff} \Delta f_i, \quad i = fl,\ fr,\ rl,\ rr. \tag{2.32}$$

2.4 Multiple-Model Adaptive Control

Classical adaptive control and linear robust control methodologies can generally guarantee stability and robustness for small parametric or non-parametric uncertainties (within a certain limited range) in system modeling. However, parametric uncertainties can become

large in practice because of changes in operating conditions, component aging or failure, or variations in plant dynamics due to an external influence. Such large parametric uncertainties may cause poor transient response or instability. Furthermore, in conventional adaptive control requires persistently exited input to guarantee for the identification of true values of unknown parameters, which is very restrictive in critical condition in which safety is crucial. MMAC strategies have been developed to address such issues for larger ranges of system variations and uncertainties.

The idea of using multiple models in control design provides more comperehensive description and better control performance of uncertain time-varying systems. The intuitive idea is to use a set of models to represent the system behaviour for various operational conditions instead of a single model with a wide range of uncertainty in its dynamic equation. This approach allows a significantly less conservative setting for design of a set of controllers, one for each system model in the aforementioned system model set, to form a supervised switched or blending control structure. As an early example of multiple model control systems, multiple-model Kalman filters were introduced in the 1970s, aiming to improve the accuracy of state estimation [4, 43].

[52] utilized switching in the framework of adaptive control. Direct switching and indirect switching were proposed as two new techniques. In direct switching [27, 55], the output of the system defines the time of the switching to the next controller in a pre-determined sequence. On the other hand, indirect switching [54] determines both when and to which controller to switch. [58, 59, 60] considered set-point regulation for uncertain linear SISO systems and proposed a high-level controller called a *supervisor* to orchestrate the switching of a sequence candidate set-point controllers such that the system output tracked a costant reference input. These paper assumed that the uncertain system belonged to a combination of a sub-families of systems and each sub-family had a linear controller to achieve set-point regulation. In these papers, output-squared estimation errors used for comparison and a candidate controller with the smallest performance index was selected to generate control input. [31] considered a continuous-time linear SISO system with large modelling errors. The paper employed a family of linear candidate controllers supervised by a high-level switching logic. This paper mainly focused on the switching logics in the literature. The paper also emphasized the modularity in switching based multiple-model adaptive control, i.e., the switching logic, the multiple-model system identifier and the candidate controllers can be independently designed, which provides grater flexibility in applications. [32] compared switching based multiple-model adaptive control with conventional adaptive control techniques and emphasized the advantages of switching based control schemes, such as the simplicity of parameterization, computational cost, capable of handling non-convex or discrete parameter sets, and modularity. The paper also di-

vided the switching logic into two categories: those based on process estimation (using either certainty equivalence or model validation) and those based on direct performance of candidate controllers. However, the paper mostly focused on estimator-based supervisory control based on certainty equivalence. The Chapter 6 of [48] was dedicated to control of systems with large modelling uncertainty, and it presented switching control algorithms for some specific problems such as stabilization of nonholonomic systems, and switching adaptive control of uncertain systems.

The certainty equivalance based multiple-model system identification has also attracted attention for estimation of unkonwn vehicle dynamics since it requires less sensor data and does not require persistent excitated input for identification. [76] utilized switching based multiple-model system identifier for the real time estimation of unknown constant parameters of vehicle dynamics. The paper used 2-DOF linear lateral vehicle dynamics, sideslip angle and yaw-rate, for the identification of front and rear tire cornering stiffnesses, and longitudinal position of vehicle CG. These unknown parameters were assumed to lie in a certain continuous parameter space, and the paper considered 140 identification models to cover the parameter space. The proposed multiple-model estimation method was simulated and it was observed that all of three constant parameters were exactly estimated. The same paper used 1-DOF linear roll vehicle dynamic for the identification of uncertain spring stiffness, damping coefficient, and the vertical position of vehicle CG. Similarly, the closed parameter space of these uncertain parameters was known and the paper designed 240 models for the identification. In simulation results, precise estimations were achieved for the spring stiffness and the vertical CG position, while the damping coefficient was estimated with 20% parametric error. The paper also presented a comparison of multiple-model approach with recursive linear least-square method for the online identification of the vertical CG position. The multiple-model approach achieved faster and more accurate convergence.

To avoid unsatisfactory response due to switching between fixed controllers, the switching and tuning idea in multiple-model adaptive control was proposed and improved in [62, 63]. The main idea was to use switching logic for fast adaptation, and then tuning (using adaptive law) the controller gain to improve performance. Furthermore, the switching based multiple-model adaptive control strategies were for uncertain LTI systems, whereas switching and tuning can be implemented to uncertain LTV systems. The authors of the paper [76] utilized the switching and tuning idea in [75] for identification of the same unknown constant parameters with the same number of identification models. However, there was no comparison with these two different approach.

In [36, 26], parameter switching based performance improvement was applied for backstepping and sliding mode type controllers, respectively. Transient performance improve-

ment for a class of systems along with a quantitative evaluation was investigated in [14]. [79] used only adaptive identification models in order to control nonlinear systems in parametric-strict-feedback form and provided a model convergence proof. Recently in [42, 5] the authors proposed the adaptive mixing control method that makes available the use of the full suite of powerful design tools from LTI theory and also they combined the controller mixing strategy with a multiple parameter estimation architecture plus a hysteresis switching logic in order to eliminate the dependence on the initial conditions of the parameter estimator. [12] studied the stability of mixing based multiple LQ controllers for LTV decoupled MIMO systems.

In the field of conventional multiple-model adaptive control, there have been some signifant works [29, 65] which focused on the number of adaptive and fixed estimation models, and the source of information for every model. These papers proposed to blend the predefined controller gains based on the identification errors from all model. This approah has led to a faster convergence and to better performance than other previous multiple-model based techniques [61]. The stabiliy analysis of these new works have been focused in [66]. However, the control scheme has been developed for LTI and LTV SISO systems.

In Fig. 2.2, the general architecture of a conventional multiple-model adaptive control scheme in the scope of this chapter is given. There is an unknown time-varying/invariant plant whose input u and output y_p, a multiple-model system identifier consisting of N identification models, and a set of controllers corresponding to designed identification models. Identification of the unknown plant is performed based on either comparison or weighting of identification errors. These approaches also determine the control input applied to the system by either switching to the corresponding controller or blending all predefined controller gains. In the following, the conventional multiple-model system identifier is presented at first. Then, the switching based control and adaptive law based control schemes are examined in detail.

2.4.1 Conventional Multiple-Model System Identifier

In this section, the conventional multiple-model system identifier in Fig.2.2 is presented. These models could be either fixed or adaptive. If each designed models consists of fixed parameters (called fixed models), these models may relate to different conditions where the plant operates. Since each model gives different output for the same input, these outputs can be considered as the response of the plant with different parameters.

In adaptive models, the parameters of the identification models are online updated.

These adaptive models are used to start adaptive laws with different initial parameter estimates. If one of the models is closer than others in initial parameter estimates to the original plants, this identification model may achieve faster convergence speed. As shown in Fig.2.2, the same input simultaneously applied to N multiple stable identification models and original plant. The output of corresponding identification model is $y_i(t)$. Thus, the identification error is defined as

$$e_i(t) = y_i(t) - y_p(t), \tag{2.33}$$

and the tracking control error is

$$e_c(t) = y_p(t) - y_d(t). \tag{2.34}$$

In this study, it assumed that the states of the unknown plant in Fig.2.2 are fully accessible. Thus, the system output can be view as $y_p(t) = x_p(t)$.

Various multiple-model control approaches have been proposed as an alternative to conventional adaptive control in the literature. Two different approaches are presented here due to relation with the multiple-model system identifier and adaptive control schemes proposed in this study.

2.4.2 Switching Based Control

The effectiveness of the switching based control strategies in the literature has been verified for the identification and control of uncertain LTI systems. Thus, this section considers an uncertain LTI MIMO system in the form

$$\dot{x}_p(t) = A_p x_p(t) + B_p u(t), \tag{2.35}$$

where $A_p \in R^{n\times n}$, $B_p \in R^{n\times r}$ are unknown constant system matrices; $x_p(t) \in R^n$ and $u(t) \in R^r$ are the (measurable) system state, and the system input, respectively.

The N fixed models in Fig. 2.2 are distributed to cover the region of uncertainty in parameter space of A_p and B_p. Each model i, for $i = 1, \cdots, N$, is formulated in the form

$$\dot{x}_i(t) = A_i x_i(t) + B_i u(t), \quad x_p(t_0) = x_i(t_0) \in R^n, \tag{2.36}$$

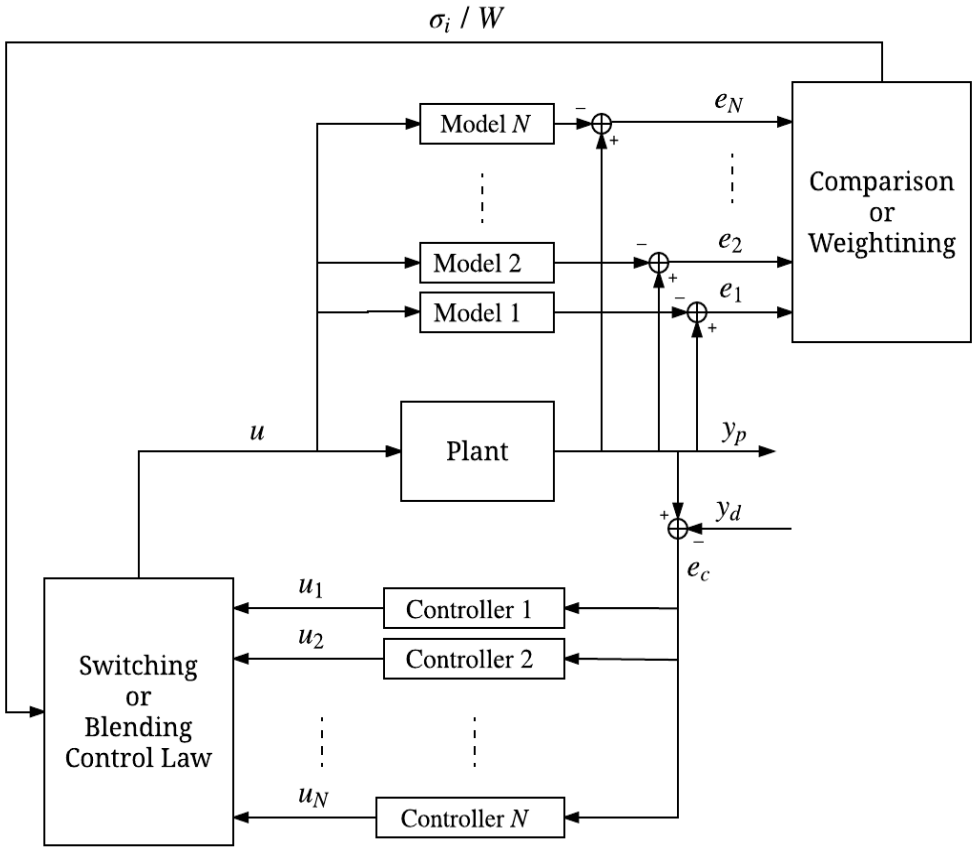

Figure 2.2: Conventional multiple-model adaptive control approaches.

having the same input as the unknown plant (2.35), where $A_i \in R^{n\times n}$, $B_i \in R^{n\times r}$ are known constant parameter matrices. The number N of fixed models to be used can be determined based on many factors influencing the uncertainties in the plant system in (2.35). Note that all designed identification models in (2.36) are assumed to be stable. The identification output error (or state error in our case) for each designed model is defined as

$$e_i(t) = x_p(t) - x_i(t). \tag{2.37}$$

The identification errors in (2.37) are used in cost functions (performance indices) to compare model matching at any time instant t. The cost function $J_i(t)$ is typically defined in one of the forms

$$J_i(t) = ||e_i(t)||^2, \tag{2.38a}$$
$$J_i(t) = \int_0^t ||e_i(\tau)||^2 d\tau, \tag{2.38b}$$
$$J_i(t) = \alpha||e_i(t)||^2 + \beta \int_0^t ||e_i(\tau)||^2 d\tau, \quad \beta, \alpha > 0 \tag{2.38c}$$
$$J_i(t) = \alpha||e_i(t)||^2 + \beta \int_0^t e^{(-\lambda(t-\tau))}||e_i(\tau)||^2 d\tau, \quad \lambda > 0, \tag{2.38d}$$

to define, respectively, the instantaneous, the integral (or least squares), a weighted instantaneous + integral, an weighted instantaneous + integral with forgetting factor λ. A high level decision maker called the *supervisor* evaluates and compares the cost functions $J_i(t)$ to identify the best matching model as the one having the minimum $J_i(t)$ at time instant t. The supervisor's output is denoted by the index signal $\sigma_i(t) \in \{1, \ldots, N\}$, defined by

$$\sigma_i(t) = \arg \min_{i \in \{1, \cdots, N\}} J_i(t).$$

For each Model i, there is a fixed robust Controller i for meeting the tracking or regulation task. Utilizing the best matching model index $\sigma_i(t)$ generated by the supervisor, at each time t, the fixed Controller $\sigma_i(t)$ is enabled. If Model $\sigma_i(t)$ is sufficiently close to or perfectly matches with the plant, then Controller $\sigma_i(t)$ stabilizes the plant.

Selection and distribution of the N plant models in parameter space is essential in guaranteeing existence of a set of N robust controllers to meet the control requirements for the system parameter range of interest. If the selected models are not close enough to each other in parameter space, the overall system in Fig. 2.2 can be subject to instability in switching transitions.

The main idea in the switching based control schemes with fixed models is that there should be a fixed controller for each possible value of an uncertain system parameter. This fixed controllers should have enough robustness to stabilize the nearby plants when the perfect match between the plant and one of the models happen.

2.4.3 Adaptive Law Based Control

In practice, the conventional switching based approaches have two major challenges. First, since at least one of the fixed models is required to be sufficiently close to the original plant in the system parameter space at any time instant t, the corresponding number N of fixed models may be large and grows exponentially with the dimension of the unknown

parameter vector [64]. Second, the models other than best matching one do not contribute to the estimation of the unknown parameters. Particularly, the performance indices of the fixed models or any other data from all models are not used efficiently to achieve a closer model. To use such data, [29] has proposed a method called *second level adaptation* for plant identification using a set of fixed identification models, for each of which there is a fixed controller gain. The resultant control gain is obtained by blending these fixed control gains based on the identification errors. Thus, the method combines information from all fixed models for the plant parameter estimation by using very few models ($n+1$ as compared to c^n, where n is the dimension of unknown parameter vector) for uncertain LTI/LTV SISO systems.

[29] has developed the second level adaptation method for uncertain LTI SISO systems in companion form using a set of adaptive identification models at first. This method is developed using the indirect model reference adaptive control scheme. The result from the method with multiple adaptive identification models formed the theoretical background of the second level adaptation with fixed identification models. Then, the paper extended the method to the control of uncertain LTV SISO systems in companion form using fixed identification models.

Adaptive Identification Models for Uncertain LTI SISO Systems

An uncertain LTI SISO plant, whose all state variables are accessible, is described by

$$\dot{x}_p = A_p x_p(t) + bu(t), \tag{2.39}$$

where $x_p(t) \in R^n, u(t) \in R$. A_p and b are in the following companion form

$$A_p = \begin{bmatrix} 0 & 1 & 0 & \cdots & 0 \\ 0 & 0 & 1 & \cdots & 0 \\ \vdots & \vdots & \vdots & \vdots & \vdots \\ 0 & 0 & 0 & \cdots & 1 \\ a_1 & a_2 & a_3 & \cdots & a_n \end{bmatrix}, b = \begin{bmatrix} 0 \\ 0 \\ 0, \\ \vdots \\ 1 \end{bmatrix}$$

where the parameters a_i are unknown. The unknown plant parameter vector is defined as

$$\theta_p^T = [a_1, a_2, \cdots, a_n]. \tag{2.40}$$

To design a direct model reference adaptive control, the reference model is described as follow:

$$\dot{x}_d = A_m x_d(t) + br(t), \tag{2.41}$$

where $x_d(t) \in R^n, r(t) \in R$ are the desired state trajectory, and uniformly bounded reference input, respectively. A_m is the reference model dynamics and in companion form. The last row of A_m, defined as θ_m^T, is designed to make A_m stable.

N adaptive identification models are simultaneously used to estimate the unknown plant parameter vector θ_p or (A_p). Each identification Model i $(i = 1, \cdots, N)$ is considered to have the form

$$\dot{x}_i(t) = A_m x_i(t) + [A_i(t) - A_m]x_p(t) + bu, \quad x_i(t_0) = x_p(t_0), \tag{2.42}$$

$$\dot{\theta}_i(t) = -e_i^T(t)Pbx_p(t), \quad \theta_i(t_0) = \theta_{i0}, \tag{2.43}$$

where $A_i(t)$ is constrained to be in companion form with the last row equal to estimate $\theta_i^T(t)$ of the unknown plant parameter vector θ_p^T, generated by the adaptive law (2.43). P is positive definite and solution of the following Lyapunov equation

$$A_m^T P + PA_m = -I. \tag{2.44}$$

It is assumed that that θ_p is in the convex hull of the vectors θ_i (or equivalently A_p) lies in the convex hull of the matrices A_i, that is $A_p \in \mathbf{Co}\{A_1, A_2, \cdots, A_N\}$, where $\mathbf{Co}\{\cdot\}$ stands for convex set. Thus, the theorem 2.1 in [29] is used

Theorem 2.1. *If N adaptive identification models described in (2.42) with initial conditions $x_i(t_0) = x_p(t_0)$ are adjusted using adaptive laws (2.43) with initial conditions $\theta_i(t_0)$ and $x_i(t_0) = x_p(t_0)$, and if the plant parameter vector θ_p lies in the convex hull of $\theta_i(t_0)(i \in \Omega)$, then θ_p lies in the convex hull of $\theta_i(t)(i \in \Omega)$ for all $t \geq t_0$.*

This theorem follows that if

$$\theta_p(t_0) = \sum_{i=1}^{N} \alpha_i \theta_i(t_0), \tag{2.45}$$

$$\sum_{i=1}^{N} \alpha_i e_i(t_0) = 0, \tag{2.46}$$

where $\alpha_i > 0$ and $\sum_{i=1}^{N} \alpha_i = 1$, then it also satisfies the equation

$$\theta_p = \sum_{i=1}^{N} \alpha_i \theta_i(t), \tag{2.47}$$

$$\sum_{i=1}^{N} \alpha_i e_i(t) = 0. \tag{2.48}$$

Therefore, α_i is considered as an alternative parametric model of the unknown LTI plant in (2.39), and the identification the system is performed by estimating the constant vector $\alpha = \begin{bmatrix} \alpha_1 & \alpha_2 & \cdots & \alpha_N \end{bmatrix}^T$, where (2.48) is utilized.

If the unknown parameter vector θ_p is in R^n, then at least $n+1$ models are required to cover this uncertain parameter set by a convex hull in practice. For the case $N = n+1$, the relation (2.48) becomes

$$\sum_{i=1}^{n+1} \alpha_i e_i(t) = 0, \tag{2.49}$$

where $e_i(t)$ are identification errors, which are continuously monitored. (2.49) is expressed in matrix form

$$E(t)\alpha = 0, \quad E(t) = \begin{bmatrix} e_1(t) & e_2(t) \cdots e_{n+1}(t) \end{bmatrix} \in R^{n \times n+1}. \tag{2.50}$$

By subtracting e_{n+1} from both sides of (2.50), the following property is obtained

$$\begin{aligned} &E_R(t)\alpha_R = -e_{n+1}(t), \\ &E_R(t) = \begin{bmatrix} e_1(t) - e_{n+1}(t) & e_2(t) - e_{n+1}(t) & \cdots, e_n(t) - e_{n+1}(t) \end{bmatrix}, \\ &\alpha_R = \begin{bmatrix} \alpha_1 & \alpha_2 & \cdots \alpha_n \end{bmatrix}, \end{aligned} \tag{2.51}$$

The α_R can be computed using the inversion of matrix $E_R(t)$ and $\alpha_{n+1} = 1 - \sum_{i=1}^{n} \alpha_i$ by convexity property for any time instant. For robustness, the estimate $\hat{\alpha}_R(t)$ of α_R can also be determined by the following differential equation;

$$\dot{\hat{\alpha}}_R(t) = -E_R^T(t)E_R(t)\hat{\alpha}_R(t) - E_R^T(t)e_{n+1}(t) \tag{2.52}$$

with $\hat{\alpha}_{n+1}(t) = 1 - \sum_{i=1}^{n} \hat{\alpha}_i(t)$. Since the constant vector α_R satisfies the algebraic equation

$$E_R^T(t)E_R(t)\alpha_R + E_R^T(t)e_{n+1}(t) = 0, \tag{2.53}$$

the estimate error $\tilde{\alpha}_R(t) = \hat{\alpha}_R(t) - \alpha_R$ satisfies the differential equation

$$\dot{\tilde{\alpha}}_R(t) = -E_R^T(t)E_R(t)\tilde{\alpha}_R(t). \tag{2.54}$$

By the Lyapunov equation $V(\tilde{\alpha}_R^T(t)\tilde{\alpha}_R(t))$, the condition

$$\frac{dV(\tilde{\alpha}_R(t))}{dt} = -\|E_R(t)\tilde{\alpha}_R(t)\|^2 < 0 \tag{2.55}$$

is followed, which guarantees the asymptotic stability of (2.54) (i.e., $\tilde{\alpha}_R$ asymptotically converges to zero). The convergence rate depends only on the positive definite matrix $E_R^T(t)E_R(t)$ and thus on the location of the n models represented by $\theta_1, \theta_2, \cdots, \theta_n$.

After computing (or estimating) the vector α (or $\hat{\alpha}$), the control input applied to the actual plant and identification models is adjusted with respect to weights of the models as shown in Fig. 2.2.

Fixed Identification Models for Uncertain LTI/LTV SISO systems

Second level adaptation with multiple adaptive models provides fast convergence for uncertain LTI SISO systems. However, it cannot be extended for uncertain LTV systems without reinitialization periodically. Thus, [65] proposed to use multiple fixed models for the identification of uncertain LTI and LTV SISO systems. With a few changes, the result in the preceding procedure can still be used. To this end, adaptive models in the previous analysis replaces with fixed models, and hence $\theta_i(t)$ (or $A_i(t)$) becomes constant θ_i (or A_i) for any time instant. To obtain the estimate $\hat{\alpha}_R$, the same equations (2.51, 2.52) could be

used for LTI SISO systems. To extend this approach for LTV SISO systems, α becomes time-varying parameter $\alpha(t)$ representing the time-variation in the parameter vector $\theta_p(t)$ (or $A_p(t)$). Then, (2.51) is converted into

$$E_R(t)\alpha_R(t) = -e_{n+1}(t). \tag{2.56}$$

For the dynamic estimation, the equation (2.52) is still valid and $\hat{\alpha}_{n+1}(t) = 1 - \sum_{i=1}^{n} \hat{\alpha}_i(t)$ by convexity property for any time instant. The applied control input is continuously tuned based on the estimate $\hat{\alpha}(t)$ or computed $\alpha(t)$.

Chapter 3

Blending based Multiple-Model Adaptive Control for Linear Systems with Polytopic Uncertainities

In this chapter, we develop multiple fixed model blending based adaptive parameter identification schemes for linear systems with polytopic parameter uncertainty utilizing gradient and RLS based methods. The developed adaptive schemes are further combined with a bank of predefined multiple LQ based optimal controllers to design an optimal MMAC scheme. In the proposed blending based MMAC design, the uncertain system is expressed in terms of PLDIs. For each vertex of such a polytopic inclusion, a fixed model is selected and a corresponding LQ controller is designed. Based on the input and output of the system, the controller gains of models are blended using the weights generated by the developed multiple-model adaptive law. The asymptotic stability of the proposed adaptive identification and the developed LQ based optimal MMAC schemes are proved for LTI MIMO systems with polytopic parameter uncertainties.

3.1 Preliminaries

The purpose of this section is to give certain definitions and properties of the norms and functions used throughout this thesis. We will use the following corollary of Barbalat's Lemma and definition for the stability analysis of the proposed adaptive identification and control schemes.

Lemma 3.1. *[34, 35] if $f, \dot{f} \in L_\infty$ and $f \in L_p$ for some $p \in [1, \infty)$, then $f(t) \to 0$ as $t \to \infty$.*

Definition 3.1. *[35] The exponentially weighted L_2 norm of a function x of time t, for a given constant $\delta \geq 0$, is defined as*

$$\|x_t\|_{2\delta} \triangleq \left(\int_0^t e^{-\delta(t-\tau)} x^T(\tau) x(\tau) d\tau \right)^{0.5}.$$

Further, $x \in L_{2\delta}$ denotes that $\|x_t\|_{2\delta}$ exists. For finite time t, the $L_{2\delta}$ norm satisfies the following properties:

(i) $\|x_t\|_{2\delta} \geq 0$

(ii) $\|\alpha x_t\|_{2\delta} = |\alpha| \|x_t\|_{2\delta}$ *for any scalar* α

(iii) $\|(x+y)_t\| x_t\|_{2\delta} \leq \|x_t\|_{2\delta} + \|y_t\|_{2\delta}$

(iv) $\|\alpha x_t\|_{2\delta} \leq \|x_t\|_{2\delta} \sup_t |\alpha(t)|$ *for any* $\alpha \in L_\infty$.

3.2 Problem Statement

Consider a linear polytopic uncertain MIMO system in the form

$$\dot{x}_p(t) = A_p(\eta) x_p(t) + B_p(\eta) u(t), \tag{3.1}$$

where $A_p(\eta) \in R^{n \times n}$ and $B_p(\eta) \in R^{n \times r}$ are plant matrices dependent on the uncertain system parameter vector $\eta \in R^q$; $x_p(t) \in R^n$ and $u(t) \in R^r$ are the (measurable) system state, and the system input, respectively. The control objective is to design control signal $u(t)$ such that $x_p(t)$ converges to zero, under the following PLDI assumption:

Assumption 3.1. *There exist N known system matrix pairs $A_i \in R^{n \times n}$, $B_i \in R^{n \times r}$, $i = 1, \cdots, N$, for some known integer $N > 0$, such that, for any possible η, we have*

$$[A_p(\eta) \ B_p(\eta)] \in \boldsymbol{Co}\{[A_i \ B_i] : i = 1, \cdots, N\}, \tag{3.2}$$

where $\mathbf{Co}\{\cdot\}$ *denotes the convex hull of a set of matrices.*

3.3 Blending Based Multiple-Model Identification

To address the control problem stated in section 3.2, we propose a new blending based multiple-model adaptive parameter identification scheme, as depicted in Fig.3.1. In this scheme, the uncertain linear system (3.1) is considered as a PLDI whose vertices are known per Assumption 1. For each vertex $i \in \{1, \cdots, N\}$, one fixed model is considered in the form

$$\dot{x}_i(t) = A_i x_i(t) + B_i u(t). \tag{3.3}$$

Then, using the convexity property of PLDI, a blending based adaptive law is developed. The convexity property (3.2) can be reexpressed as

$$A_p(\eta)x_p(t) + B_p(\eta)u(t) = \sum_{i=1}^{N} w_i(t) \left[A_i x_p(t) + B_i u(t)\right], \tag{3.4}$$

where $w_i(t)$ refer to the weights of the corresponding models at time instant t, satisfying

$$\sum_{i=1}^{N} w_i(t) = 1 \quad \text{and} \quad w_i(t) \geq 0. \tag{3.5}$$

w_i are constant for uncertain LTI plants, i.e., if η is constant.

Noting that the fixed parameter matrices A_i, B_i are already known, estimation of the unknown weights w_i is equivalent to identification of the unknown matrices $A_p(\eta)$ and $B_p(\eta)$.

3.3.1 Selection of Linear Parametric Models

The linear parametric models required for online identification of the system (3.1) with polytopic uncertainty are selected, considering (3.1) in the form of linear parametric model ([34]):

$$z(t) = \Theta_p(\eta)\Phi(t), \tag{3.6}$$

where

$$\begin{aligned}\Theta_p(\eta) &= \begin{bmatrix} A_p(\eta) & B_p(\eta) \end{bmatrix}, \\ \Phi &= \frac{1}{s+\lambda}\begin{bmatrix} x_p \\ u \end{bmatrix}, \\ z &= \frac{s}{s+\lambda}x_p, \quad \lambda > 0,\end{aligned} \tag{3.7}$$

where s denotes the differentiation operator and λ is a constant design parameter. The N fixed models in (3.3) are parameterized similarly, as follows:

$$z_i(t) = \Theta_i \Phi(t), \quad \Theta_i = \begin{bmatrix} A_i & B_i \end{bmatrix} \text{ for } i = 1, \cdots, N, \tag{3.8}$$

where $z_i = \frac{s}{s+\lambda}x_i$. The (output) estimation errors for the N fixed models are defined as

$$\varepsilon_i(t) = z(t) - \Theta_i \Phi(t), \quad i = 1, \cdots, N. \tag{3.9}$$

Using convexity property (3.4), the following relations are obtained:

$$\Theta_p(t) = \sum_{i=1}^{N} w_i(t)\Theta_i, \quad \sum_{i=1}^{N} w_i(t)\varepsilon_i(t) = 0, \tag{3.10}$$

which can be reexpressed in matrix form as

$$\begin{aligned} &E(t)W(t) = 0, \; E(t) = \begin{bmatrix} \varepsilon_1(t) & \varepsilon_2(t) & \cdots & \varepsilon_N(t) \end{bmatrix} \in R^{n \times N}, \\ &W(t) = \begin{bmatrix} w_1(t) & w_2(t) & \cdots & w_N(t) \end{bmatrix}^T \in R^N. \end{aligned} \tag{3.11}$$

By (3.5) and (3.11), the weight of the last model, Model N can be computed as $w_N = 1 - \sum_{i=1}^{N-1} w_i$. Thus, we obtain the following equation by subtracting $\varepsilon_N(t)$ from both sides of (3.11):

$$\begin{aligned} &E_R(t)W_R(t) = -\varepsilon_N(t), \\ &E_R(t) = [\varepsilon_1(t) - \varepsilon_N(t) \; \cdots \; \varepsilon_{N-1}(t) - \varepsilon_N(t)] \in R^{n \times (N-1)}, \\ &W_R(t) = \begin{bmatrix} w_1(t) & w_2(t) & \cdots & w_{N-1}(t) \end{bmatrix}^T \in R^{N-1}. \end{aligned} \tag{3.12}$$

By (3.12), the estimate $\hat{w}_i(t)$ of $w_i(t)$ can be obtained either batch linear algebraic calculation or using differential equation.

3.3.2 Estimation of the Weighting Vector

The matrix $E_R(t)$ in (3.12) is only dependent on the output of designed models since its all columns are of the form $\varepsilon_i(t) - \varepsilon_N(t)$. If the matrix $E_R(t)$ in (3.12) is full-rank, then $W_R(t)$ can be algebraically estimated as

$$\begin{aligned} W_R(t) &= -(E_R^T(t)E_R(t))^{-1}E_R^T(t)\varepsilon_N(t) \text{ for } n \geq N-1, \\ W_R(t) &= -E_R^T(t)(E_R(t)E_R^T(t))^{-1}\varepsilon_N(t) \text{ for } n < N-1, \end{aligned} \tag{3.13}$$

which also satisfies

$$E_R^T(t)E_R(t)W_R(t) + E_R^T(t)\varepsilon_N(t) = 0. \tag{3.14}$$

Since differential equations are more robust to rank deficiency and measurement noise effects than algebraic methods, they are more preferable in practice. Utilizing (3.13), the estimate $\hat{W}_R(t)$ of W_R is generated applying the following recursive adaptive law:

$$\dot{\hat{W}}_R(t) = -\Gamma E_R^T(t)E_R(t)\hat{W}_R(t) - \Gamma E_R^T(t)\varepsilon_N(t), \tag{3.15a}$$

$$\hat{w}_N(t) = 1 - \sum_{i=1}^{N-1} \hat{w}_i(t), \tag{3.15b}$$

where $\Gamma \in R^{(N-1)\times(N-1)}$ is a diagonal matrix with positive constant entries, to tune the convergence speed, where (3.15b) is based on (3.5).

Remark 3.1. *The adaptive law (3.15a) is a gradient algorithm minimizing the cost (Lyapunov) function*

$$V(\tilde{W}_R(t)) = \frac{1}{2}\tilde{W}_R^T(t)\Gamma^{-1}\tilde{W}_R(t).$$

For the cases where any noise or inaccuracies exist in the measured data, least-squares based identification schemes are expected to provide better performance than gradient based schemes.

3.3.3 Recursive Least-Squares Based Adaptation

A recursive least-squares based alternative to the gradient adaptive law (3.15) can be designed, aiming to minimize the following integral cost function:

$$\begin{aligned} J(\hat{W}_R) =& \frac{1}{2}\int_0^t e^{-\beta(t-\tau)}\tilde{W}_R^T(\tau)E^T(\tau)E(\tau)\tilde{W}_R(\tau)d\tau \\ &+ \frac{1}{2}e^{-\beta t}(\hat{W}_R - \hat{W}_{R0})^T Q_0(\hat{W}_R - \hat{W}_{R0}), \end{aligned} \tag{3.16}$$

where $\hat{W}_{R0} = \hat{W}_R(0)$ is the initial estimate; $\beta \geq 0$ is a design parameter acting as a forgetting factor; $Q_0 = Q_0^T \in R^{(N-1)\times(N-1)}$ penalizes the initial parameter estimation error. The corresponding recursive least-squares based adaptive algorithm is obtained, similarly to the procedure in [34], as

$$\dot{\hat{W}}_R = -P\ (E_R^T\varepsilon_N + E_R^T E_R\hat{W}_R), \tag{3.17a}$$

$$\dot{P} = \beta P - PE_R^T E_R P, \quad P(0) = P_0 = Q_0^{-1}, \tag{3.17b}$$

$$\hat{w}_N(t) = 1 - \sum_{i=1}^{N-1}\hat{w}_i(t) \tag{3.17c}$$

where $P_0 \in R^{(N-1)\times(N-1)}$ is a diagonal positive definite matrix. The LS based on-line update of the adaptive gain matrix P leads to significant improvement in the convergence speed and robustness to measurement noise, as will be observed in Section 4.4 through simulations. However, when $\beta > 0$, $P(t)$ may grow without bound since $\dot{P}$ satisfy $\dot{P} > 0$ because $\beta P > 0$ and the fact that $PE_R^T E_R P$ is only positive definite. To avoid this issue, we modify the least-squares algorithm (3.17) as follows:

$$\dot{\hat{W}}_R = -P\ (E_R^T\varepsilon_N + E_R^T E_R\hat{W}_R), \tag{3.18a}$$

$$\dot{P} = \begin{cases} \beta P - PE_R^T E_R P & if\ ||P(t)|| \leq R_0, \\ 0 & otherwise \end{cases} \tag{3.18b}$$

$$\hat{w}_N(t) = 1 - \sum_{i=1}^{N-1}\hat{w}_i(t) \tag{3.18c}$$

where $||P|| \leq R_0$ and R_0 is a constant upper bound for $||P||$, which guarantees $P \in L_\infty$.

3.3.4 Stability and Convergence

The adaptive laws (3.15) and (3.18) can be used for both LTI and LTV systems. In the following theorems, Theorem 3.2 and Theorem 3.3, we establish the stability of (3.15) and (3.18), respectively, for uncertain LTI systems, for which W_R is constant.

Theorem 3.2. *Consider the MIMO system (3.1). Assume that* $\Theta_p(\eta) = [A_p(\eta)\ B_p(\eta)]$ *is constant. If* $\Theta_p \in \boldsymbol{Co}\{\Theta_i : i = 1, \cdots, N\}$ *and* $\Phi, \dot{\Phi} \in L_\infty$*, the adaptive law (3.15a) guarantees that*

(i) ε_i, $\dot{\varepsilon}_i$ $(i = 1, \cdots, N)$, $\dot{\hat{W}}_R$, $\hat{W}_R$, $E_R\tilde{W}_R \in L_\infty$

(ii) $E_R\tilde{W}_R \in L_2$

(iii) $E_R(t)\hat{W}_R(t) + \varepsilon_N(t)$ *asymptotically converges to* 0.

Proof. Consider a constant W_R that satisfies (3.12), whose existence is guaranteed by Assumption 3.1. For such W_R, (3.12) can be rewritten as $E_R\hat{W}_R + \varepsilon_N - E_R\tilde{W}_R = 0$, for the estimation error $\tilde{W}_R = \hat{W}_R - W_R$. Hence, $E_R\tilde{W}_R = E_R\hat{W}_R + \varepsilon_N$. Multiplying both sides of (3.14) with Γ, we obtain

$$\Gamma E_R^T(t)E_R(t)W_R + \Gamma E_R^T(t)\varepsilon_N(t) = 0. \tag{3.19}$$

Adding (3.19) to both sides of (3.15a), the following dynamic equation is obtained:

$$\dot{\tilde{W}}_R(t) = \dot{\hat{W}}_R(t) = -\Gamma E_R^T(t)E_R(t)\tilde{W}_R(t). \tag{3.20}$$

Hence, the Lyapunov function

$$V(\tilde{W}_R(t)) = \frac{1}{2}\tilde{W}_R^T(t)\Gamma^{-1}\tilde{W}_R(t), \tag{3.21}$$

satisfies

$$\frac{dV(\tilde{W}_R(t))}{dt} = -\|E_R(t)\tilde{W}_R(t)\|^2 \leq 0, \tag{3.22}$$

which implies $V \geq 0$ is a non-increasing function of time, the $\lim_{t\to\infty} V(\tilde{W}_R) = V_\infty$ exists. This further implies that $\tilde{W}_R \in L_\infty$ and hence $\hat{W}_R \in L_\infty$. Further, since $\dot{\Phi} \in L_\infty$ implies

$z \in L_\infty$ by definition and $\Phi \in L_\infty$, by definition we have ε_i, $\dot{\varepsilon}_i \in L_\infty$ for all $i \in \{1, \ldots, N\}$. Hence, $E_R(t)$ is bounded and (3.20) implies that $\dot{\hat{W}}_R$, $E_R\tilde{W}_R \in L_\infty$, completing proof of (i). To prove (ii), observe that $E_R\tilde{W}_R \in L_2$ since, by (3.22), we have

$$\int_0^\infty \|E_R(t)\tilde{W}_R(\tau)\|^2 d\tau = -\int_0^\infty \dot{V}(\tau)d\tau = V_0 - V_\infty, \tag{3.23}$$

where $V_0 = V(\tilde{W}_R(0))$.

Thus, the proofs of (i) and (ii) are completed. (iii) follows by applying Lemma 2.1 with $f(t) = E_R(t)\tilde{W}_R(t)$. □

Theorem 3.3. *Consider the MIMO system (3.1). Assume that $\Theta_p(\eta) = [A_p(\eta)\ B_p(\eta)]$ is constant. If $\Theta_p \in \boldsymbol{Co}\{\Theta_i : i = 1, \cdots, N\}$ and $\Phi, \dot{\Phi} \in L_\infty$, the adaptive law (3.18a,3.18b) guarantees that*

(i) ε_i, $\dot{\varepsilon}_i$ $(i = 1, \cdots, N)$, $\dot{\hat{W}}_R$, $\hat{W}_R$, $E_R\tilde{W}_R$, $P \in L_\infty$

(ii) $E_R\tilde{W}_R \in L_2$

(iii) $E_R(t)\hat{W}_R(t) + \varepsilon_N(t)$ *asymptotically converges to* 0.

Proof. As in the case of Theorem 3.2, (3.12) can be rewritten as $E_R\tilde{W}_R = E_R\hat{W}_R + \varepsilon_N$, and hence, similar to (3.20), we have

$$\dot{\tilde{W}}_R(t) = \dot{\hat{W}}_R(t) = -P(t)E_R^T(t)E_R(t)\tilde{W}_R(t). \tag{3.24}$$

Using the identity $\frac{d}{dt}P^{-1} = -P^{-1}\dot{P}P^{-1}$, (3.18b) can be rewritten as

$$\dot{P} = \begin{cases} \beta P - PE_R^T E_R P & if\ ||P(t)|| \le R_0, \\ 0 & otherwise. \end{cases} \tag{3.25}$$

Defining the Lyapunov-like function

$$V(t) = \frac{1}{2}\tilde{W}_R^T(t)P^{-1}(t)\tilde{W}_R^T(t), \tag{3.26}$$

(3.18a), (3.24), and (3.25) lead to

$$\dot{V}(t) = \begin{cases} -\frac{1}{2}\tilde{W}_R^T E_R^T E_R\tilde{W}_R - \frac{1}{2}\beta\tilde{W}_R^T P^{-1}\tilde{W}_R & if\ ||P|| \le R_0 \\ -\tilde{W}_R^T E_R^T E_R\tilde{W}_R & otherwise \end{cases} \tag{3.27}$$

The assumption $\Phi, \dot{\Phi} \in L_\infty$ implies that $E_R, E_R^T E_R \in L_\infty$ as well. Therefore, (3.25) implies that $||P||$ is both upper and lower bounded and $P(t)$ is always positive definite. Hence, since $\dot{V} \leq -\frac{1}{2}\|E_R(t)\tilde{W}_R(t)\|^2 \leq 0$, $\forall t \geq 0$, by (3.27), we have V, $\tilde{W}_R$, $\hat{W}_R$, and $E_R\tilde{W}_R$ bounded, and $E_R\tilde{W}_R \in L_2$, which completes proof of (i) and (ii). (iii) follows by applying Lemma 3.1 with $f(t) = E_R(t)\tilde{W}_R(t)$. □

Remark 3.2. *The convergence rate is dependent on the positive constant parameters of* Γ *and the definiteness of* $E_R^T(t)E_R(t)$*, which depends on the location of* N *vertex models defining the convex parameter set.*

Remark 3.3. *Although the adaptive laws (3.15) and (3.18) guarantee* $\sum_{i=1}^{N} \hat{w}_i(t) = 1$*, they do not guarantee that* $w_i(t) \geq 0,\ i = 1, 2, \cdots, N$*.*

To guarantee both of the conditions in (3.5) simultaneously, we apply parameter projection on (3.15a) and (3.18a) in the following section.

3.3.5 Parameter Projection

The constraints in (3.5) are formulated in a compact form by the compact set

$$S = \left\{ \hat{W}_R \in R^{N-1} \mid g(\hat{W}_R) \leq 0 \right\} \tag{3.28}$$

where $g : R^{N-1} \to R$ is the function defined as follows to capture the constraints in (3.5):

$$g(\chi) = -\min \left\{ \chi_1, \cdots, \chi_{N-1}, 1 - \sum_{1}^{N-1} \chi_i \right\}, \tag{3.29}$$

where $\chi = \left[\chi_1, \cdots, \chi_{N-1}\right]$.

We denote S^0, ∂S as the interior and the boundary of S, respectively. $\hat{W}_R(0)$ is chosen to be in S. Applying the gradient projection method, the adaptive law obtained as follow:

$$\dot{\hat{W}}_R = Pr(-\Gamma\ (E_R^T \varepsilon_N + E_R^T E_R \hat{W}_R)), \tag{3.30}$$

where the $Pr(\cdot)$ operator imposes Algorithm 1.

Algorithm 1 Gradient Algorithm with Projection

if $(\hat{W}_R \in S^0)$ or $(\hat{W}_R \in \partial S$ and $\dot{\hat{W}}_R^T \nabla g \leq 0)$ **then**

$\dot{\hat{W}}_R = -\Gamma \ (E_R^T \varepsilon_N + E_R^T E_R \hat{W}_R)$

else

$\dot{\hat{W}}_R = -\ \Gamma \ (E_R^T \varepsilon_N + E_R^T E_R \hat{W}_R)$

$+\Gamma \nabla g \left(\nabla g^T \Gamma \nabla g\right)^{-1} \nabla g^T \ \Gamma \ (E_R^T \varepsilon_N + E_R^T E_R \hat{W}_R)$

end if

The gradient projection method is also adopted in the case of the least-squares as follows:

$$\dot{\hat{W}}_R = Pr(-P \ (E_R^T \varepsilon_N + E_R^T E_R \hat{W}_R)), \tag{3.31a}$$

$$\dot{P} = \begin{cases} \beta P - P E_R^T E_R P & if \ ||P(t)|| \leq R_0, \\ 0 & otherwise \end{cases} \tag{3.31b}$$

where the $Pr(\cdot)$ operator imposes Algorithm 2.

Algorithm 2 Recursive Least Squares with Projection

if $(\hat{W}_R \in S^0)$ or $(\hat{W}_R \in \partial S \ and \ -(P \ \nabla J)^T \nabla g \leq 0)$ **then**

$\dot{\hat{W}}_R = -P \ (E_R^T \varepsilon_N + E_R^T E_R \hat{W}_R)$

else

$\dot{\hat{W}}_R = -\ P \ (E_R^T \varepsilon_N + E_R^T E_R \hat{W}_R)$

$+P \nabla g^T \left(\nabla g P \nabla g^T\right)^{-1} \nabla g \ P \ (E_R^T \varepsilon_N + E_R^T E_R \hat{W}_R)$

end if

Theorem 3.4. *Theorem 3.2 and Theorem 3.3 still hold if the adaptive laws (3.15a) and (3.18a) are replaced with (3.30) and (3.34a), respectively.*

Proof. The proof follows the same rationale and steps as in the proof of Theorem 3.10.1 of [34] □

3.3.6 Discretization of Continuous-Time Adaptive Law

The implementation of an online identifier or controller to physical systems requires a discrete-time design due to digital computers. The design of the discrete-time online identifier can be done using a discrete-time approximation of the proposed continuous-time adaptive laws (3.15) and (3.18) based on state parametric model (3.7) and assume that $z_i(t)$, $\Phi(t)$ are measured at times $t = kT$, where $k = 0, 1, 2, ...$ and T is the sampling period, i.e.,

$$z_i[k] = \Theta_i \Phi[k], \tag{3.32}$$

where $z_i[k] \triangleq z_i[kT]$, $\Phi[k] = \Phi[kT]$. Let discretize $\dot{\hat{W}}_R(t)$ in the continuous adaptive law (3.15) using the Euler backward approximation method, i.e.,

$$\dot{\hat{W}}_R(t) \cong \frac{\hat{W}_R[k] - \hat{W}_R[k-1]}{T}.$$

Then, the discrete form of the gradient adaptive law (3.15) is obtained as

$$\hat{W}_R[k] = -\Gamma_1 \left(E_R^T[k] E_R[k] \ \hat{W}_R[k-1] - E_R^T[k] \varepsilon_N[k] \right) + \hat{W}_R[k-1], \tag{3.33a}$$

$$\hat{w}_N[k] = 1 - \sum_{i=1}^{N-1} \hat{w}_i[k], \tag{3.33b}$$

where $\Gamma_1 = \Gamma T$. The discrete form of the modified RLS adaptive law (3.18) is obtained by following the design procedure [34] as

$$\hat{W}_R[k] = -P[k] \left(E_R^T[k] \varepsilon_N[k] + E_R^T[k] E_R[k] \hat{W}_R[k-1] \right) + \hat{W}_R[k-1], \tag{3.34a}$$

$$P[k] = \begin{cases} \frac{1}{\beta_1} \left(P[k-1] - \frac{P[k-1] E_R^T[k] E_R[k] P[k-1]}{\beta_1 + E_R[k] P[k-1] E_R^T[k]} \right) & if \ ||P[k]|| \leq R_0, \\ 0 & otherwise \end{cases} \tag{3.34b}$$

where $0 < \beta_1 < 1$ is the forgetting factor.

3.4 Proposed Multiple-Model Adaptive Control

We utilize the adaptive scheme developed in Section 3.3 to design an optimal MMAC scheme for polytopic uncertain linear systems. An LQ optimal controller is designed for each identification model in (3.8), which enables the optimal fixed control gains to be off-line computed for all identification models (i.e., all operation conditions) in advance. Then, the adaptive control law is generated by using the proposed blending based multiple-model adaptive scheme in Section 3.3.

Since all designed (A_i, B_i) in (3.8) are fixed and known, an LQ controller gain for each fixed model, K_i, can be computed offline for $i = 1, \cdots, N$. This eliminates the computational expense of online optimal control gain calculation. Assuming that all designed fixed models in (3.8) are controllable or stabilizable, an LQ controller gain, K_i is designed for each model such that $x_p(t)$ goes zero as time t goes infinity. The cost functions are defined as

$$J_i(u_i) = \frac{1}{2}\int_0^\infty x_p^T(t)Qx_p(t) + u_i^T(t)Ru_i(t)dt, \;\; i = 1, \cdots, N; \tag{3.35}$$

where Q is constant symmetric positive semi definite matrix; R is constant symmetric positive definite matrix. The optimal input, $u_i(t)$, is computed as

$$u_i(t) = -R^{-1}B_i^T P_i x_p(t) = -K_i x_p(t) \tag{3.36}$$

where P_i is the positive definite and the solution of the following Algebraic Riccati equation

$$A_i^T P_i + P_i A_i - P_i B_i R^{-1} B_i^T P_i + Q = 0. \tag{3.37}$$

Since the original system (3.1) is an uncertain linear MIMO system and its parameter may not exactly be the same with one of the designed fixed models in (3.8), we propose to blend the control inputs in (3.36) using the estimated weighting parameters $\hat{w}_i$ generated by the adaptive law (3.15a). Then, the proposed adaptive LQ control input for the polytopic uncertain system (3.1) is designed as follow:

$$u(t) = -\sum_i^N \hat{w}_i(t) K_i x_p(t). \tag{3.38}$$

Hence, by (3.5) the following closed-loop system is obtained

$$\begin{aligned}\dot{x}_p(t) &= \left(A_p(\eta) - B_p(\eta)\sum_i^N \hat{w}_i(t)K_i\right)x_p(t), \\ &= \left(A_p(\eta) - \sum_i^N w_i(t)B_i \ \sum_i^N \hat{w}_i(t)R^{-1}B_i^T P_i\right)x_p(t),\end{aligned} \tag{3.39}$$

Assumption 3.2. *$\hat{A} - \hat{B}\hat{K}$ is Hurwitz for any time instant.*

The proposed optimal MMAC scheme is shown in Fig.3.1.

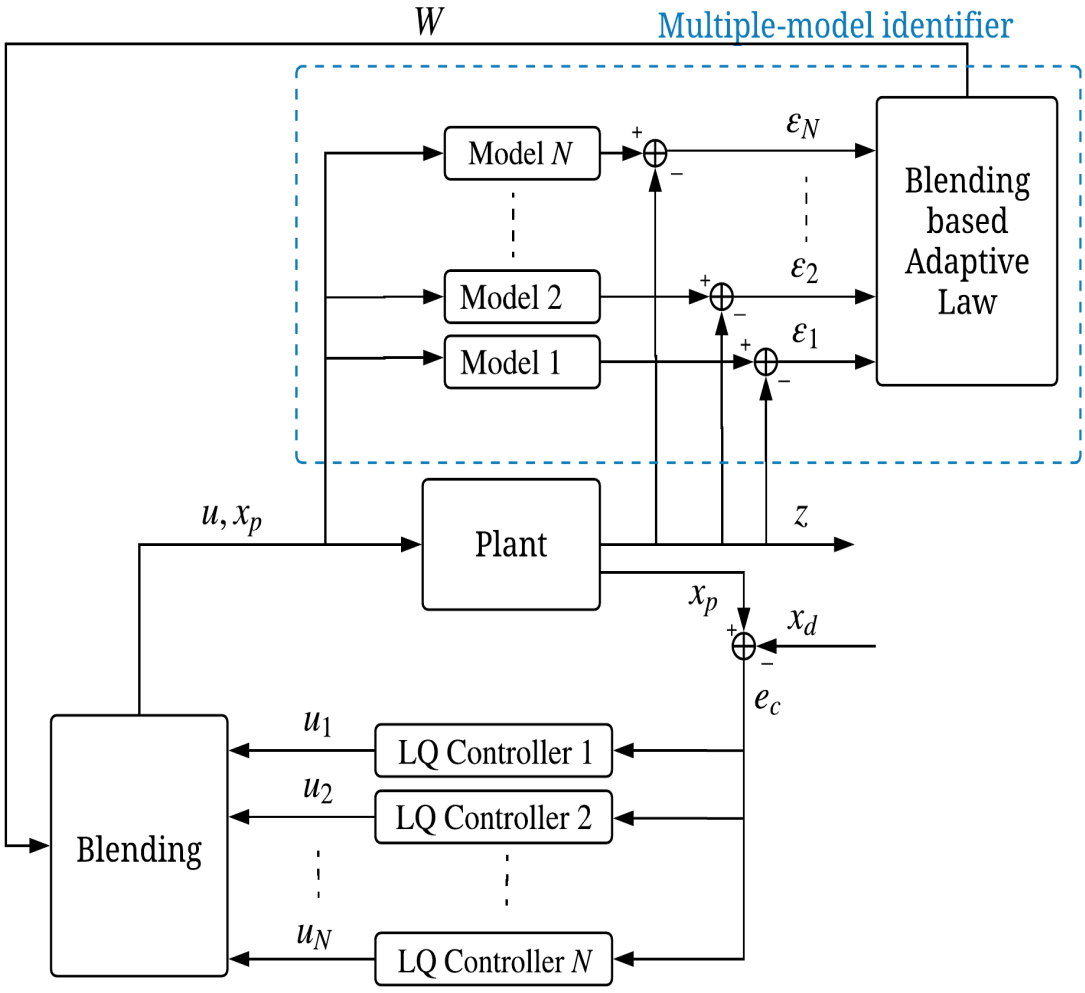

Figure 3.1: Blending based optimal MMAC scheme.

3.4.1 Stability Analysis

The stability of the closed-loop plant (3.39) is guaranteed by the following theorem under Assumption 3.2.

Theorem 3.5. *The adaptive control scheme (3.9) ,(3.12), (3.15), (3.38) guarantees that all signals in the closed-loop plant (3.39) are bounded and the state x_p converges to zero asymptotically with time under Assumption 3.2.*

Proof. To establish the stability of the closed-loop system (3.39), we rewrite (3.1) by adding and subtracting $\hat{A}x_p(t) + \hat{B}u(t)$ as

$$\dot{x}_p(t) = \hat{A}x_p(t) + \hat{B}u(t) + \tilde{A}x_p(t) + \tilde{B}u(t), \tag{3.40}$$

where

$$\begin{aligned}
\hat{A} =& \sum_i^N \hat{w}_i(t)A_i, \quad \hat{B} = \sum_i^N \hat{w}_i(t)B_i, \\
\tilde{A} =& \hat{A} - A_p(\eta) = \sum_i^N \tilde{w}_i(t)A_i, \\
\tilde{B} =& \hat{B} - B_p(\eta) = \sum_i^N \tilde{w}_i(t)B_i.
\end{aligned}$$

The closed-loop system (3.39) can be re-expressed using (3.38) and (3.40) by

$$\dot{x}_p(t) = (\hat{A} - \hat{B}\hat{K})x_p(t) + \tilde{A}x_p(t) + \tilde{B}u(t), \tag{3.41}$$

where $\hat{K} = \sum_i^N \hat{w}_i(t)K_i$. In this case, the exponential stability of the nominal part ((3.41) with $\tilde{A} \approx 0$ and $\tilde{B} \approx 0$) is established since $(\hat{A} - \hat{B}\hat{K})$ is Hurwitz.

In the next step, the boundedness of the inputs due to the parameter estimation in (3.41) is established. The estimation error equation is

$$\begin{aligned}
\xi(t) =& z(t) - \sum_i^N \hat{w}_i(t)\Theta_i\phi(t) = \sum_i^N \tilde{w}_i(t)\Theta_i\phi(t) \\
=& \frac{1}{s+\lambda}(\tilde{A}x_p(t) + \tilde{B}u(t)).
\end{aligned} \tag{3.42}$$

Operating both sides of (3.42) with $s+\lambda$ and using the property of differentiation, i.e., $s(xy) = \dot{x}y + x\dot{y}$ where s is the differential operator, the following is obtained:

$$(s+\lambda)\xi(t) = (\tilde{A}x_p(t) + \tilde{B}u(t)) + \frac{1}{s+\lambda}(\dot{\tilde{A}}x_p(t) + \dot{\tilde{B}}u(t)). \tag{3.43}$$

Therefore,

$$(\tilde{A}x_p(t) + \tilde{B}u(t)) = (s+\lambda)\xi - \frac{1}{s+\lambda}(\dot{\tilde{A}}x_p(t) + \dot{\tilde{B}}u(t)), \tag{3.44}$$

which is substituted in (3.41) to obtain

$$\dot{x}_p(t) = (\hat{A} - \hat{B}\hat{K})x_p(t) + (s+\lambda)\xi(t) - \frac{1}{s+\lambda}(\dot{\tilde{A}}x_p(t) + \dot{\tilde{B}}u(t)). \tag{3.45}$$

If we define $\bar{\xi}(t) = x_p(t) - \xi(t)$, (3.45) becomes

$$\begin{aligned} \dot{\bar{\xi}}(t) =& (\hat{A} - \hat{B}\hat{K})\bar{\xi}(t) + (\lambda I + \hat{A} - \hat{B}\hat{K})\xi(t) \\ & - \frac{1}{s+\lambda}(\dot{\tilde{A}}x_p(t) + \dot{\tilde{B}}u(t)), \\ x_p(t) =& \bar{\xi} + \xi. \end{aligned} \tag{3.46}$$

Equation (3.46) has a homogeneous part that is exponentially stable and an input that is small in the sense of $\xi, \dot{\tilde{A}}, \dot{\tilde{B}} \in L_2$, where the boundedness of $\dot{\tilde{A}}, \dot{\tilde{B}}$ follows from the boundedness of $\dot{\tilde{W}}$, guaranteed by the adaptive law (3.15a).

To analyse (3.46), the properties of the $L_{2\delta}$ norm, denoted by $\|\cdot\|_{2\delta}$, is used [35].

The fictitious normalizing signal m_f satisfies

$$m_f^2(t) = 1 + \|x_p(t)\|_{2\delta}^2 + \|u(t)\|_{2\delta}^2 \leq 1 + c_1\|x_p(t)\|_{2\delta}^2, \tag{3.47}$$

for some $c_1,\ \delta > 0$ because of the control law (3.38) and the fact that $\hat{B}, \hat{P} \in L_\infty$, where

$$\hat{P} = \sum_i^N \hat{w}_i P_i.$$

Because $x_p(t) = \bar{\xi}(t) + \xi(t)$, we have $\|x_p(t)\|_{2\delta} \leq \|\bar{\xi}(t)\|_{2\delta} + \|\xi(t)\|_{2\delta}$, which is used in (3.47) to obtain

$$m_f^2(t) \leq 1 + c_2\|\bar{\xi}(t)\|_{2\delta}^2 + c_2\|\xi(t)\|_{2\delta}^2 \tag{3.48}$$

for some $c_2 > 0$. From (3.46), for $c_3 > 0$ we have

$$\|\bar{\xi}(t)\|_{2\delta}^2 \leq c_3\|\xi(t)\|_{2\delta}^2 + c_3\|\dot{\tilde{A}}\bar{x}_p(t)\|_{2\delta}^2 + c_3\|\dot{\tilde{B}}\bar{u}(t)\|_{2\delta}^2, \tag{3.49}$$

where

$$\bar{x}_p(t) = \frac{1}{s+\lambda}x_p(t), \quad \bar{u}(t) = \frac{1}{s+\lambda}u(t).$$

By the properties of the $L_{2\delta}$ norm, it can be shown that m_f bounds from above $\bar{x}_p(t), \bar{u}$ and therefore it follows from (3.48) and (3.49) that

$$m_f^2(t) \leq 1 + c_3\|\xi(t)m_f(t)\|_{2\delta}^2 + c_3\|\dot{\tilde{A}}m_f(t)\|_{2\delta}^2 + c_3\|\dot{\tilde{B}}m_f(t)\|_{2\delta}^2, \tag{3.50}$$

which implies that

$$m_f^2(t) \leq 1 + c_3\int_0^t e^{-\delta(t-\tau)}g^T(\tau)g(\tau)\ m_f^2(\tau)d\tau, \tag{3.51}$$

where

$$g^Tg = \xi^T\xi + \|\dot{\tilde{A}}\|_{2\delta}^2 + \|\dot{\tilde{B}}\|_{2\delta}^2.$$

Since $\xi, \dot{\tilde{A}}, \dot{\tilde{B}} \in L_2$ implies that $g \in L_2$, the boundedness of m_f follows by applying the Bellman-Gronwall Lemma.

Now, $m_f \in L_\infty$ implies that $\bar{x}_p, \bar{u}$ and thus, $\phi \in L_\infty$. By the fact that $\xi, \dot{\tilde{A}}, \dot{\tilde{B}}, \bar{x}_p, \bar{u} \in L_\infty$, we establish that $\bar{\xi} \in L_\infty$ from (3.46), which implies that $x_p \in L_\infty$, and therefore, all signals in closed-loop system (3.41).

We proceed to establish $x_p \to 0$ as $t \to \infty$. Using (3.46), it is established that $\bar{\xi} \in L_2$ which together with $\xi \in L_2$ imply that $x_p = \bar{\xi} + \xi \in L_2$. As (3.45) implies that $\dot{x}_p \in L_\infty$, it follows from Lemma 3.1 that $x_p(t) \to 0$ as $t \to \infty$. □

3.5 Summary and Remarks

In this chapter, two blending based multiple-model online parameter identification schemes for MIMO systems with polytopic uncertain parameters have been developed including gradient and RLS based identification schemes. The proposed schemes use multiple linear parametric fixed models in the system identifier design. Each model represents different extreme operation condition by using different system parameters. In other words, each model is an extreme point (a vertex) of a convex polytope which is a compact convex set with a finite number of extreme points. Thus, the designed multiple fixed models guarantee that the uncertain system lies in the convex hull of the design multiple fixed model.

Multiple linear fix models approach provides a more comprehensive description of Nonlinear and/or Time-varying linear systems. For the given same input and state vectors, discrepancies between the responses of designed multiple models and the response of uncertain system are continuously observed. These discrepancies indicate how each designed model is close to actual model in terms of system parameters based on the Certainty Equivalence principle. Thus, these discrepancies and the convexity property are used to blend the designed models using a weighting vector for accurate estimation of the uncertain system. Estimation of the weighting vectors can be achieved by gradient method.

The proposed adaptive schemes provide fast adaptation for even uncertain LTV systems without reinitialisation. The proofs of asymptotic stability of the developed identification schemes for linear time-invariant MIMO systems were presented. We apply parameter projection on the proposed adaptive schemes to guarantee that the convexity condition is satisfied during adaptation especially for fast transients in system parameters. We also provide discrete version of the proposed adaptive schemes to be used in MPC control design later. Lastly, we utilize the proposed adaptive schemes to design an optimal MMAC scheme for linear systems with polytopic parameter uncertainties. An LQ optimal controller is designed for each identification model, which enables the optimal fixed control gains to be off-line computed for all identification models in advance. All LQ controllers utilize the same design parameters Q, R. The adaptive control law is generated by using the proposed blending based multiple-model adaptive scheme. Furthermore, the stability analysis of the proposed optimal MMAC scheme is provided.

Chapter 4

Multiple-Model Adaptive Vehicle Motion Control

In this chapter, the proposed optimal MMAC algorithm is applied to motion control of an uncertain lateral vehicle dynamics for validation.

4.1 Dynamic Model with Polytopic Parameter Uncertainties

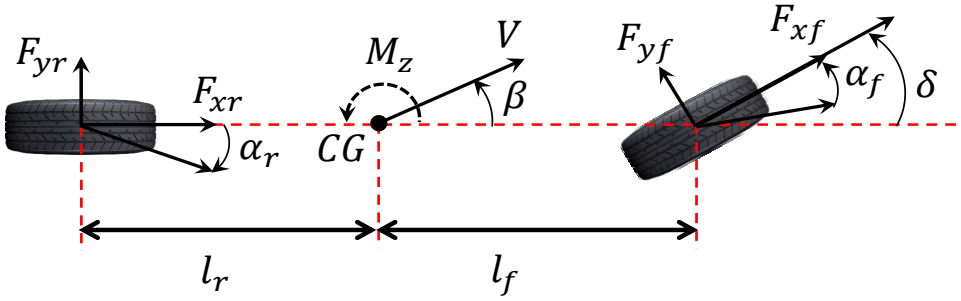

Figure 4.1: Bicycle model.

For vehicle lateral stability and handling control, the vehicle sideslip angle β and the yaw rate r are critical as stated in Section 2.1. In this section the lateral dynamics of a ground

vehicles with the capability of generating differential torque is presented for control and simulation purpose.

The lateral dynamic equations of the 2-DOF bicycle model, lateral and yaw motion, in Fig. 4.1 can be written as:

$$\dot{v}_y = -v_x r + \frac{1}{m}\left[F_{yf}\cos\delta + F_{yr} + F_{xf}\sin\delta\right), \tag{4.1}$$

$$\dot{r} = \frac{1}{I_z}\left(l_f F_{yf}\cos\delta - l_r F_{yr} + l_f F_{xf}\sin\delta\right) + \eta_x \frac{M_z}{I_z}, \tag{4.2}$$

where M_z, F_{xf}, F_{yf}, and F_{yr} are yaw moment about z-axis, front longitudinal, front lateral and rear lateral tire forces. η_x parametrizes uncertain time-variation in longitudinal tire force capacities, which has direct effect on the yaw moment M_z on vehicle CG. The uncertain front lateral and rear lateral tire forces computed by

$$\begin{aligned} F_{yf} &= \eta_f C_f \alpha_f, \\ F_{yr} &= \eta_r C_r \alpha_r, \end{aligned} \tag{4.3}$$

where C_f, C_r are total nominal tire cornering stiffness coefficients for front and rear tires. η_f, η_r parametrize the uncertain time-variation in cornering stiffness in front and rear tires, respectively; α_f, α_r are the front and rear tire slip angles, respectively, and for small angles computed as

$$\begin{aligned} \alpha_f &= \left[\delta - \left(\frac{v_y + r l_f}{v_x}\right)\right], \\ \alpha_r &= \left(\frac{r l_r - v_y}{v_x}\right). \end{aligned} \tag{4.4}$$

The sideslip angle is defined as the angle between the vehicle lateral velocity and the longitudinal velocity

$$\beta = \frac{v_y}{v_x}. \tag{4.5}$$

By rearranging and simplifying (4.1) -(4.5), the state-space model of the uncertain lateral dynamics is expressed in the following state-space form:

$$
\begin{aligned}
\dot{x}_p(t) =& A_p(\eta)x_p(t) + B_p(\eta)u(t),\\
A_p(\eta) =& A_{p1} + \eta_f A_{p2} + \eta_r A_{p3},\\
B_p(\eta) =& \eta_f B_{p1} + \eta_x B_{p2},
\end{aligned}
\tag{4.6}
$$

where $x_p(t) = [\beta, r]^T$, $u(t) = [\delta, M_z]^T$, $\eta = [\eta_f, \eta_r, \eta_x]^T$ are the vehicle system state, input, and uncertain parameter vectors, respectively; δ is the total steering angle of the front wheels including driver command δ_d and corrective steering control input δ_c (i.e., $\delta = \delta_d + \delta_c$);

$$
\begin{aligned}
A_{p1} &= \begin{bmatrix} 0 & -1 \\ 0 & 0 \end{bmatrix}, \quad A_{p2} = \begin{bmatrix} \frac{-C_f}{mv_x} & \frac{l_f C_f}{mv_x^2} \\ \frac{-l_f C_f}{I_z} & \frac{-l_f^2 C_f}{I_z v_x} \end{bmatrix},\\
A_{p3} &= \begin{bmatrix} \frac{-C_r}{mv_x} & \frac{l_r C_r}{mv_x^2} \\ \frac{l_r C_r}{I_z} & \frac{-l_r^2 C_r}{I_z v_x} \end{bmatrix}, \quad B_{p1} = \begin{bmatrix} \frac{C_f}{mv_x} & 0 \\ \frac{l_f C_f}{I_z} & 0 \end{bmatrix},\\
B_{p2} &= \begin{bmatrix} 0 & 0 \\ 0 & \frac{1}{I_z} \end{bmatrix}.
\end{aligned}
\tag{4.7}
$$

The uncertainty ranges of the parameters in η are assumed to be known as

$$
\underline{\eta}_f < \eta_f < \bar{\eta}_f, \quad \underline{\eta}_r < \eta_r < \bar{\eta}_r, \quad \underline{\eta}_x < \eta_x < \bar{\eta}_x. \tag{4.8}
$$

Note that although the system in (4.6) is linear in the state variables, it is a nonlinear system with respect to unknown parameter variations which are represented by η.

4.2 Multiple-Model Identifier Design

Since there are three uncertain parameters, we need 2^3 polytopes, i.e., 8 fixed models (A_i, B_i) to be designed using the constant known bound values of uncertain parameters in (4.8) such that

$$
(A_p(\eta), B_p(\eta)) \in \mathbf{Co}\{(A_i, B_i) : i = 1, \cdots, 8\}. \tag{4.9}
$$

Assuming that the states, side-slip angle $\beta(t)$ and yaw rate $r(t)$, are perfectly measured using or computed for any instant using the fusion of vehicle on-board sensors, including inertia measurement unit (IMU), steering wheel angle, wheel speed sensors, Global positioning system (GPS), etc., the identification error in (3.9) is defined as

$$\varepsilon_i(t) = z(t) - \Theta_i \Phi(t), \quad i = 1, 2, \cdots, 8, \tag{4.10}$$

with

$$\begin{aligned}
\Theta_i &= \begin{bmatrix} A_i & B_i \end{bmatrix}, \\
\Phi(t) &= \frac{1}{s+\lambda} \begin{bmatrix} \beta & r & \delta & M_z \end{bmatrix}^T, \\
z(t) &= \frac{s}{s+\lambda} \begin{bmatrix} \beta \\ r \end{bmatrix}.
\end{aligned}$$

Thus, we obtained the following equation

$$\begin{aligned}
&E_R(t) W_R(t) = -\varepsilon_8(t), \\
&E_R(t) = \begin{bmatrix} \varepsilon_1(t) - \varepsilon_8(t) & \cdots & \varepsilon_7(t) - \varepsilon_8(t) \end{bmatrix} \\
&W_R(t) = \begin{bmatrix} w_1(t) & w_2(t) & \cdots & w_7(t) \end{bmatrix}^T,
\end{aligned} \tag{4.11}$$

where the estimate $\hat{W}_R(t)$ of $W_R(t)$ is continuously generated by either gradient based adaptive law (3.30) or RLS based adaptive law (3.34) and the weight of the last model, Model 8, can be computed by $\hat{w}_8(t) = 1 - \sum_1^7 \hat{w}_i(t)$.

4.3 LQ Optimal Robust MMAC Design

Multiple model LQ controllers are designed for the tracking problem of a vehicle under uncertain time-varying operation conditions. First, the desired response of a vehicle under critical conditions are defined. By these defined state trajectories, the trajectory tracking problem for the vehicle is converted into regulation problem. Then, for each designed model (A_i, B_i) in (4.9) (i.e., each operation condition), an LQ controller is designed. The control gains for LQ controllers of fixed models are calculated off-line in advance, which save the time spent for the computation of optimum control input in corresponding operation condition. The overall diagram of the proposed LQ based MMAC is shown in Fig. 4.2.

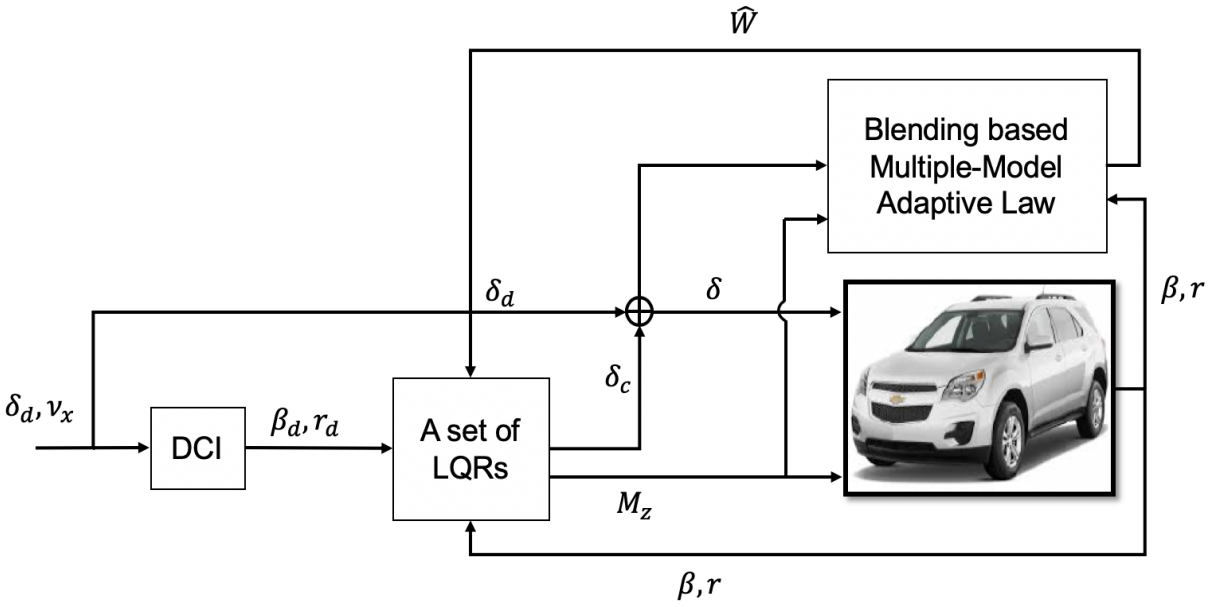

Figure 4.2: Proposed overall LQ based MMAC diagram.

The objective of tracking control is to improve vehicle handling performance and maintaining stability during cornering manoeuvres, i.e., the vehicle is expected to achieve the desired yaw rate r_d while maintaining the closeness of side-slip angle to zero, i.e., $\beta_d = 0$. The desired vehicle yaw rate is defined depending on the steering angle, vehicle velocity and vehicle geometry [47] as follows:

$$r_d = \frac{v_x}{L + k_{us}\ v_x^2}\delta_d, \tag{4.12}$$

where δ_d, L, g are the steering angle of the front wheels commanded by driver, the vehicle wheel base, the gravitational constant, respectively, and k_{us} is the desired understeer gradient.

For fixed models (A_i, B_i) in (4.9), we design LQ controllers. To this end, the tracking problem is converted into a regulation problem by defining the control error as

$$e_c(t) = x_d(t) - x_p(t), \quad x_d(t) = \begin{bmatrix}\beta_d & r_d\end{bmatrix}^T, \tag{4.13}$$

where $x_d(t)$ is the desired state trajectory including desired yaw-rate r_d and side-slip angle β_d. Now, we have the following general LQR problem for each designed Model i:

$$\dot{e}_c(t) = A_i e_c(t) + B_i u_i(t),\ e_c(t_0) = 0,\ i = 1, \cdots, 8. \tag{4.14}$$

The optimum controller gain for each fixed model, K_i is computed offline based on the bound values of the uncertain parameter vector η before the operation. For the LTI error dynamics in (4.14), the cost functions are defined as

$$J(e_c, u_i) = \frac{1}{2}\int_0^\infty e_c^T(t) Q e_c(t) + u_i^T(t) R u_i(t) dt, \quad i = 1, \cdots, 8, \tag{4.15}$$

where $e_c \in R^n$, $u \in R^r$, are state and input vector; $Q \in R^{n\times n}$ is symmetric positive semi definite matrix; $R \in R^{r\times r}$ is symmetric positive definite matrix. Then the optimal input for each model, $u_i(t)$, is computed as

$$u_i(t) = -R^{-1} B_i^T P_i x(t) = -K_i e_c(t), \tag{4.16}$$

where P_i is the positive definite and the solution of the following Riccati equation

$$A_i^T P_i + P_i A_i - P_i B_i R^{-1} P_i + Q = 0. \tag{4.17}$$

For the discrete time case, the optimal input $u_i[k]$ is

$$u_i[k] = -R^{-1} B_i^T P_i\ e_c[k] = -K_i\ e_c[k] \tag{4.18}$$

where P_i is the solution of discrete time Riccati equation

$$A_i^T P_i A_i - A_i^T P_i B_i (B_i^T P_i B_i + R)^{-1} B_i^T P_i A_i + Q = P_i. \tag{4.19}$$

Thus, the optimal input, $u_i[k]$, for each model is computed as

$$u_i[k] = -R_i^{-1} B_i^T P_i\ e_c[k] = -K_i\ e_c[k],\ i = 1, \cdots, 8. \tag{4.20}$$

The control inputs (4.20) are blended to obtain the overall control input to be applied to the lateral vehicle dynamics (4.6) as follow:

$$u_i[k] = -\sum_{i=1}^{8} \hat{w}_i[k]\ K_i\ e_c[k]. \tag{4.21}$$

4.4 Simulations

In this section, simulation tests are performed on the proposed multiple model approach to identify the uncertain time-varying lateral vehicle dynamics in Simulink environment. The parameters of vehicle used in the simulation are $m = 1140\ kg$, $I_z = 1020\ kgm^2$, $C_f = 86849\ N/rad$, $C_r = 90950\ N/rad$, $l_f = l_r = 1.165\ m$.

For the simulations, it is assumed that $\eta = \begin{bmatrix}\eta_f & \eta_r & \eta_x\end{bmatrix}^T$ are changing within certain ranges as stated in (4.8) during operation. These lower and upper bounds are determined as $\underline{\eta}_f = \underline{\eta}_r = \underline{\eta}_x = 0.1$, and $\bar{\eta}_f = \bar{\eta}_r = \bar{\eta}_x = 1.3$, respectively.

The design parameters of fixed LQ controllers are selected the same for all fixed models (operation condition) as $Q = diag([4, 10^4])$, $R = diag([10^4, 1])$. The tuning parameters, Γ in (3.15a), P_0, R_0, and β in (3.18b) are $diag([1, 1, \cdots, 1])$, $diag([2, 2, \cdots, 2])$, 0.01, and 0.96, respectively. The value of λ in (3.7) is 5. The operational vehicle speed is constant at $v_x = 100\ kph$. Lastly, for performance comparison purpose, a single model based LQ controller with the same design parameters (Q, R) is designed for the constant values $\eta_f = \eta_r = \eta_x = 1$.

The simulations are performed under two cases including noise-free state measurement and noisy state measurement. For the latter case, the white noises $N(0, 10^{-3})$, $N(0, 10^{-4})$ with the sample time $T_s = 0.001$ are added to system states β, r, respectively. The driver steering command δ_d and the drastic variation of uncertain parameters of the vector (η) during maneuver are shown in Fig.4.3 for the both cases.

Even though, the uncertain parameters in Fig.4.3, and hence the plant parameters drastically change during the harsh maneuver, the estimated values generated by the RLS and gradient identification schemes achieve to converge to their true values within a short time for noise-free state case and noisy state case as depicted in Figs. 4.6, 4.8, 4.12, 4.14. The estimated entries of the plant matrices in these Figures are computed using the estimated weighting parameters, shown in Figs. 4.7, 4.9, 4.13, 4.15, respectively. Furthermore, the developed MMAC scheme using the proposed gradient and RLS schemes achieve better tracking performance compared to single-model based LQ controller as seen in Figs. 4.4, 4.10.

Although the tracking performances of gradient and RLS based MMAC are similar for both noise-free states and noisy states, RLS based parameter identification scheme demonstrates faster and smoother convergence to true values of uncertain parameters during transition (i.e., while the uncertain parameters are changing) as depicted in Figs 4.6, 4.8, 4.12, 4.14.

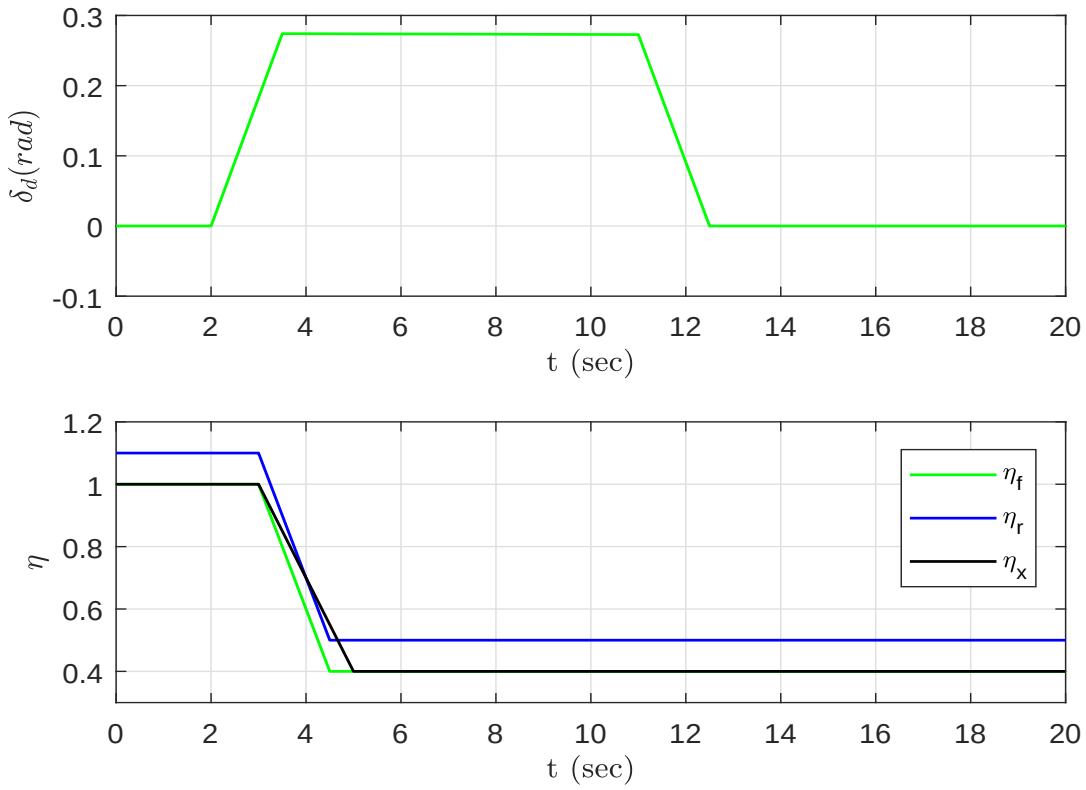

Figure 4.3: Driver input and time-varying unknown parameters.

4.4.1 Results for Noise-free System States

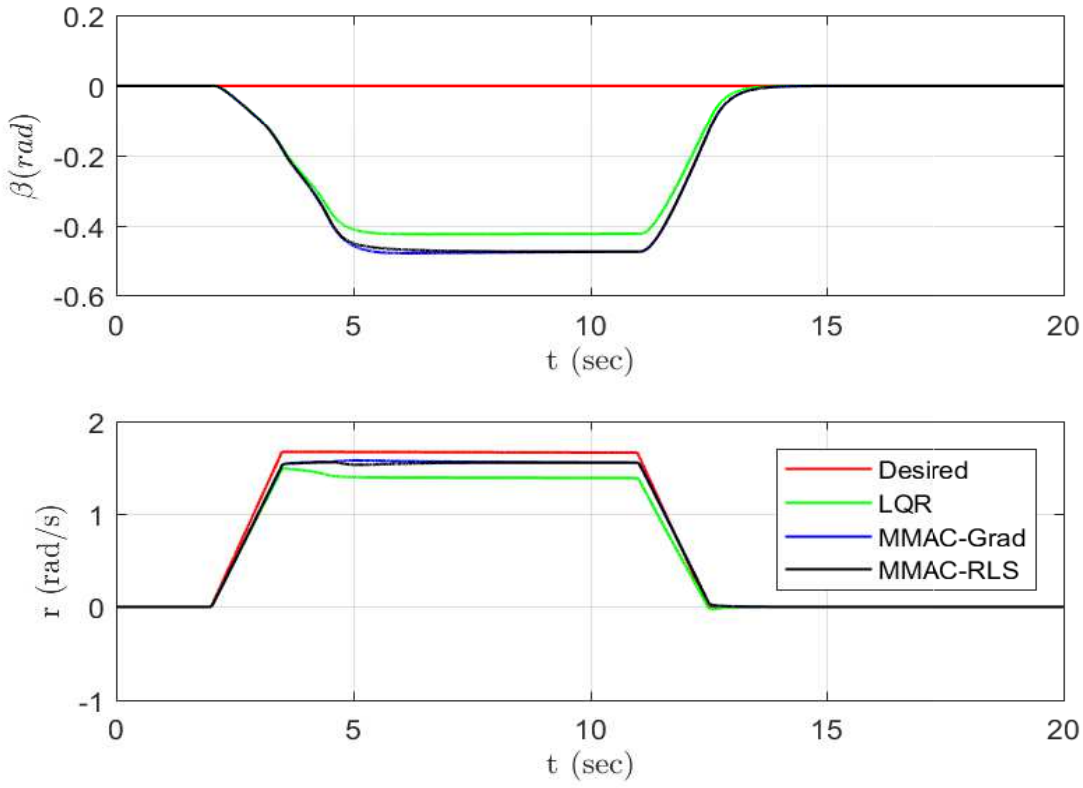

Figure 4.4: States

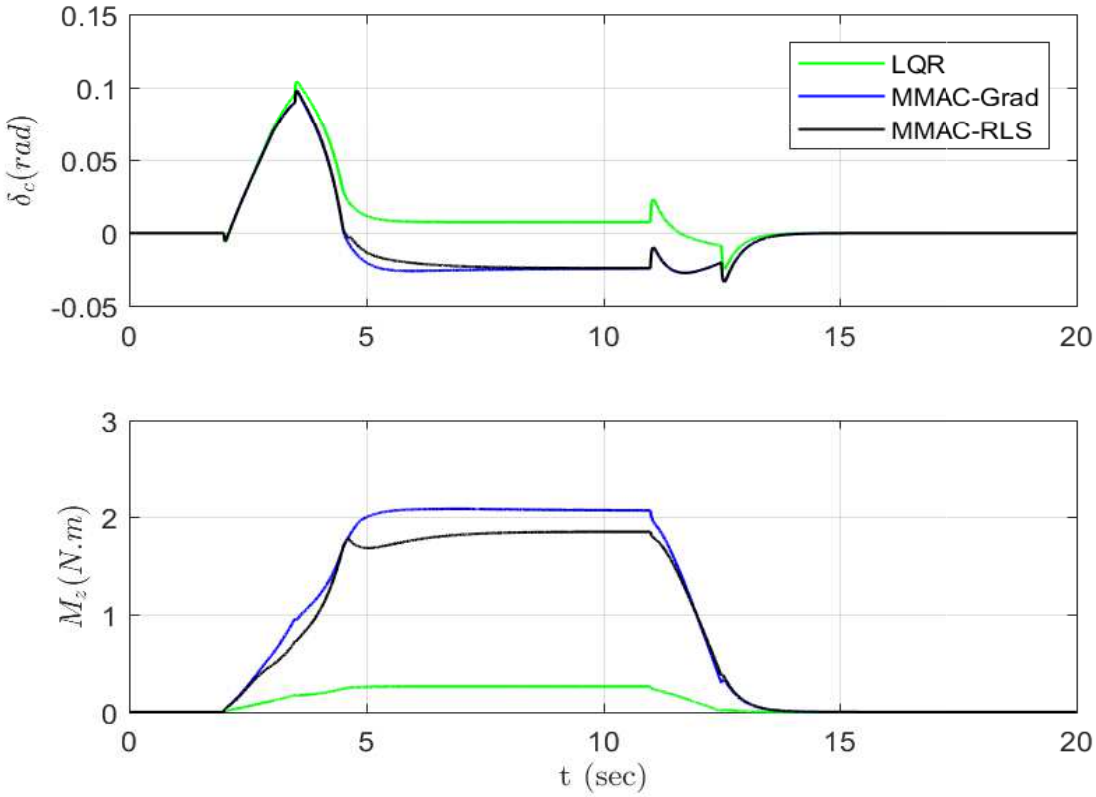

Figure 4.5: Control inputs

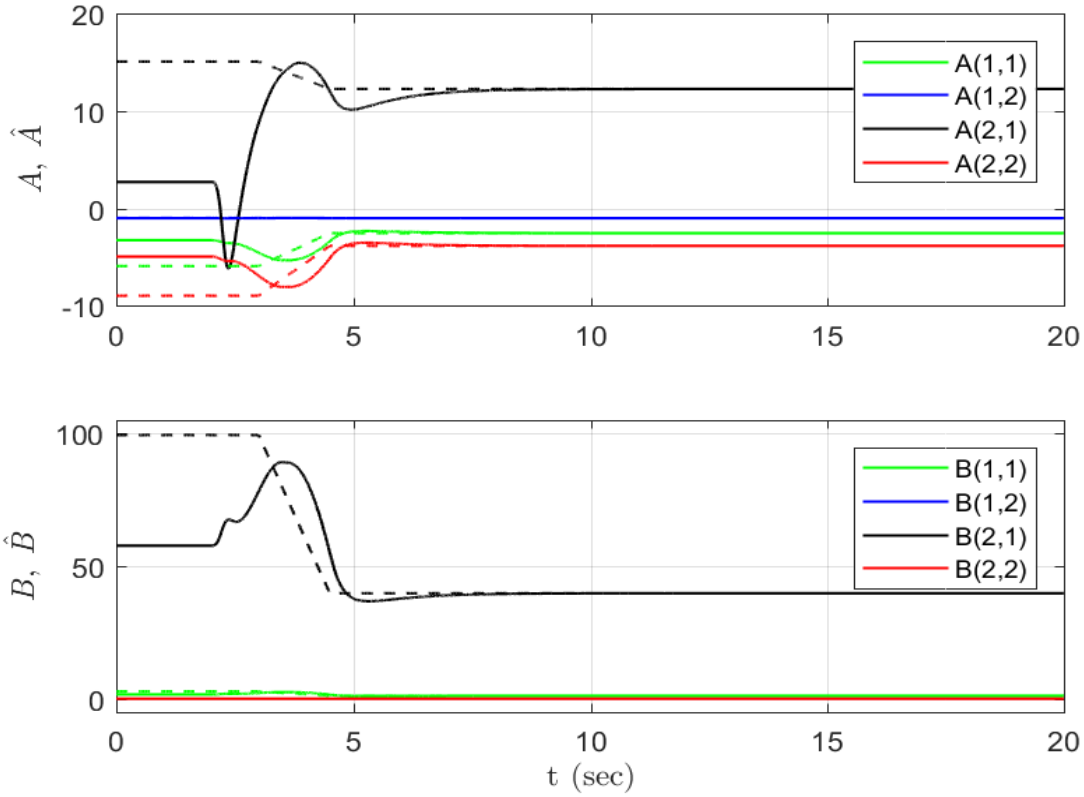

Figure 4.6: Estimated plant matrices

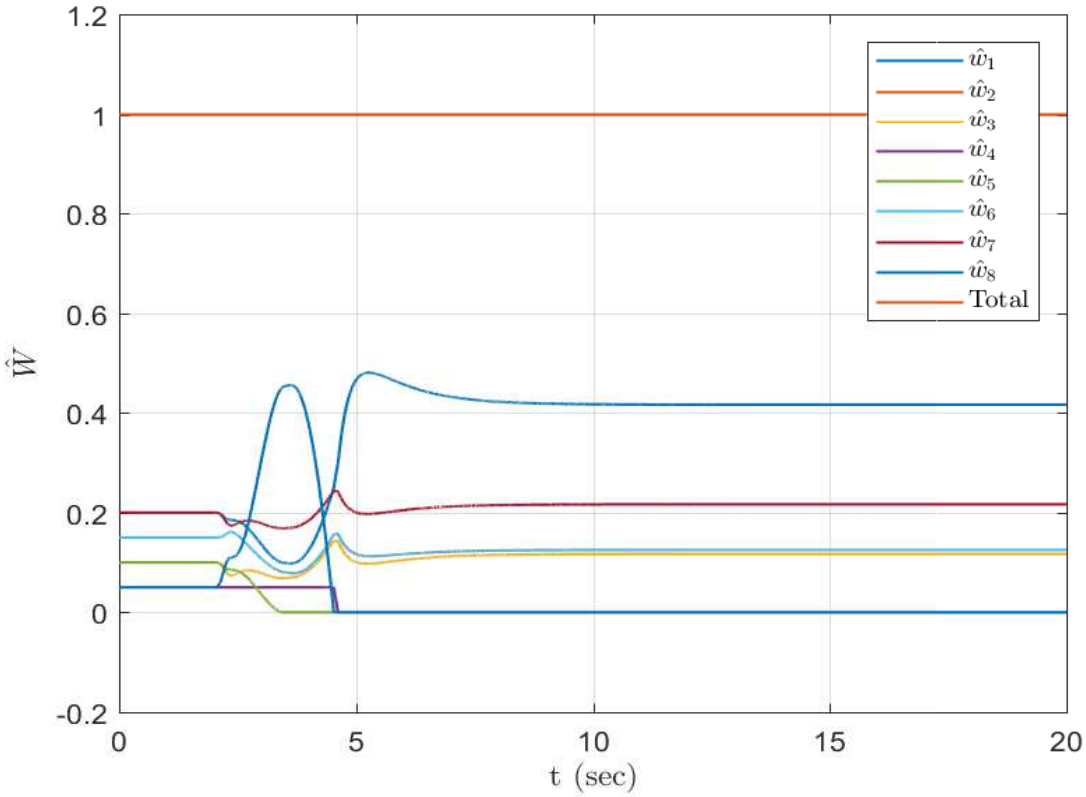

Figure 4.7: Estimated weighted parameters

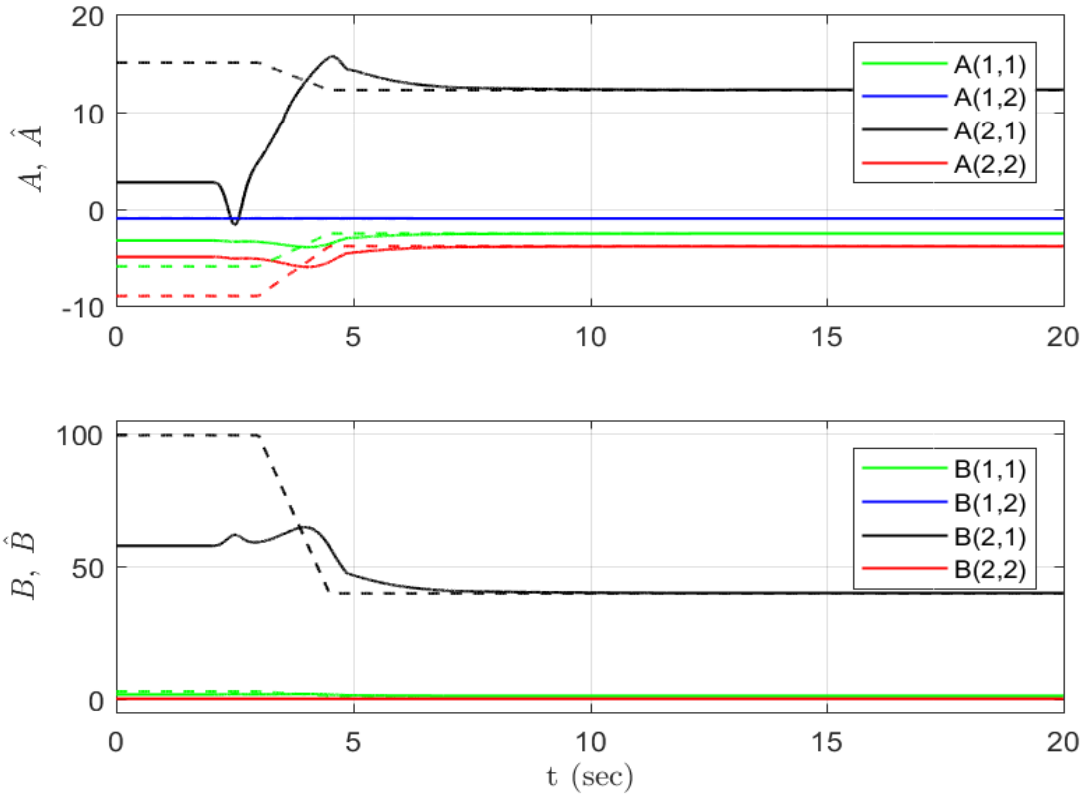

Figure 4.8: Estimated plant matrices

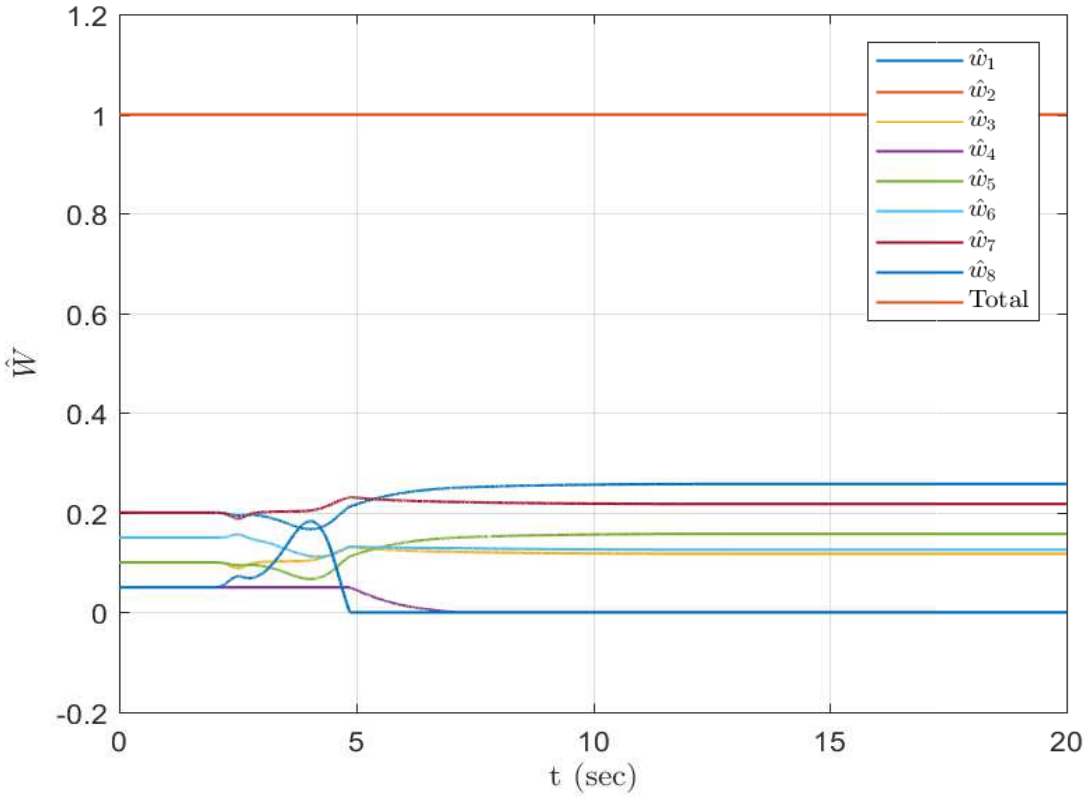

Figure 4.9: Estimated weighted parameters

4.4.2 Results for Noisy System States

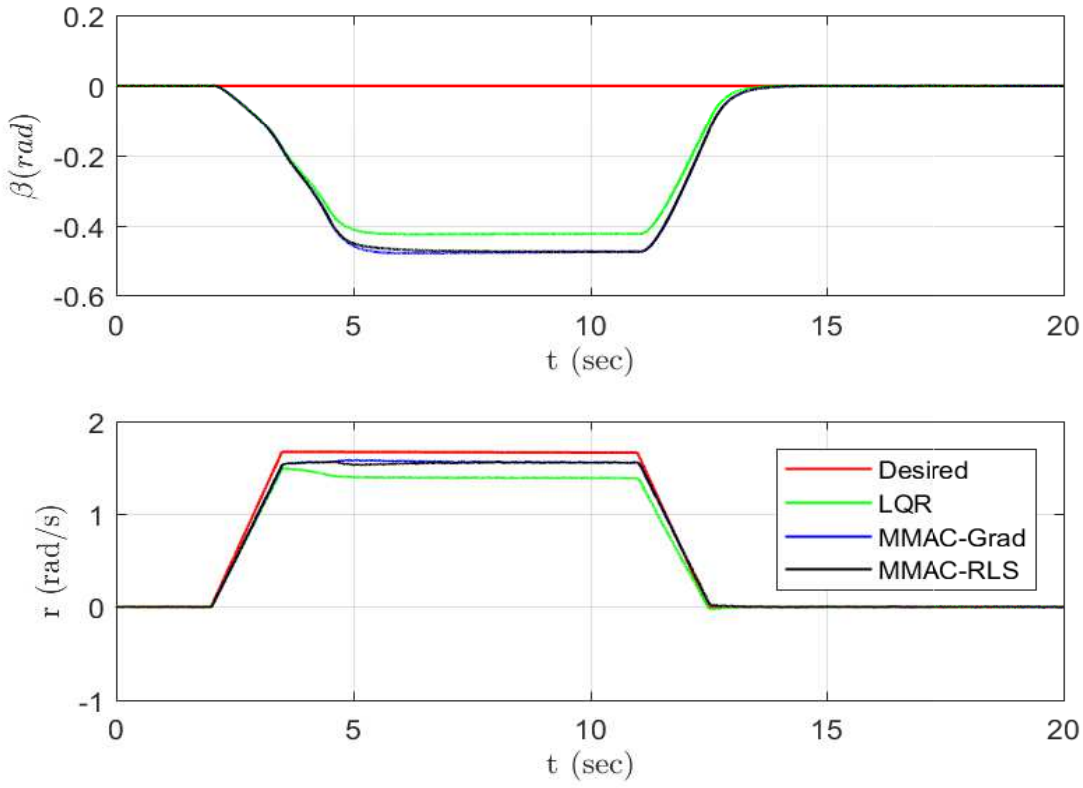

Figure 4.10: States

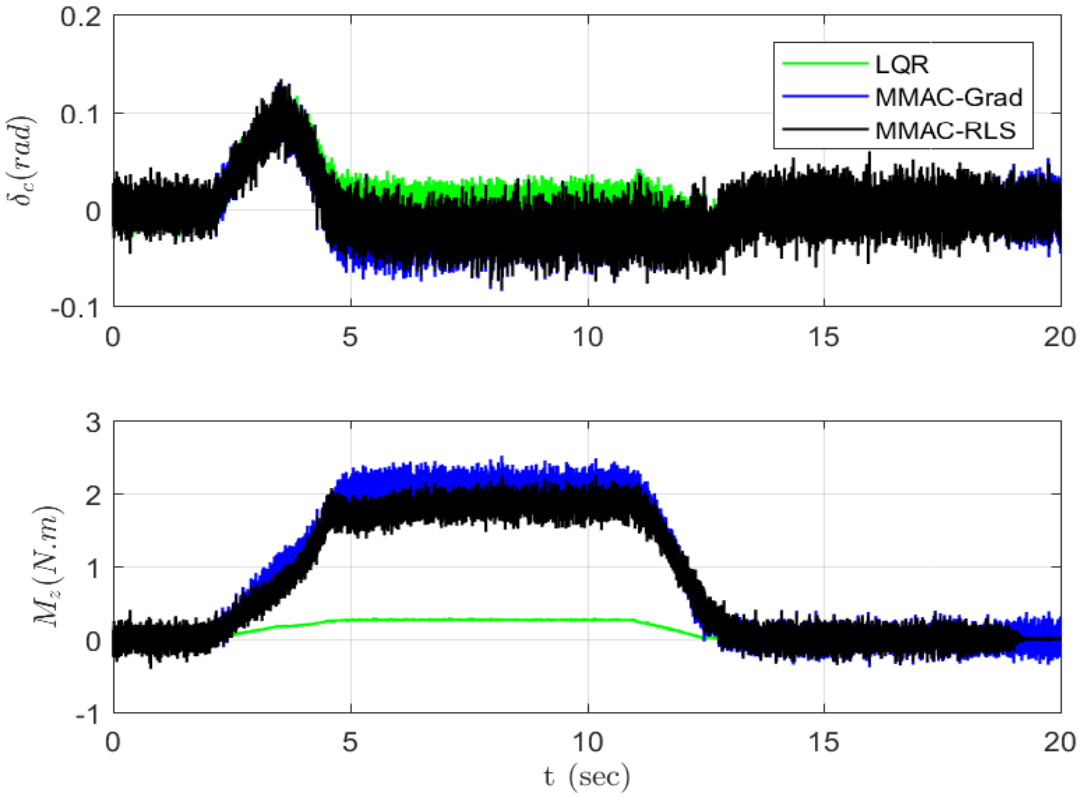

Figure 4.11: Control inputs

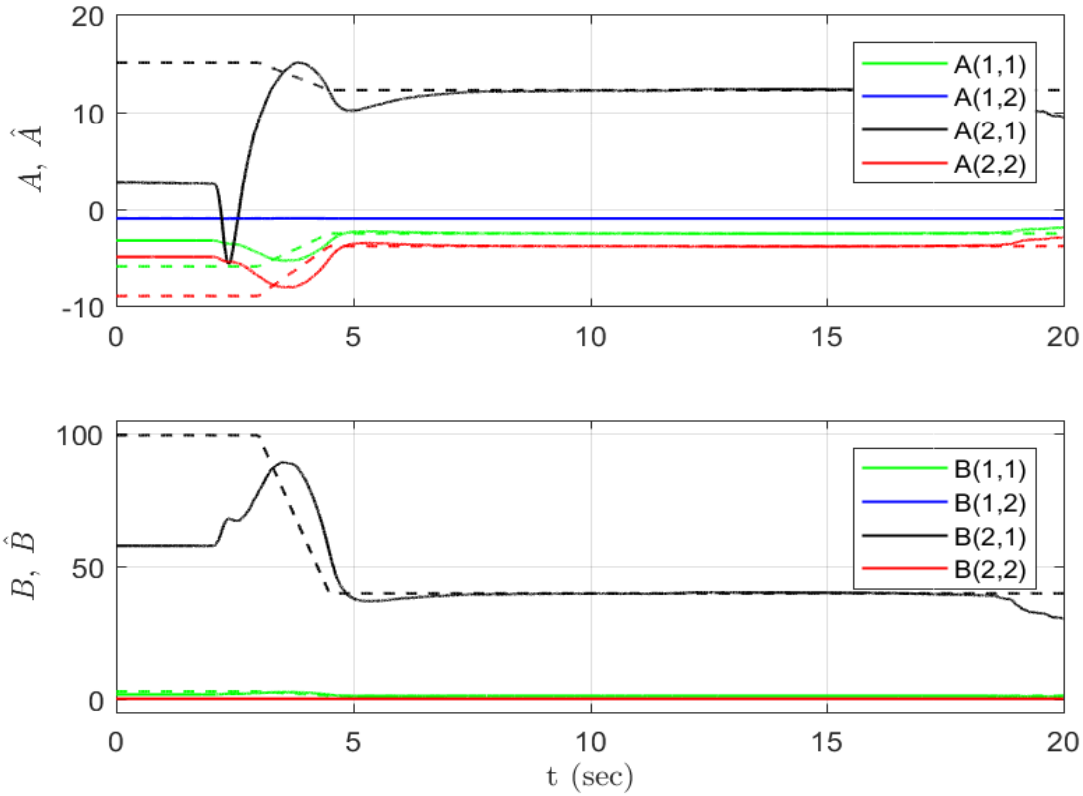

Figure 4.12: Estimated plant matrices

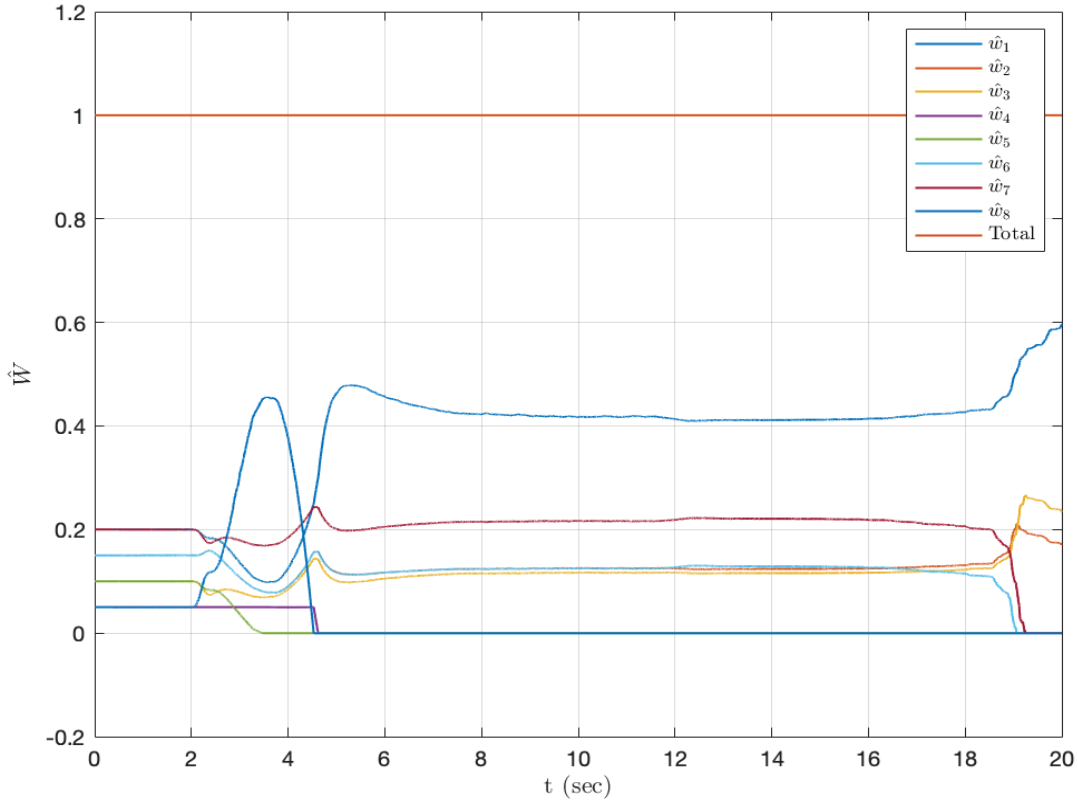

Figure 4.13: Estimated weighted parameters

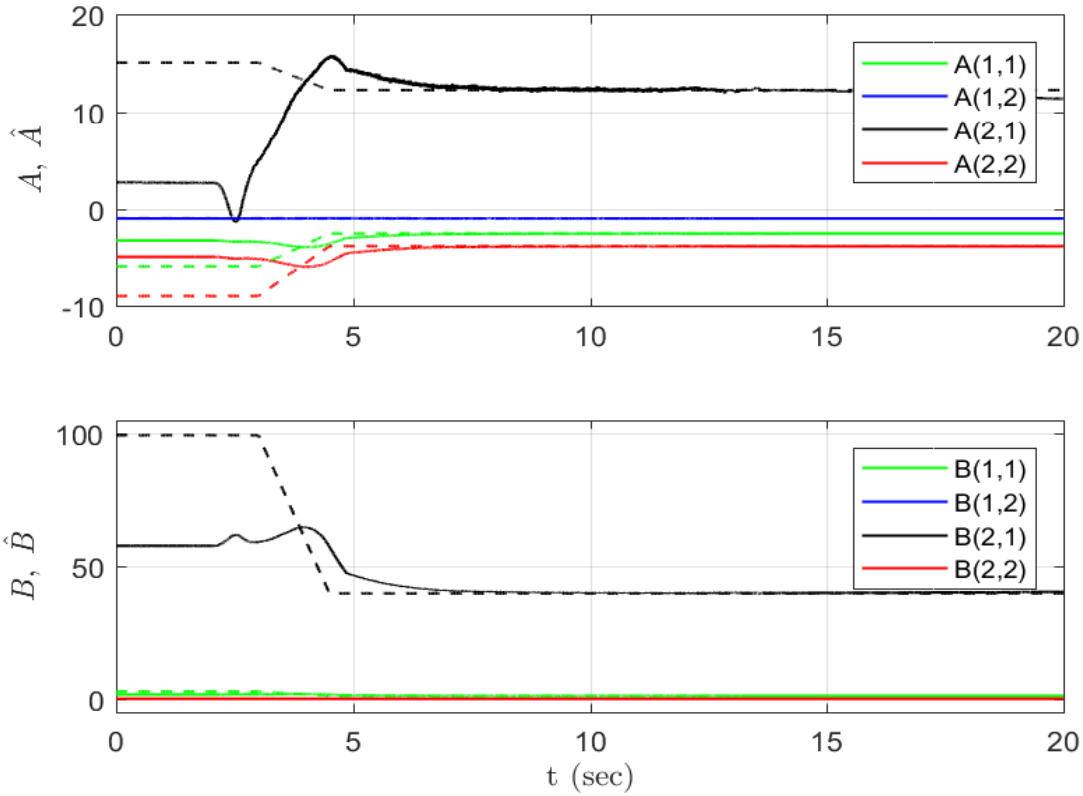

Figure 4.14: Estimated plant matrices

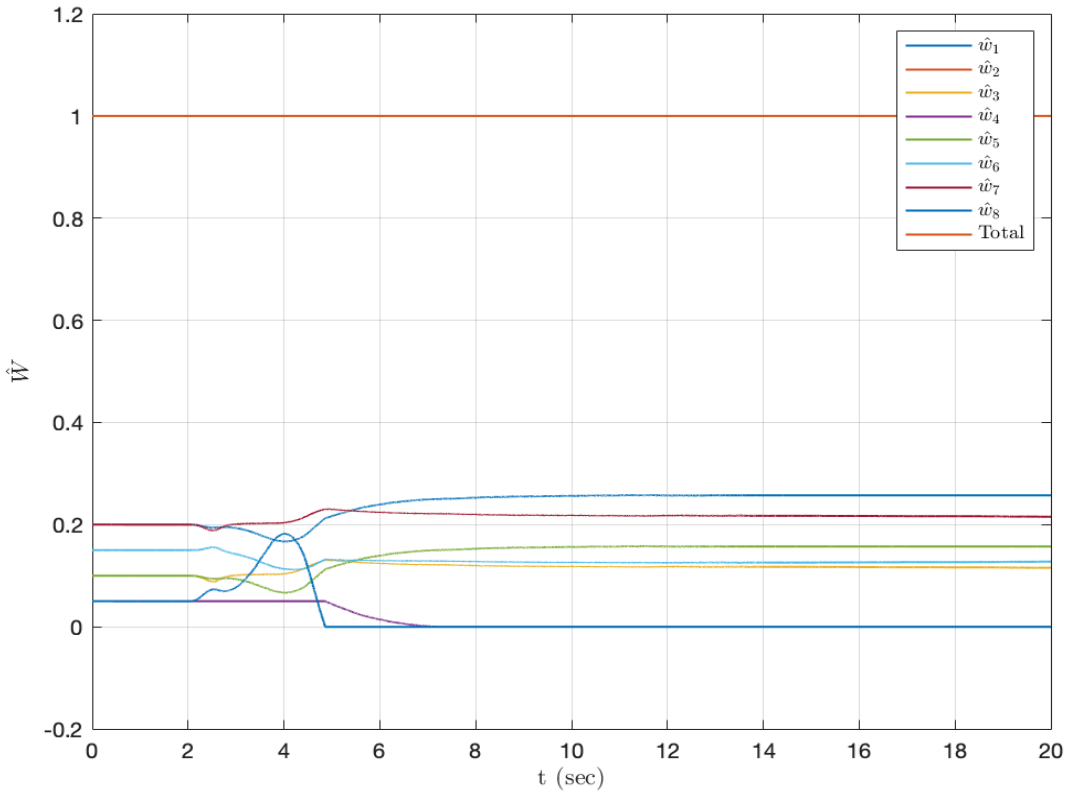

Figure 4.15: Estimated weighted parameters

4.5 Summary and Remarks

In this chapter, the proposed LQ based optimal MMAC scheme in Chapter 3 has been applied to vehicle motion control. The objective was to improve vehicle handling performance and to maintain stability during cornering manoeuvres, i.e., the vehicle was controlled to track the desired yaw rate while the side-slip angle is close to zero. First, we considered nonlinear vehicle dynamics equipped with active front steering system and direct yaw control system that uses independent in-wheel motor at corners to generate torque at vehicle CG in Section 2.2. The nonlinear vehicle dynamic model includes uncertain time-invariant/varying parameters due to uncertain tire characteristics, tire-road friction coefficient, and combined-slip effect. We lumped all these system uncertainties and readdressed them as the uncertain time varying longitudinal and lateral tire stiffness with their known upper and lower bounds. Since it is assumed that the upper and lower

bounds (extreme values) of these uncertain parameters are known, the uncertain nonlinear vehicle dynamic model has been addressed as a linear MIMO system with polytopic uncertain parameters. These bounds have been used to design the multiple fixed models for the system identifier. For each fixed model (i.e., each operation condition) and given performance matrices Q, R, an optimal LQ control gain is computed off-line for the corresponding model in advance. This saves time for the computation of optimum control input in real-time implementation. The generated control inputs for all fixed models are blended on-line using weighting vector. The weighting vector is continuously estimated by the proposed either gradient or RLS based adaptive scheme.

The simulation application to uncertain lateral vehicle dynamics is presented 2-DOF dynamic model in Simulink environment. The performances of proposed LQ based MMAC utilizing the proposed gradient and RLS based schemes have been compared to each other and an LQ controller which is designed using the same performance matrices Q, R and fixed nominal values of the uncertain parameters. The results validated the stability and effectiveness of the proposed LQ based MMAC algorithm and demonstrate that the proposed adaptive LQ control schemes outperform over the LQ control scheme for tracking tasks.

Chapter 5

Multiple-Model Adaptive Predictive Control for Vehicle Motion

In this chapter, the constraints on actuation systems, active front steering system and torque vectoring, are considered to design an MPC based MMAC. First, maximum and minimum limits are determined to generate steering angle and steering angle rate. Second, the maximum and minimum torque and torque rate for each corner (each in-wheel electric motor) are determined. These bound values and vehicle kinematic structure will be later used to determine the constraints on torque vectoring at vehicle CG. Third, we present how to estimate the prediction model for each time step using the proposed MMA scheme in Chapter 3. For validation of effectiveness of the proposed control algorithm, several critical driving scenarios are simulated using an high-fidelity model CarSim/Simulink environment. The proposed MPC based MMAC is depicted in Fig. 5.1.

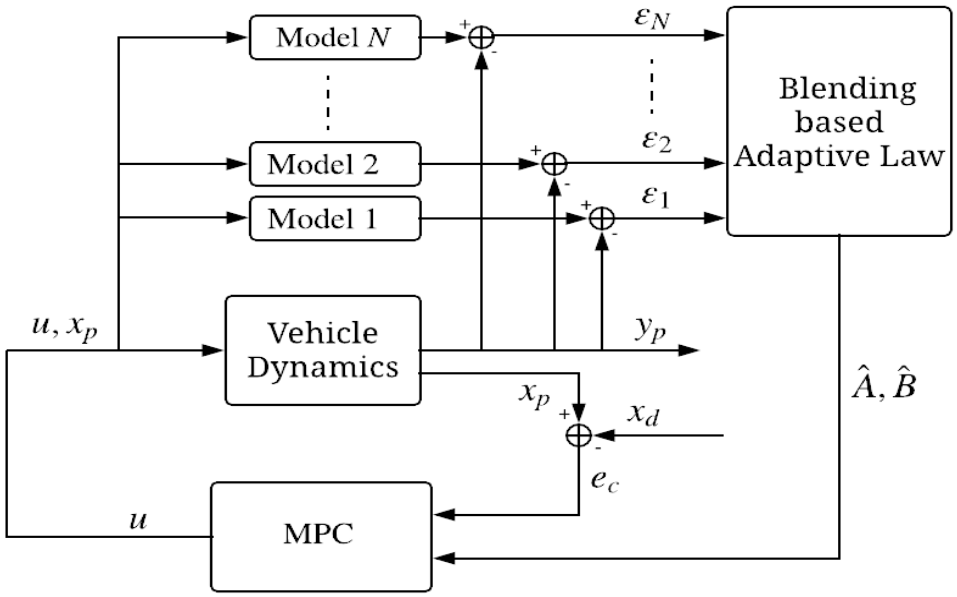

Figure 5.1: Proposed Model Predictive Control based MMAC diagram.

5.1 Actuator Constraints

MPC based MMAC has to be designed in an optimal way such that it considers actuator constraints and take measurements to correct these constraint violations for long range predictive control horizon. In this study, two sets of constraints are considered for each actuation systems including active steering system and torque vectoring.

5.1.1 Constraints for Active Steering System

Active steering system is one of the significant ways to control the vehicle lateral motion. However, it has two constraints to be considered: maximum limit on the steering input δ and angle rate $\Delta\delta$. These constraints are very effective to guarantee stable and smooth vehicle motion, and thus comfortable and safe ride. If the maximum and minimum that can be generated steering angles are denoted by δ_{max} and δ_{min} , the total applied steering angle $\delta = \delta_d + \delta_c$ in (4.6) must satisfy the following constraints;

$$\delta_{min} \leq \delta \leq \delta_{max}. \tag{5.1}$$

Denoting $\Delta\delta_{max}$ and $\Delta\delta_{min}$ to the maximum and minimum that can be generated steering angle rates, the total applied steering angle rate $\Delta\delta$ must satisfy the following constraints;

$$\Delta\delta_{min} \leq \Delta\delta \leq \Delta\delta_{max}. \tag{5.2}$$

The maximum steering angle δ_{max} and angle rate $\Delta\delta_{max}$ are chosen as 30 deg and 10 deg/s, respectively.

5.1.2 Constraints for Torque Vectoring

The vehicle, used for simulation, has independent electric motor at each corner, which is capable of generating a torque vector at vehicle CG. However, electric motor has a limited range of actuation and a limited slew rate. If the maximum and minimum torques that can be generated are denoted by Q_{max} and Q_{min} , the applied torque (i.e., Q_i for $i = fl, fr, rl, rr$) on each corner should satisfy

$$Q_{min} \leq Q_i \leq Q_{max}. \tag{5.3}$$

Denoting ΔQ_{max} and ΔQ_{min} to the maximum and minimum that can be generated torque rates, the total applied torque rate ΔQ_i on each corner must satisfy the following constraints;

$$\Delta Q_{min} \leq \Delta Q_i \leq \Delta Q_{max}. \tag{5.4}$$

The electric motor constraints (5.3), (5.4) at each corner can be mapped into generated torque vectoring at vehicle CG. The generated torque M_z at CG is computed using vehicle kinematic with front steering system and generated tire forces:

$$M_z = \begin{bmatrix} -0.5l_s\cos\delta + l_f\sin\delta & 0.5l_s\cos\delta + l_f\sin\delta & -0.5l_s & 0.5l_s \end{bmatrix} \begin{bmatrix} F_{fl} \\ F_{fr} \\ F_{rl} \\ F_{rr} \end{bmatrix}. \tag{5.5}$$

where longitudinal tire forces F_i relates to applied torques Q_i as in (2.5). Assuming wheel moment of inertia I_w and wheel rotational accelerations $\dot{w}_i$ are enough small to ignore, M_z can be reexpressed in terms of applied torques Q_i as

$$M_z = \frac{1}{R_{eff}} \begin{bmatrix} -0.5l_s \cos\delta + l_f \sin\delta & 0.5l_s \cos\delta + l_f \sin\delta & -0.5l_s & 0.5l_s \end{bmatrix} \begin{bmatrix} Q_{fl} \\ Q_{fr} \\ Q_{rl} \\ Q_{rr} \end{bmatrix} \tag{5.6}$$

If the maximum and minimum torque at vehicle CG that can be generated are denoted by $M_{z_{max}}$ and $M_{z_{min}}$, which can be computed by (5.3) and (5.6), the applied CG torque M_z should be within the following range

$$M_{z_{min}} \leq M_z \leq M_{z_{max}}. \tag{5.7}$$

Denoting $\Delta M_{z_{min}}$ and $\Delta M_{z_{max}}$ to the maximum and minimum that can be generated CG torque rates, the total applied CG torque rate ΔM_z must satisfy the following constraints;

$$\Delta M_{z_{min}} \leq \Delta M_z \leq \Delta M_{z_{max}}, \tag{5.8}$$

where $\Delta M_{z_{min}}$ and $\Delta M_{z_{max}}$ can be computed by (5.4) and (5.6).

5.2 Model Predictive Controller Design

In this section, we design an MPC based controller considering actuator constraints for the same tracking problem in Section 4.3 on a slippery road condition (i.e., $\eta_x = \eta_f = \eta_r = 0.4$ in (4.6)). The objective of tracking control is to improve vehicle handling performance while maintaining stability during cornering manoeuvres and considering the actuator constraints. In other words, the vehicle is expected to achieve the desired yaw rate r_d defined in (4.12) while maintaining the closeness of side-slip angle to zero, i.e., $\beta_d = 0$ and satisfying the input range constraints (5.1, 5.7) and the input rate constraints (5.2, 5.8). To this end the objective function is defined as

$$J_{MPC} = arg\min_{u} \sum_{k=1}^{N_p} (x_p[t+k|t] - x_{des}[t+k|t])^T \;\; Q \;\; (x_p[t+k|t] - x_{des}[t+k|t]) + \sum_{k=0}^{N_c-1} u[t+k|t]^T \;\; R \;\; u[t+k|t] \tag{5.9}$$

subject to

$$\begin{aligned} & x_p[t+k+1|t] = A_{pd}[t+k|t]x_p[t+k|t] + B_{pd}[t+k|t]u[t+k|t], \\ & u_{LB} \leq u[t+k|t] \leq u_{UB}, \quad k = 1, \cdots, N_c, \\ & \Delta u_{LB} \leq u[t+k|t] - u[t+k-1|t] \leq \Delta u_{UB}, \quad k = 1, \cdots, N_c, \end{aligned} \tag{5.10}$$

where $u_{LB} = \begin{bmatrix} \delta_{min} & M_{z_{min}} \end{bmatrix}^T$, $u_{UB} = \begin{bmatrix} \delta_{min} & M_{z_{min}} \end{bmatrix}^T$ denote lower bound and upper bound, respectively, on control input; $\Delta u_{LB} = \begin{bmatrix} \Delta\delta_{min} & \Delta M_{z_{min}} \end{bmatrix}^T$, $\Delta u_{UB} = \begin{bmatrix} \Delta\delta_{min} & \Delta M_{z_{min}} \end{bmatrix}^T$ denote lower bound and upper bound, respectively, on control input rate; $x_{des} = \begin{bmatrix} \beta_d & r_d \end{bmatrix}^T$ is desired state and assumed to be constant over prediction horizon. The prediction model in (5.10) can be expressed by the current state and prospective control inputs. Based on the assumption that the control and prediction horizons have the same length, the future system state

$$X_p = S_x x_{p0} + S_u U, \;\; x_{p0} = x_p[0], \tag{5.11}$$

where $X_p = \begin{bmatrix} x_p^T[1] & x_p^T[2] & \cdots & x_p^T[N_p] \end{bmatrix}^T$, $U = \begin{bmatrix} u^T[0] & u^T[1] & \cdots & u^T[N_p-1] \end{bmatrix}^T$, and

$$S_x = \begin{bmatrix} A_{pd} \\ A_{pd}^2 \\ \vdots \\ A_{pd}^{N_p} \end{bmatrix}, \;\; S_u = \begin{bmatrix} B_{pd} & 0 & \cdots & 0 \\ A_{pd}B_{pd} & B_{pd} & \cdots & 0 \\ \vdots & \ddots & \ddots & \vdots \\ A_{pd}^{N_p-1}B_{pd} & \cdots & \cdots & B_{pd} \end{bmatrix},$$

and the desired states over the prediction horizon is $X_{des} = \begin{bmatrix} x_{des}^T[1] & x_{des}^T[2] & \cdots & x_{des}^T[N_p] \end{bmatrix}^T$. The input U is expressed as

$$U = S_{\Delta u}\Delta U + U_{-1}, \tag{5.12}$$

where $\Delta U = \begin{bmatrix}\Delta u^T[0] & \Delta u^T[1] & \cdots & \Delta u^T[N_p-1]\end{bmatrix}^T$ in which $\Delta u^T = \begin{bmatrix}\Delta\delta & \Delta M_z\end{bmatrix}$, $U_{-1} = \begin{bmatrix}u^T[-1] & u^T[-1] & \cdots & u^T[-1]\end{bmatrix}^T$ in which $u[-1]$ denotes the input applied in previous time step, and

$$S_{\Delta u} = \begin{bmatrix} I & 0 & \cdots & 0 \\ I & I & \cdots & 0 \\ \vdots & \ddots & \ddots & \vdots \\ I & \cdots & \cdots & I \end{bmatrix}.$$

To consider the input rate, the cost function (5.9) is reexpressed as follow

$$J_{A_{MPC}} = arg\min_{\Delta U} (X - X_{des})^T \ \mathbf{Q} \ (X - X_{des}) + U^T \ \mathbf{R} \ U + \Delta U^T \ \mathbf{R_2} \ \Delta U, \tag{5.13}$$

where $\mathbf{Q} = blockdiag\{Q, Q, \cdots, Q\}$, $\mathbf{R} = blockdiag\{R, R, \cdots, R\}$ and $\mathbf{R_2} = blockdiag\{R_2, R_2, \cdots, R_2\}$. Once similar steps are followed in Subsection 2.3.2, the optimization problem (5.13) can be expressed as a constrained quadratic programming (QP) problem

$$J_{A_{MPC}} = arg\min_{\Delta U} \frac{1}{2}\Delta U^T H_A \Delta U + F_A^T \Delta U + \Upsilon_A, \tag{5.14}$$

subject to

$$\begin{aligned} u[t+k|t] &\in \mathcal{U}, \quad k = 0, \cdots, N_p - 1, \\ u[t+k|t] - u[t+k-1|t] &\in \Delta\mathcal{U}, \quad k = 0, \cdots, N_p - 1, \end{aligned} \tag{5.15}$$

where

$$\begin{aligned} H_A =& S_u^T S_{\Delta u}^T \mathbf{Q} S_{\Delta u} S_u + S_{\Delta u}^T \mathbf{R} S_{\Delta u} + \mathbf{R_2}, \\ F_A =& 2(S_u U_{-1} + S_x x_0 + S_D)^T \mathbf{Q} S_u S_{\Delta u} - 2X_{des}^T \mathbf{Q} S_u S_{\Delta u} + 2U_{-1}^T \mathbf{R} S_{\Delta u}, \\ \Upsilon_A =& (S_u U_{-1} + S_x x_0 + S_D)^T \mathbf{Q} (S_u U_{-1} + S_x x_0 + S_D) + U_{-1}^T \mathbf{R} U_{-1} \\ & - 2\left(X_{des}^T \mathbf{Q} (S_u U_{-1} + S_x x_0 + S_D)\right). \end{aligned}$$

In real-time, the QP problem (5.14) with the constraints (5.15) is solved using interior-point algorithm in Optimization Toolbox/MATLAB each time step. The solution of the

quadratic programming problem provides the series of MPC input increments ΔU, including steering angle increments $\Delta\delta$ and torque increments at vehicle CG ΔM_z. The first input vector of ΔU is added to the control input applied in previous time step $u[-1]$. The total control steering is applied to system (2.6) while the total control torque vector inputs M_z is distributed to each corner based on HCC principles in (2.30) and (2.30).

5.3 Design of Multiple-Model Adaptive Predictive Control

In the previous section, an MPC controller was designed for a wet road condition, i.e., $\eta_x = \eta_f = \eta_r = 0.4$ which implies the system parameters $A_p,\ B_p$ in prediction model are fixed. In this section, MMAC is redesigned for the same tracking problem in previous section considering MPC and actuator constraints. We consider the uncertain vehicle dynamics (4.6) with its known input and input rate constraints (5.1), (5.7), and (5.8), (5.2), respectively.

For multiple-model identifier, the same fixed models $(A_i,\ B_i)$ in (4.9) for the known range of the uncertainty in (4.8) are discritized by backward euler approach to $(A_{di},\ B_{di})$ which are used in the discritized adaptive law (3.33a, 3.33b) to obtain weighting vector $\hat{W}$. After obtaining estimate weighting vector $\hat{W}$, uncertain discritized parameter matrices $\hat{A}_{pd}$, $\hat{B}_{pd}$ are estimated by

$$\begin{aligned} \hat{A}_{pd} &= \sum_{i=1}^{N} \hat{w}_i A_{di}, \\ \hat{B}_{pd} &= \sum_{i=1}^{N} \hat{w}_i B_{di}. \end{aligned} \tag{5.16}$$

The estimated parametric models $\hat{A}_{pd},\ \hat{B}_{pd}$ are used as a prediction model in (5.10) for MPC design and assummed to be constant during prediction horizon N_p. The proposed MPC based MMAC block diagram is given in Fig. 5.2. In order to validate our control algorithm, several critical driving scenarios has been simulated in CarSim/Simulink environment in the next section.

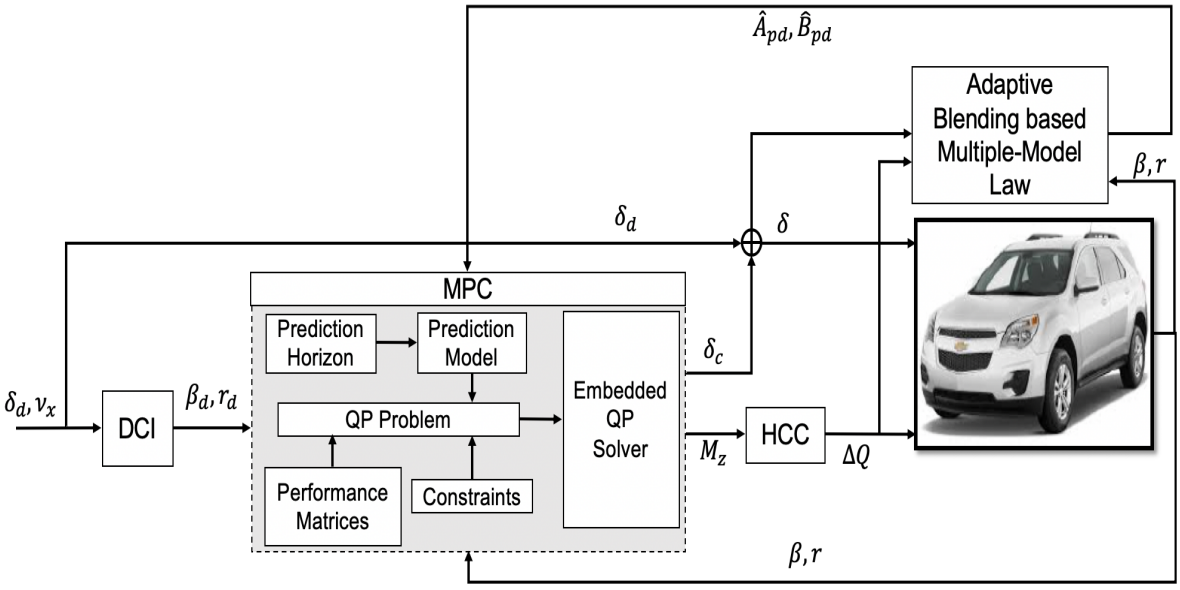

Figure 5.2: Proposed overall MPC based MMAC diagram.

5.4 Simulations

In this section, simulation tests are performed on the proposed MPC to identify the uncertain time-varying lateral vehicle dynamics in Simulink and CarSim environment. The vehicle used for simulation is D-Class sedan car, one of the pre-built models in CarSim 8.2.2, which can independently generate torque in each corner to provide torque vectoring moment at vehicle CG. The CarSim vehicle is a high-fidelity dynamic model unlike the simulink model used in Chapter 3 which is 2-DOF model. Table 5.1 shows the main properties of the simulated vehicle.

Parameter	Description	Value	Unit
m	Vehicle mass	1530	kg
I_z	Yaw moment of inertia	2315.3	kgm^2
I_ω	Wheel moment of inertia	0.8	kgm^2
L	Wheel base	2.78	m
l_s	Track width	1.55	m
R_{eff}	Wheel effective radius	0.325	m
l_f	CG distance to Front axle	1.11	m
l_r	CG distance to Rear axle	1.67	m
C_f	Nominal Front tire stiffness	80400	N/rad
C_r	Nominal Rear tire stiffness	82700	N/rad

Table 5.1: Carsim vehicle parameters.

The parameters of the MPC are defined next. The sample time of the controller is set equal to $T_s = 5\ ms$. The size of the prediction horizon is set equal to $N_p = 6$ and the size of the control horizon is also $N_c = 6$. The size of the prediction horizon is selected after several computations such that the online computation time is reduced to maintain an acceptable closed-loop performance. The design parameters MPC scheme are selected as $Q = diag([3 \cdot 10^4, 10^4])$, $R = diag([2 \cdot 10^4, 10^{-5}])$, $R_2 = diag([2 \cdot 10^4, 10^{-5}])$. The tuning parameter of MMA scheme, Γ in (3.30) is $diag([50, 50, \cdots, 50])$. The parameters of HCC are selected as $W_{\Delta f} = diag([1, 1, 1, 1])$ and $W_E = diag([1, 1, 10])$.

5.4.1 Case 1: No Acceleration/Braking During Maneuver

Double lane change maneuver is performed to induce vehicle drift without applying acceleration or braking. This maneuver is performed with the given vehicle parameters in Table 5.1.

Two different road conditions are considered including a slippery road with the friction coefficient of $\mu = 0.4$ and a dry road with the friction coefficient of $\mu = 0.9$. We first run the simulation for dry road. The driving scenario is given in the following way: the vehicle is cruising at the constant initial speed of 80 kph on slippery road and 120 kph on the dry road, and then double lane change steering input is applied by the driver. The driver steering input is shown in Fig. 5.3.

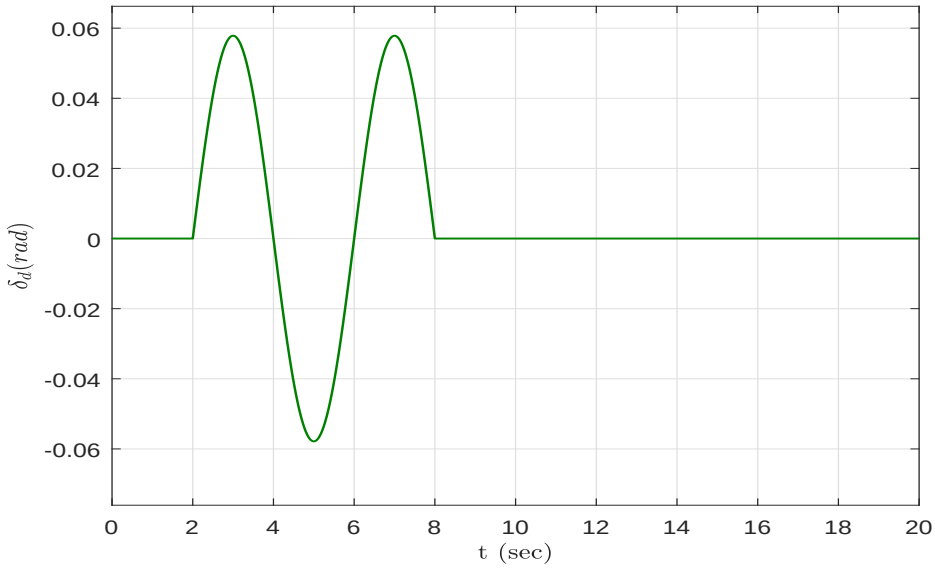

Figure 5.3: Driver steering input during maneuver.

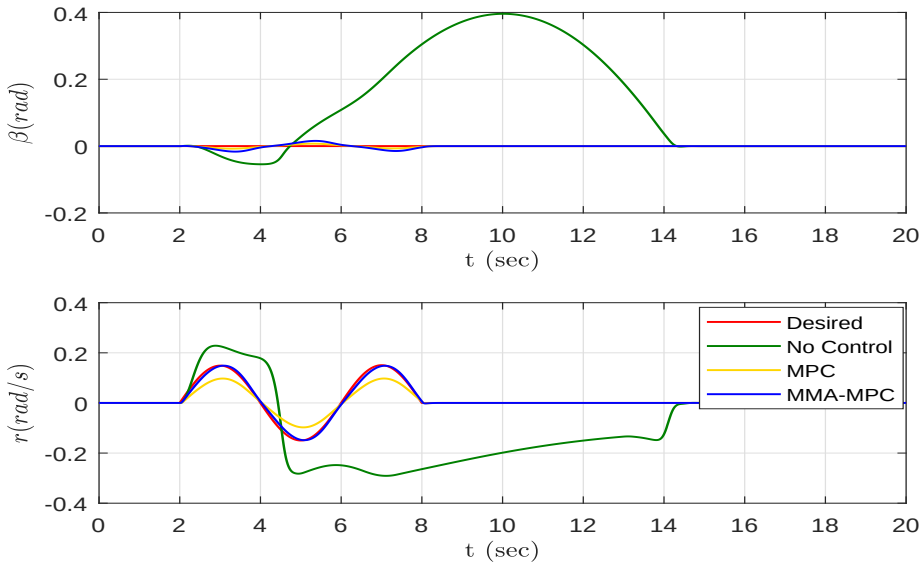

Figure 5.4: Tracking performance of designed controller on a slippery road.

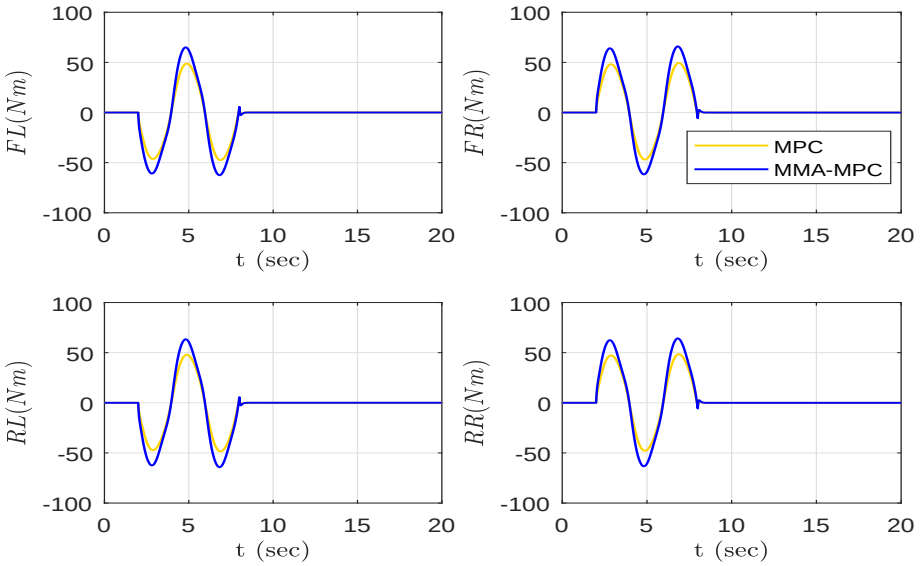

Figure 5.5: Generated torques by designed controller on a slippery road.

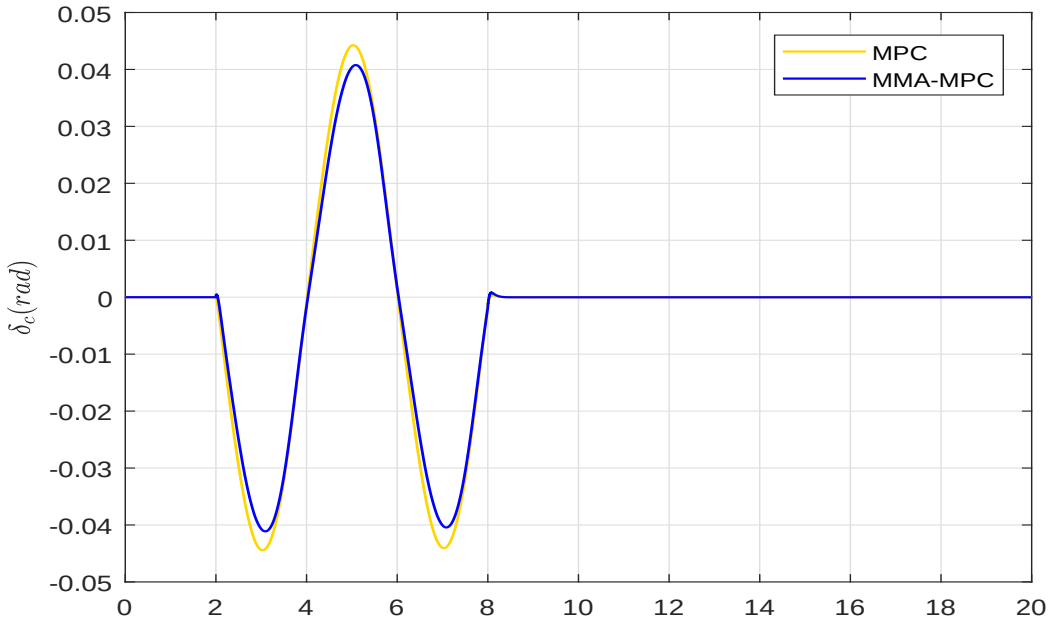

Figure 5.6: Corrected steering input by designed controller on a slippery road.

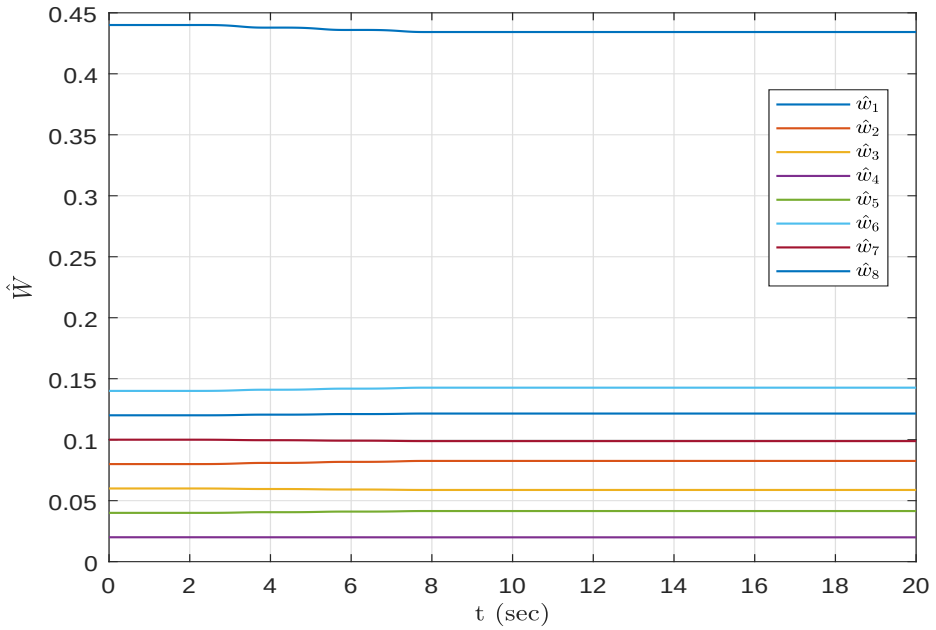

Figure 5.7: Estimates of weighting parameters for a slippery road.

Fig. 5.4 shows the yaw rate and the sideslip angle tracking performance of the vehicle without controller, with MPC controller, and with MMA-MPC controller. In the uncontrolled maneuver, the vehicle is unable to track the desired yaw rate and demonstrate unstable motion. On the other hand, the MPC based controllers successfully maintain the vehicle stability during manoeuvre. However, the proposed MMA-MPC controller achieves better performance increasing yaw tracking performance by almost 100% while keeping sideslip angle small.

Generated torque adjustments of the designed MPC and MMA-MPC controllers are given in Fig. 5.5. As can be seen that the torque differentials required to maintain vehicle stability are away from saturation, smooth and symmetric. Fig. 5.6 displays the corrected steering input is almost same with the driver input in Fig. 5.3. This results indicate that the designed controller does not involve in the driver steering input much and provides confidence.

In Fig. 5.7, the estimates of the weighting parameters are shown during maneuver. As seen, the estimate parameters show small changes when the vehicle start double lane change maneuver on a slippery road.

For the second scenario, the steering input in Fig. 5.3 is applied by driver while cruising at 80 *kph* on a dry road.

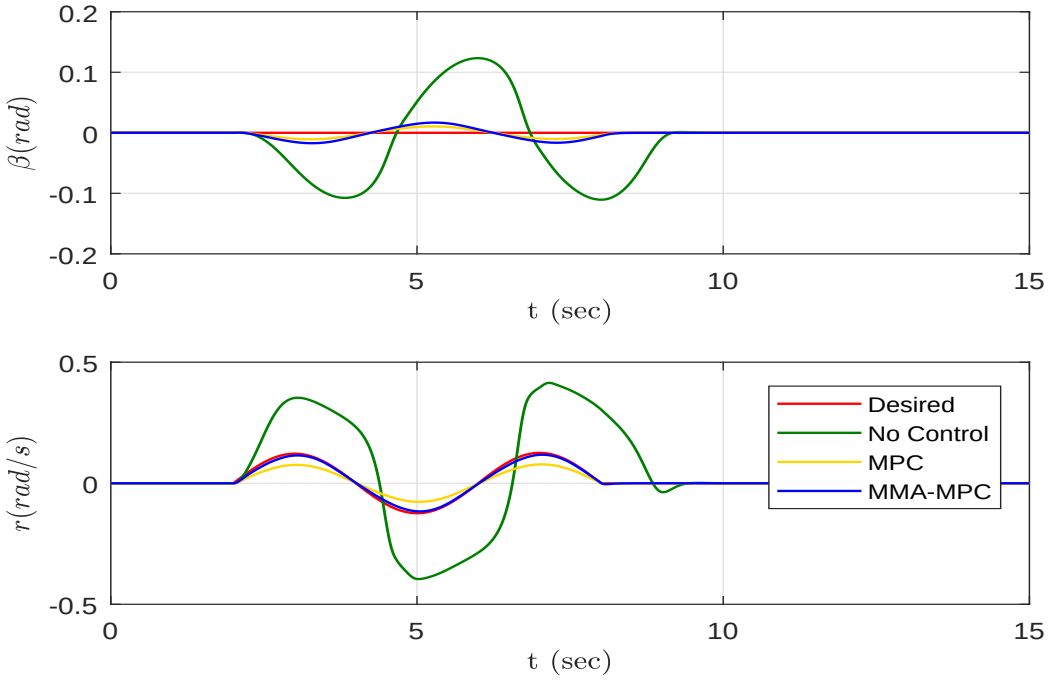

Figure 5.8: Tracking performance of designed controller on a dry road.

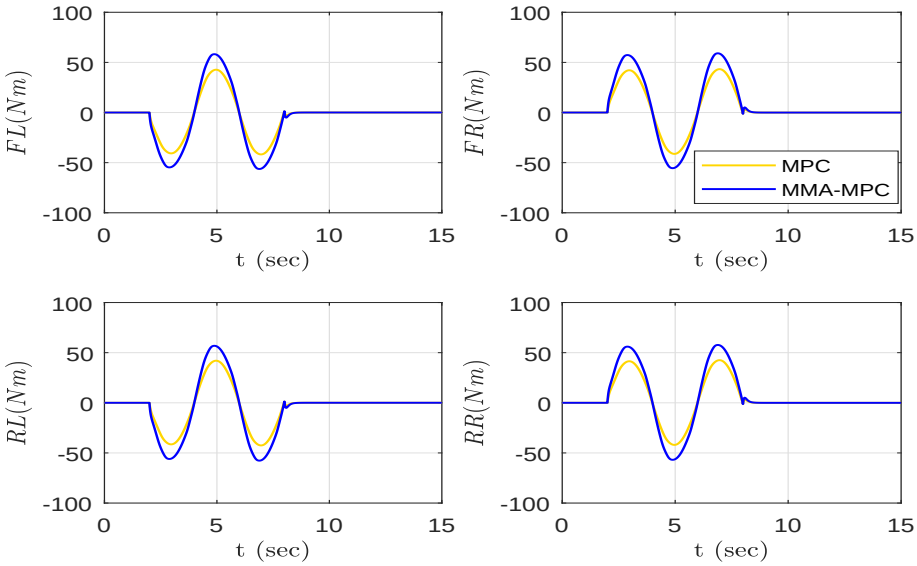

Figure 5.9: Generated torques by designed controller on a dry road.

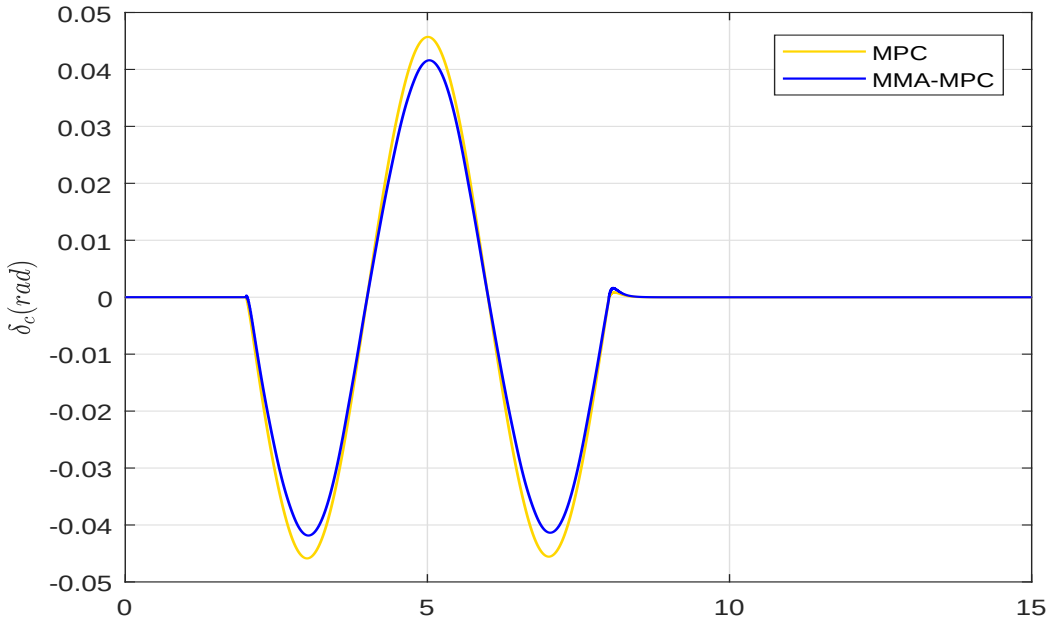

Figure 5.10: Corrected steering input by designed controller on a dry road.

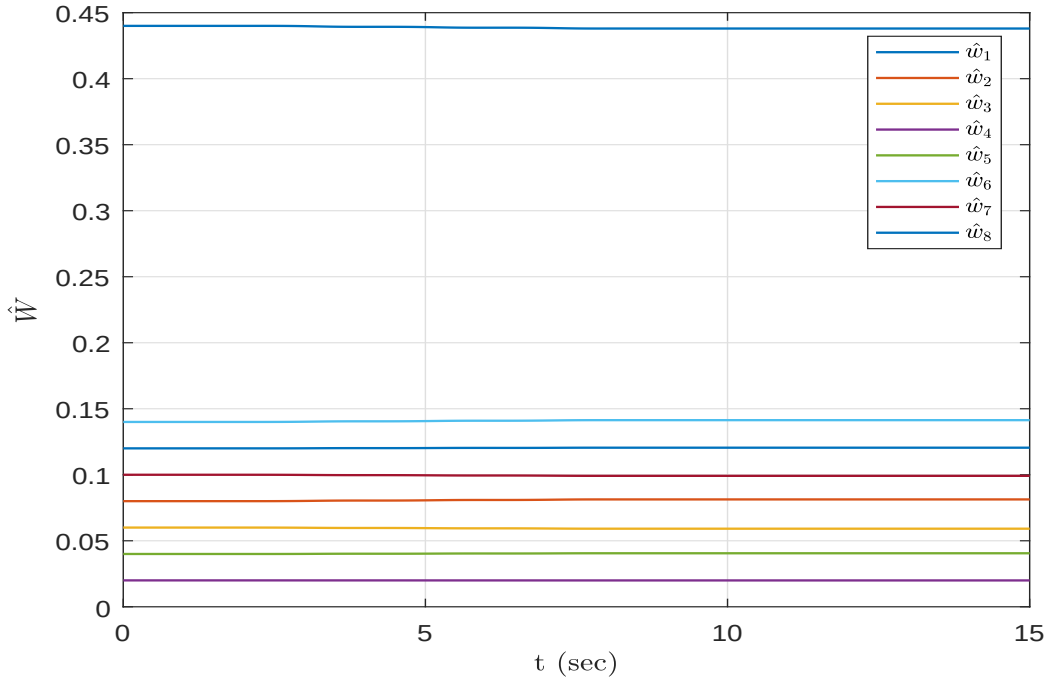

Figure 5.11: Estimates of weighting parameters for a dry road.

Fig. 5.8 shows the yaw rate and the sideslip angle tracking performance of the vehicle without controller, with MPC controller, and with MMA-MPC controller. In the uncontrolled maneuver, the vehicle is unable to track the desired yaw rate and demonstrate unstable motion. On the other hand, the MPC based controllers successfully maintain the vehicle stability during manoeuvre. However, the proposed MMA-MPC controller achieves better performance increasing yaw tracking performance by around 30% while keeping sideslip angle small.

The torque adjustments generated by the designed MPC and MMA-MPC controllers are given in Fig. 5.5. As can be seen that the torque differentials required to maintain vehicle stability are away from saturation, smooth and symmetric. Fig. 5.6 displays the corrected steering input is almost same with the driver input in Fig. 5.3. This results indicate that the designed controller does not involve in the driver steering input much and provides confidence.

In Fig. 5.11, the estimates of the weights are shown during maneuver. As seen, the estimate parameters show relatively smaller changes compared to ones for vehicle motion on the slippery road.

5.4.2 Case 2: Acceleration/Braking During Maneuver

Two different road conditions are considered including a slippery road with the friction coefficient of $\mu = 0.4$ and a dry road with the friction coefficient of $\mu = 0.9$.

The driving scenario is defined as the vehicle is cruising at at the constant initial speed of 80 *kph* on slippery road and 120 *kph* on the dry road, and then steering for double lane change and applying first acceleration and then braking while maneuver. The steering and the acceleration/braking commands by driver are shown in Figs. 5.12-5.13, respectively, assuming the total torque for acceleration/braking are distribute equally to corners when the vehicle is uncontrolled. We first run the simulation for a slippery road.

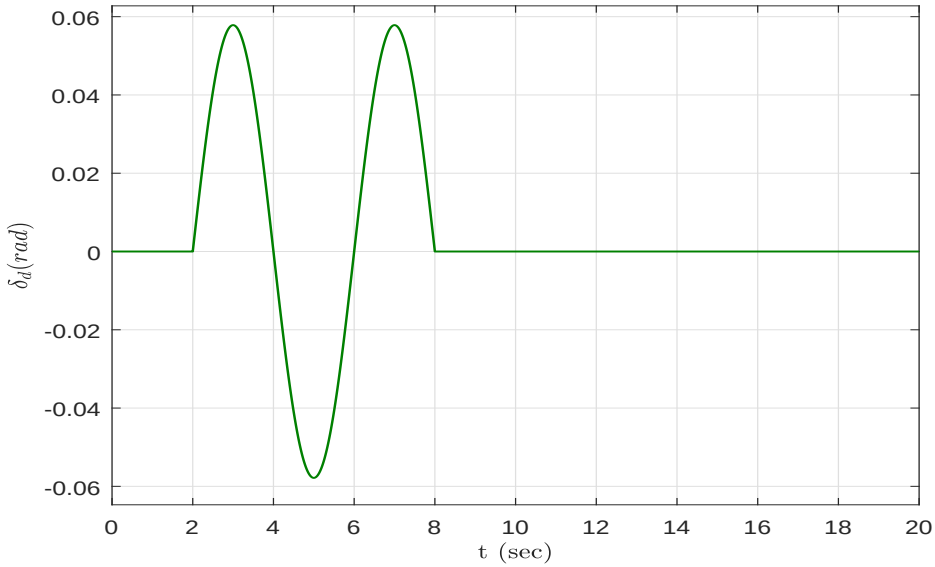

Figure 5.12: Driver steering input during maneuver.

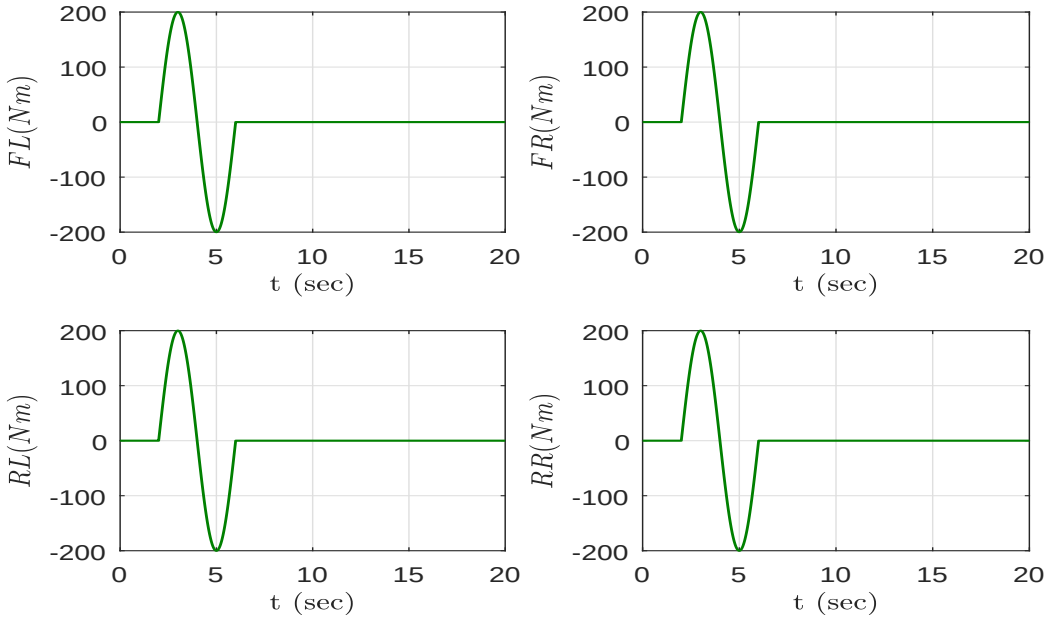

Figure 5.13: Driver acceleration/braking input during maneuver.

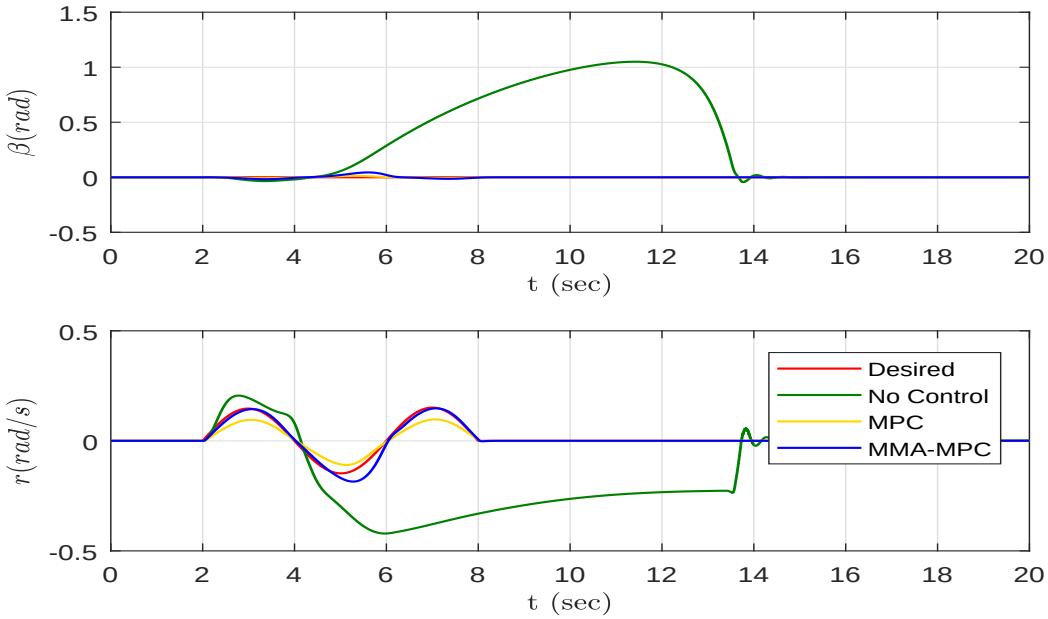

Figure 5.14: Tracking performance of designed controller on a slippery road.

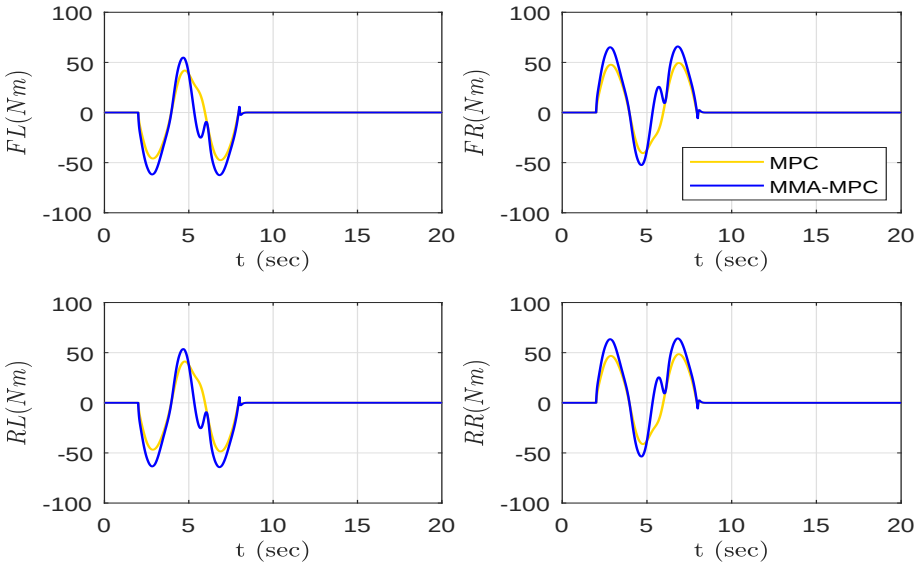

Figure 5.15: Generated torques by designed controller on a slippery road.

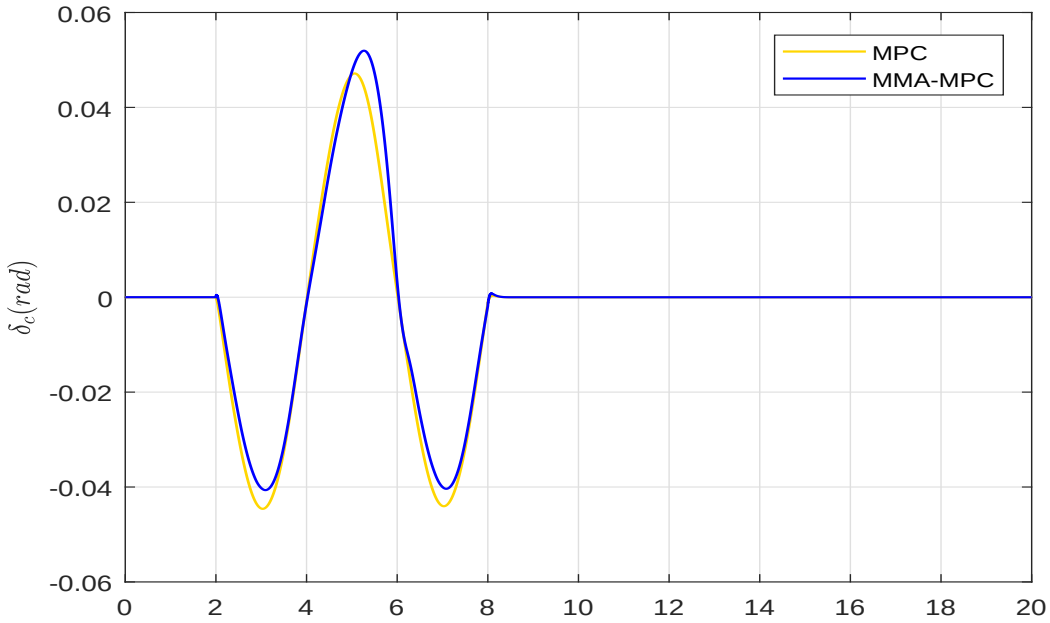

Figure 5.16: Corrected steering input by designed controller on a slippery road.

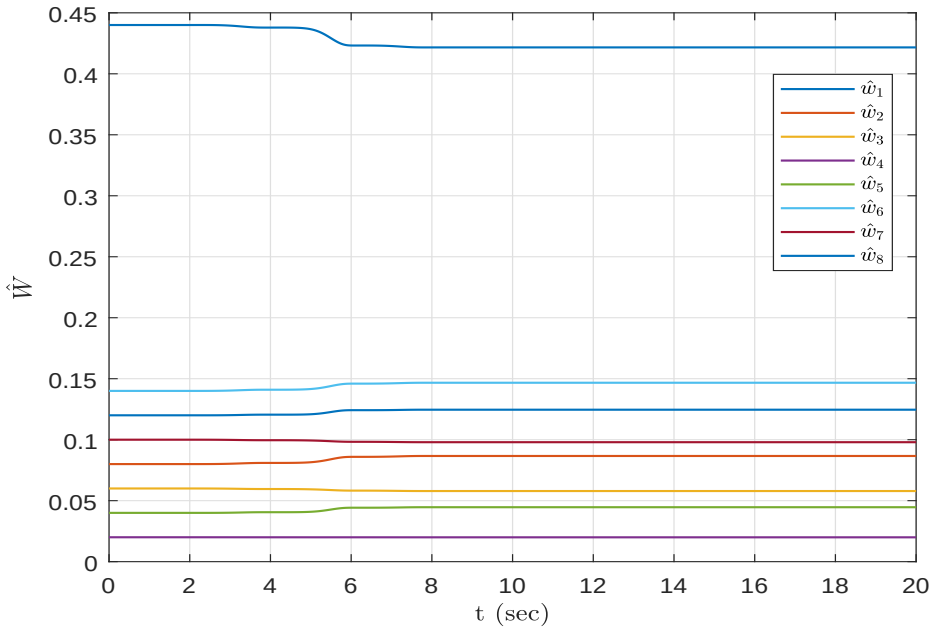

Figure 5.17: Estimates of weighting parameters for a slippery road.

Fig. 5.14 shows the yaw rate and the sideslip angle tracking performance of the vehicle without controller, with MPC controller, and with MMA-MPC controller. In the uncontrolled case, the vehicle becomes unstable as soon as the driver applies acceleration and steering. On the other hand, the MPC based controllers successfully maintain the vehicle stability during manoeuvre. However, the proposed MMA-MPC controller achieves better performance increasing yaw tracking performance by around 50% with a small overshoot around $t = 5$ *sec* while keeping sideslip angle small.

The torque adjustments generated by the designed MPC and MMA-MPC controllers are given in Fig. 5.15. As can be seen that the torque differentials required to maintain vehicle stability are away from saturation, smooth and symmetric. Fig. 5.16 displays the corrected steering input is almost same with the driver input in Fig. 5.12. This results indicate that the designed controllers do not involve in the driver steering input much as desired.

In Fig. 5.17, the estimates of the weights are shown during maneuver. The estimate parameters show relatively larger changes than the case without braking/acceleration.

For the second scenario, the driver inputs are the same in Figs. 5.12-5.13 and the vehicle started cruising at 120 *kph* on dry road.

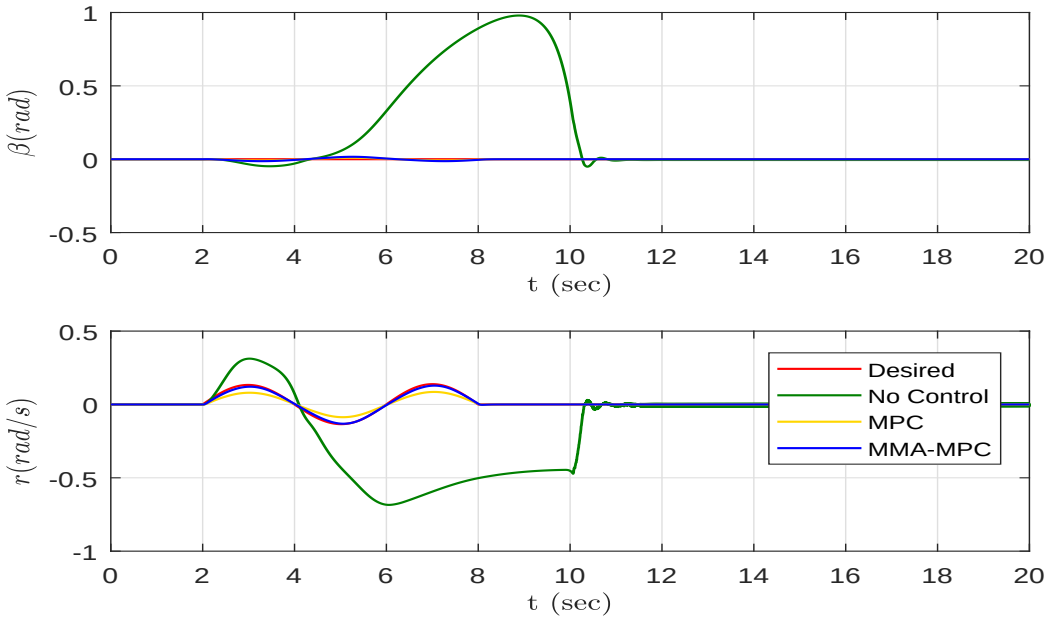

Figure 5.18: Tracking performance of designed controller on a dry road.

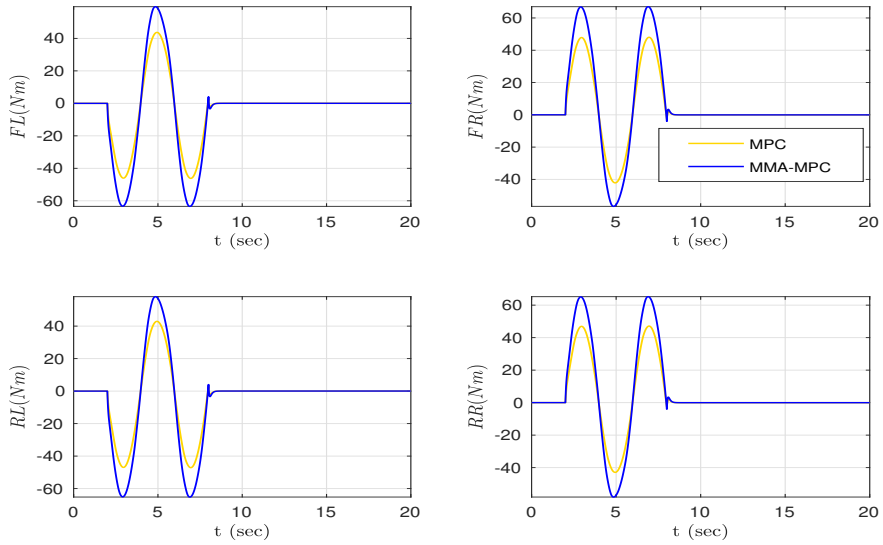

Figure 5.19: Generated torques by designed controller on a dry road.

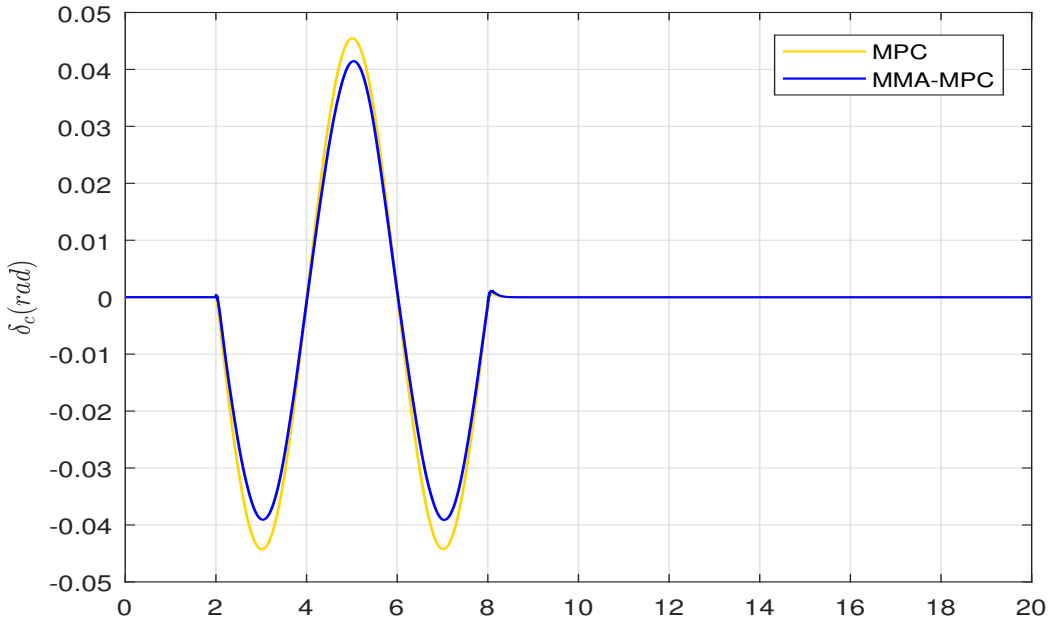

Figure 5.20: Corrected steering input by designed controller on a dry road.

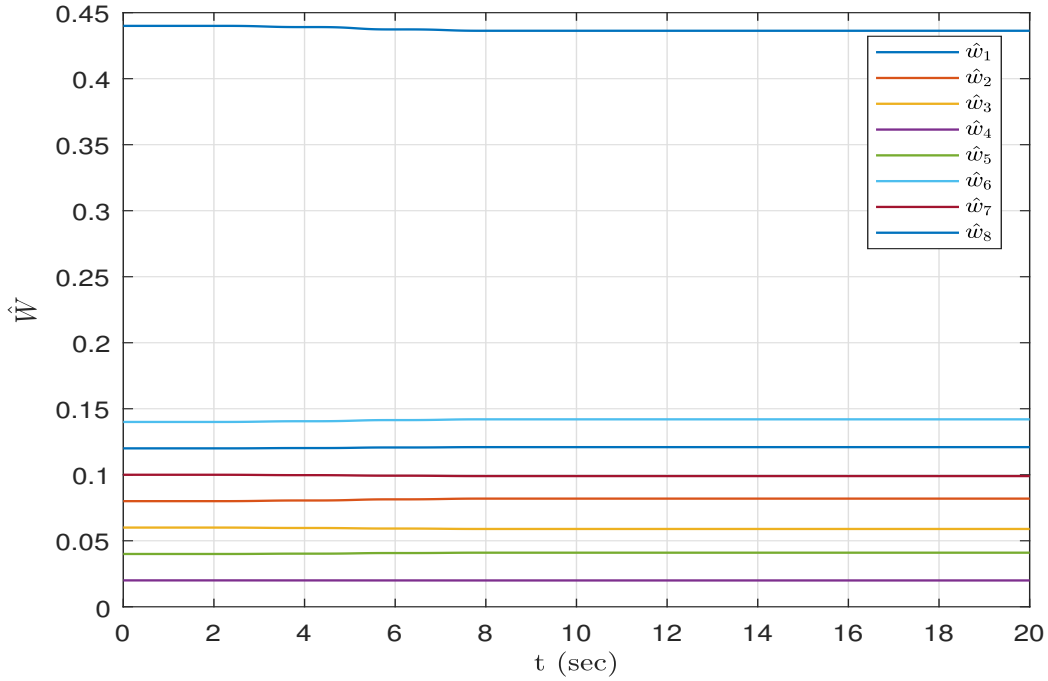

Figure 5.21: Estimates of weighting parameters for a dry road.

Fig. 5.18 shows the yaw rate and the sideslip angle tracking performance of the vehicle without controller, with MPC controller, and with MMA-MPC controller. In the uncontrolled case, the vehicle becomes unstable as soon as the driver applies acceleration and steering. On the other hand, the MPC based controllers successfully maintain the vehicle stability during manoeuvre. However, the proposed MMA-MPC controller achieves better performance increasing yaw tracking performance by around 25% while keeping sideslip angle small.

The torque adjustments generated by the designed MPC and MMA-MPC controllers are given in Fig. 5.19. As can be seen that the torque differentials required to maintain vehicle stability are away from saturation, smooth and symmetric. Fig. 5.20 displays the corrected steering input is almost same with the driver input in Fig. 5.12. This results indicate that the designed controllers do not involve in the driver steering input much as desired.

In Fig. 5.21, the estimates of the weights are shown during maneuver. The estimate parameters show relatively smaller changes than the ones for slippery road.

5.4.3 Case 3: No Acceleration/Braking During Maneuver on Changing Road Condition

Two different road conditions are considered including a slippery road with the friction coefficient of $\mu = 0.4$ and a dry road with the friction coefficient of $\mu = 0.9$.

The first driving scenario is defined as the vehicle is cruising at at the constant initial speed of 80 kph on slippery road and then start steering for double lane change. The steering command by driver are shown in Fig. 5.22. After vehicle starts the double lane change maneuver, the vehicle pass the dry road with the friction coefficient of $\mu = 0.9$.

The second driving scenario is defined as the vehicle is cruising at at the constant initial speed of 120 kph on dry road and then start steering for double lane change. After vehicle starts the double lane change maneuver, the vehicle pass the slippery road with the friction coefficient of $\mu = 0.4$.

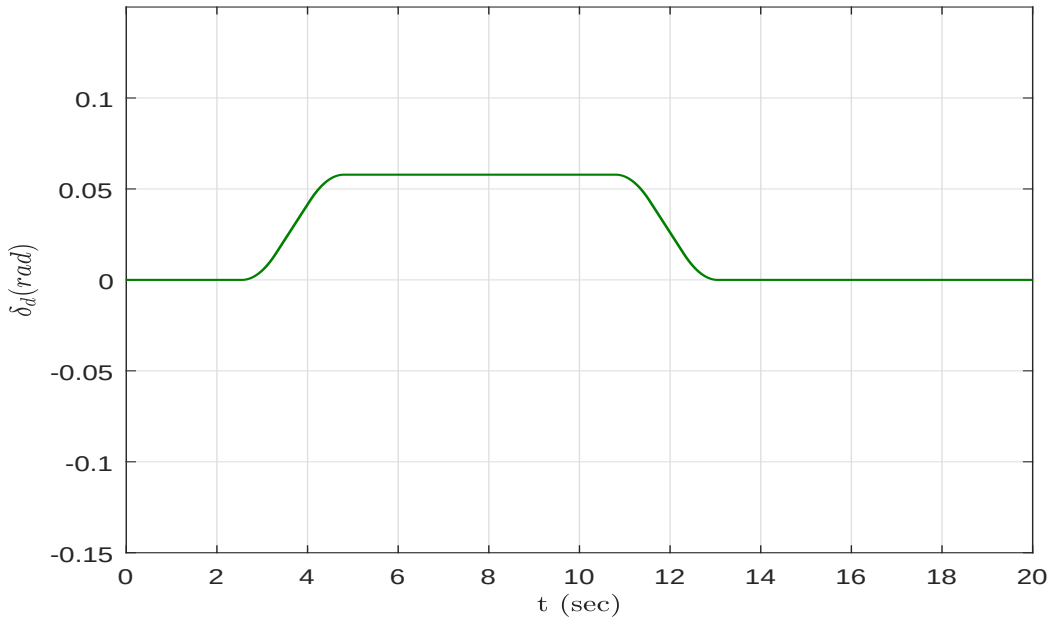

Figure 5.22: Driver steering input during maneuver.

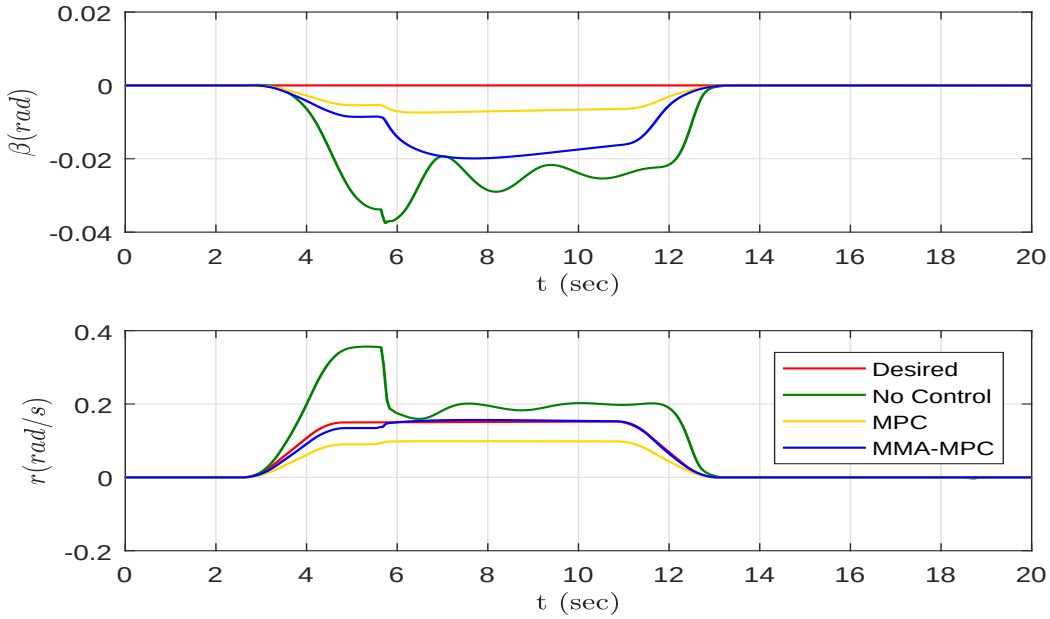

Figure 5.23: Tracking performance of designed controller on a slippery road.

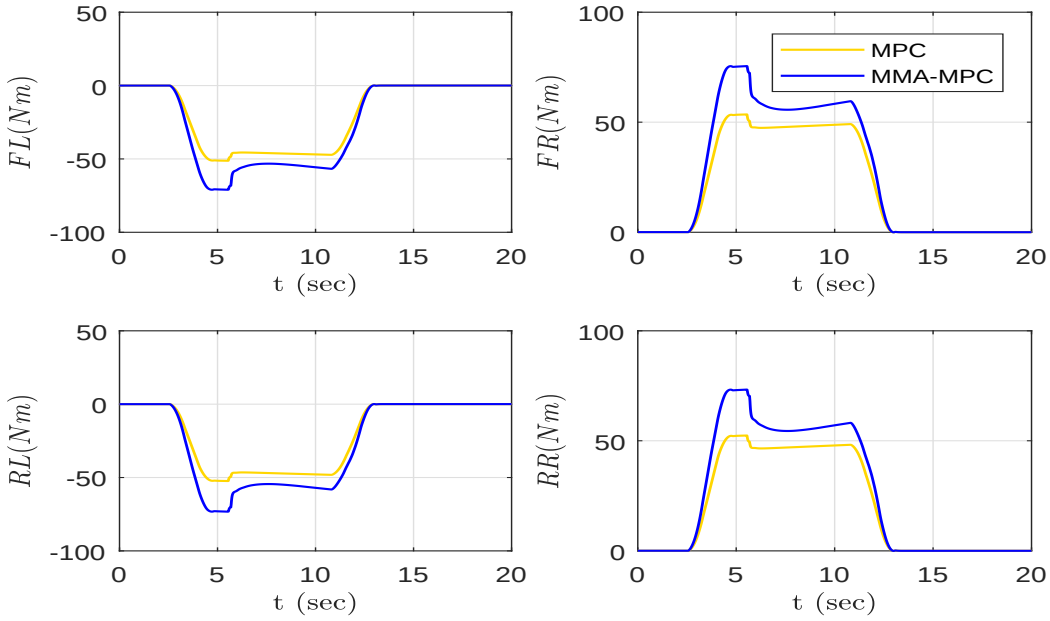

Figure 5.24: Generated torques by designed controller on a slippery road.

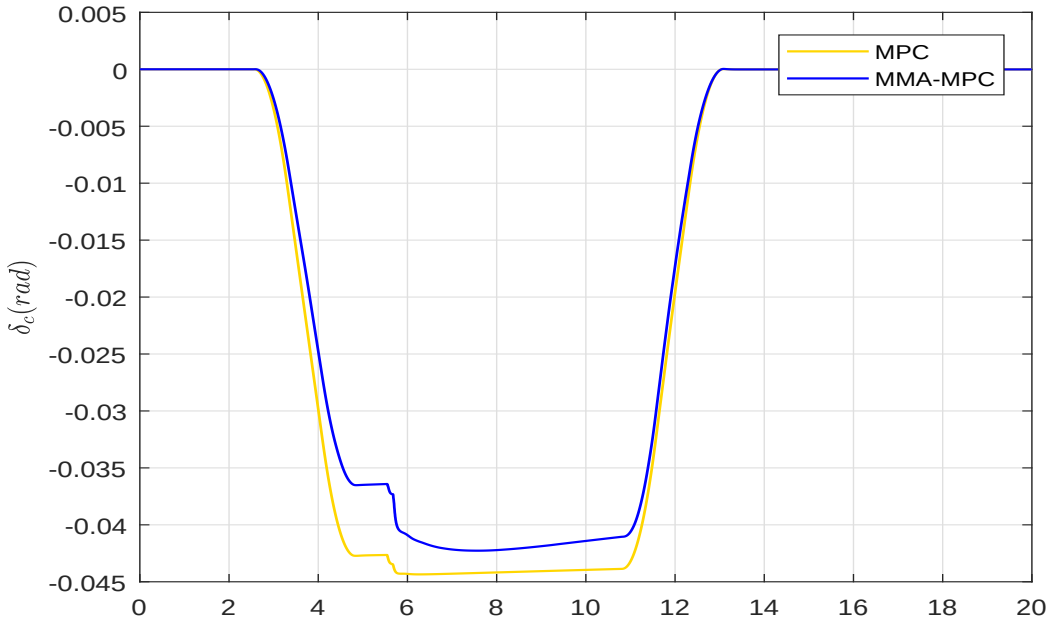

Figure 5.25: Corrected steering input by designed controller on a slippery road.

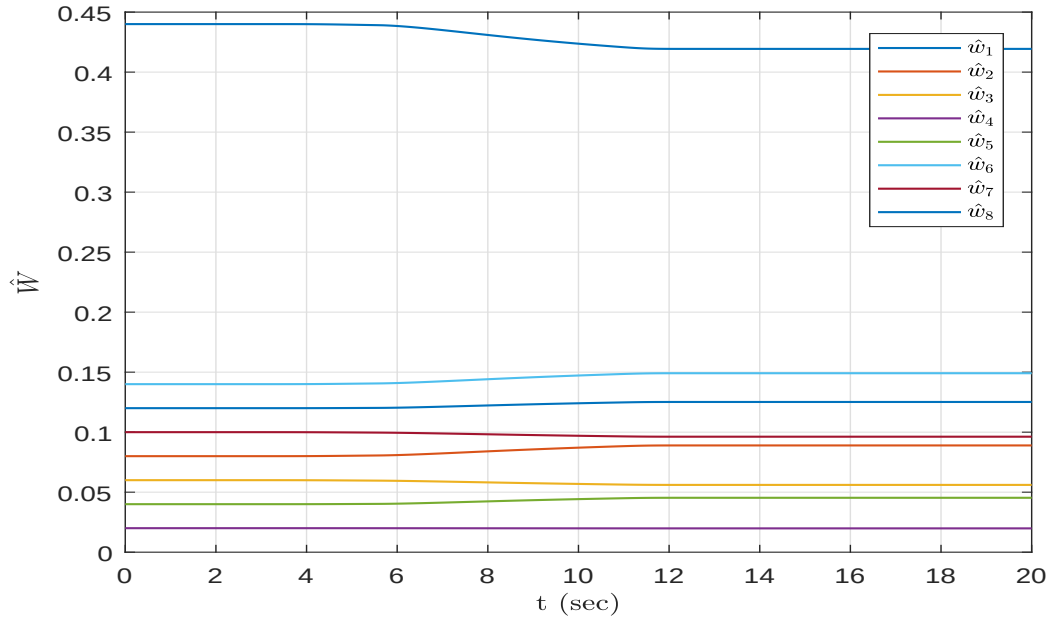

Figure 5.26: Estimates of weighting parameters for a slippery road.

Fig. 5.23 shows the yaw rate and the sideslip angle tracking performance of the vehicle without controller, with MPC controller, and with MMA-MPC controller. In the uncontrolled case, the vehicle becomes unstable as soon as the driver applies acceleration and steering. On the other hand, the MPC based controllers successfully maintain the vehicle stability during manoeuvre. However, the proposed MMA-MPC controller achieves better performance increasing yaw tracking performance by around 50% with a small overshoot around $t = 5$ *sec* while keeping sideslip angle small.

The torque adjustments generated by the designed MPC and MMA-MPC controllers are given in Fig. 5.24. As can be seen that the torque differentials required to maintain vehicle stability are away from saturation, smooth and symmetric. Fig. 5.25 displays the corrected steering input is almost same with the driver input in Fig. 5.22. This results indicate that the designed controllers do not involve in the driver steering input much as desired.

In Fig. 5.26, the estimates of the weights are shown during maneuver. The estimate parameters show relatively larger changes than the case without braking/acceleration.

For the second scenario, the driver input is the same in Fig. 5.22 and the vehicle started cruising at 120 *kph* on dry road.

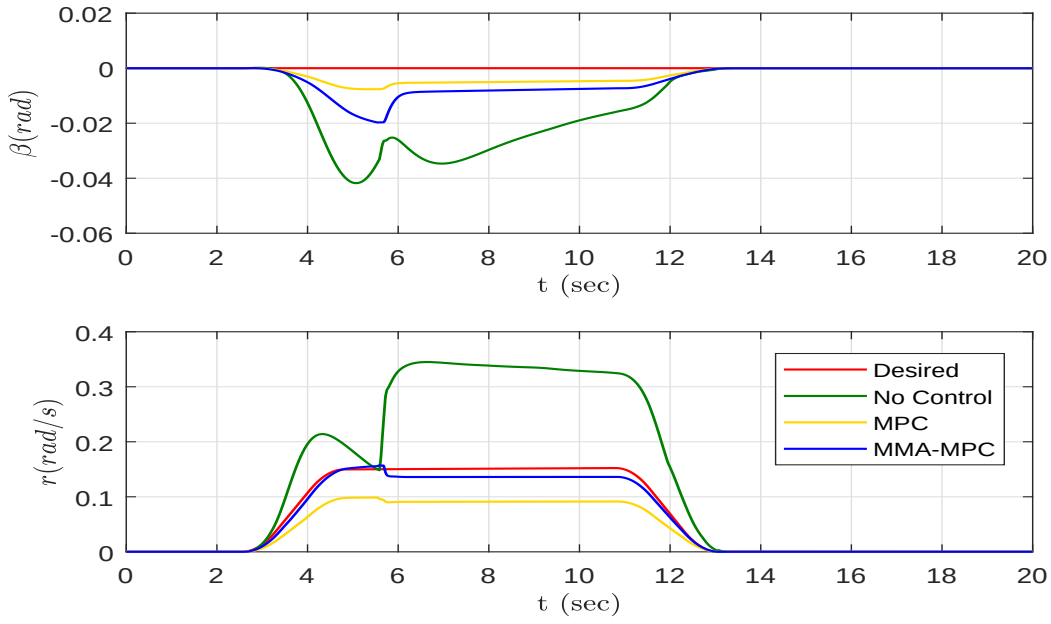

Figure 5.27: Tracking performance of designed controller on a dry road.

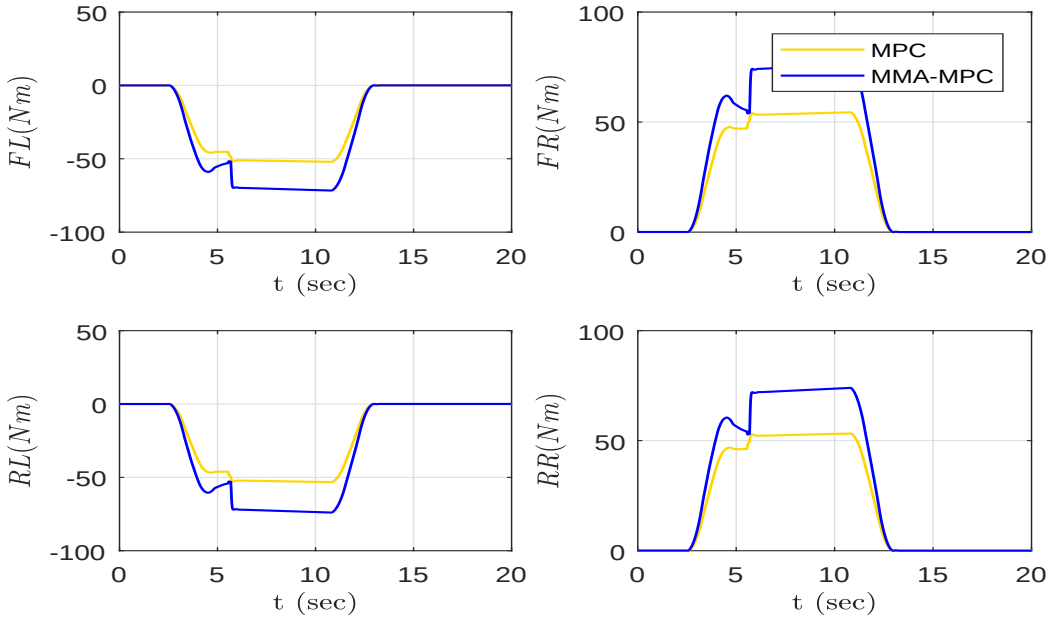

Figure 5.28: Generated torques by designed controller on a dry road.

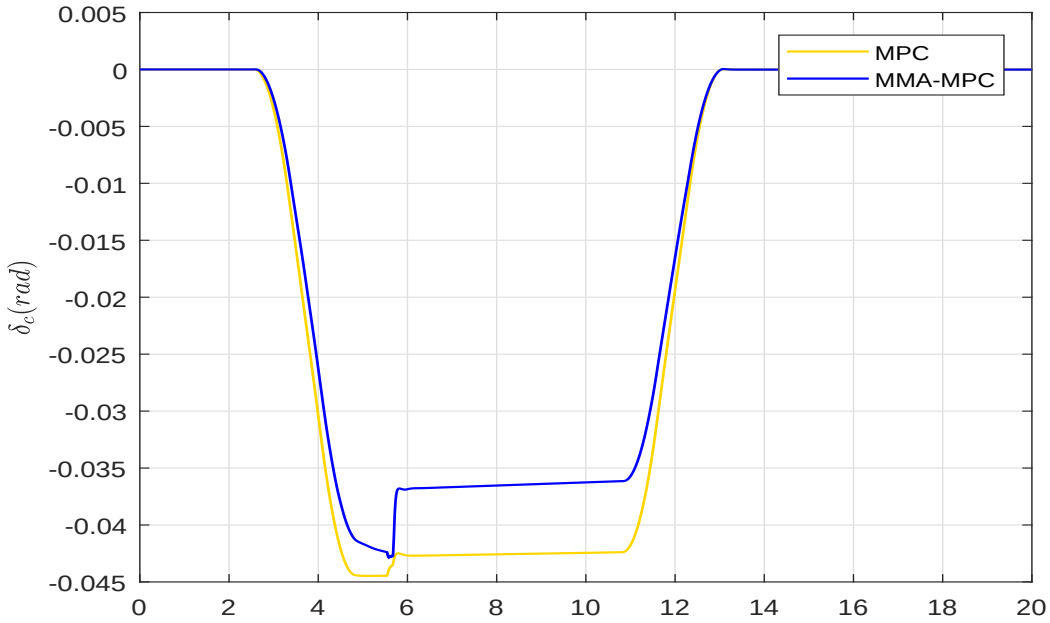

Figure 5.29: Corrected steering input by designed controller on a dry road.

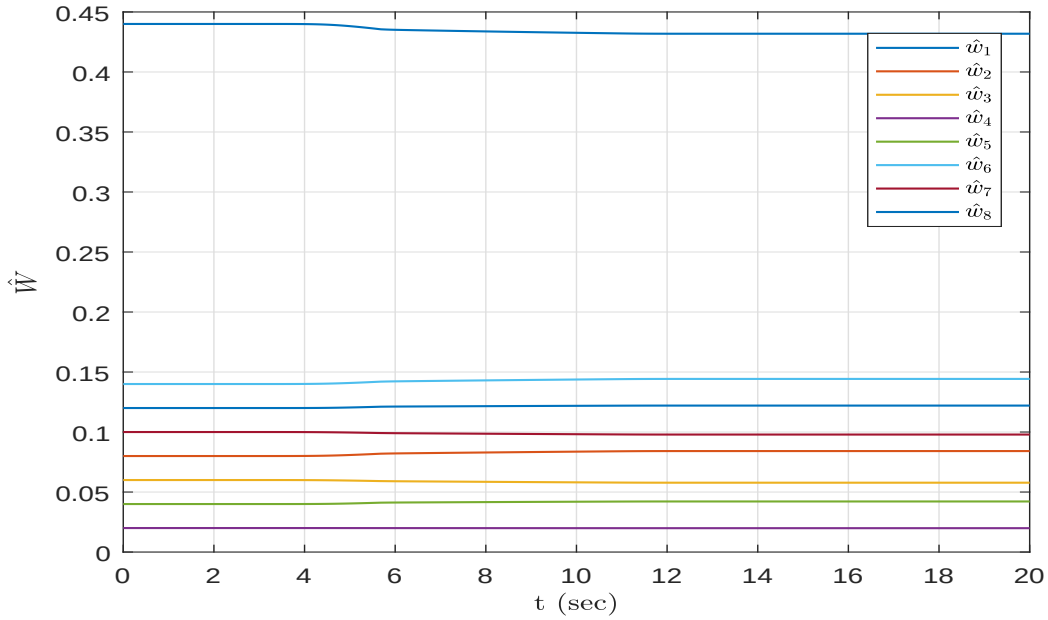

Figure 5.30: Estimates of weighting parameters for a dry road.

Fig. 5.27 shows the yaw rate and the sideslip angle tracking performance of the vehicle without controller, with MPC controller, and with MMA-MPC controller. In the uncontrolled case, the vehicle becomes unstable as soon as the driver applies acceleration and steering. On the other hand, the MPC based controllers successfully maintain the vehicle stability during manoeuvre. However, the proposed MMA-MPC controller achieves better performance increasing yaw tracking performance by around 25% while keeping sideslip angle small.

The torque adjustments generated by the designed MPC and MMA-MPC controllers are given in Fig. 5.28. As can be seen that the torque differentials required to maintain vehicle stability are away from saturation, smooth and symmetric. Fig. 5.29 displays the corrected steering input is almost same with the driver input in Fig. 5.22. This results indicate that the designed controllers do not involve in the driver steering input much as desired.

In Fig. 5.30, the estimates of the weights are shown during maneuver. The estimated parameters show relatively smaller changes than the ones for slippery road.

5.5 Summary and Remarks

This chapter has addressed the constraints on actuation systems, including active front steering system and torque vectoring, for an MPC based MMAC design. First, the maximum and minimum that can be generated steering angle and steering angle rate have been determined. Second, the maximum and minimum torque and torque rate for each corner (each in-wheel electric motor) have been determined. These bound values and vehicle kinematic structure have been used to determine the constraints on torque vectoring at vehicle CG. Third, we have presented how to estimate the prediction model for each time step using the proposed MMA scheme in Chapter 3.

The prediction model and the input constraints have been used to define a constrained optimization problem for MPC design. This optimization problem was redefined as a constrained QP problem following the standard steps in Subsection 2.3.2. The QP problem is solved via interior-point algorithm in Optimization Toolbox/MATLAB each time step. The solution of the quadratic programming problem provides MPC inputs, including total steering angle and torque at vehicle CG which is optimally distributed to each corned based on HCC principles.

In order to validate our control algorithm, several critical driving scenarios were simulated using a high-fidelity vehicle simulation environment CarSim/Simulink. Three diffiernt cases were considered as follows: No acceleration/braking during maneuver, Acceleration/braking during maneuver, No Acceleration/braking during maneuver on changing road condition. The performance of the proposed MPC based MMAC was compared to an MPC controller which was designed for a wet road condition using the same tuning parameters in objective function design. The results validated the stability and effectiveness of the proposed MPC based MMAC algorithm and showed that the proposed adaptive control scheme outperformed over a nonadaptive MPC controller for tracking tasks.

Chapter 6

Conclusions and Future Work

6.1 Conclusions

In this thesis, a blending based multiple-model on-line identification scheme for MIMO systems with polytopic uncertain parameters has been developed. The proposed identification scheme has been used to design optimal adaptive control schemes.

In Chapter 3, new blending based multiple-model on-line identification schemes for MIMO systems with polytopic uncertain parameters is proposed utilizing gradient and RLS based approaches. The proposed schemes used multiple linear parametric fixed models in the system identifier design. Each model represented different extreme operation condition (i.e., an extreme point of a convex polytope which was a compact convex set with a finite number of extreme points) by using different system parameters. Thus, the designed multiple fixed models guaranteed that the uncertain system lied in the convex hull of the design multiple fixed model.

More comprehensive description of Nonlinear and/or Time-varying Linear systems were provided using multiple linear fixed models approach. For the given input and state vectors, discrepancies between the responses of designed multiple models and the response of uncertain system were continuously observed. These discrepancies showed how each designed model was close to actual model in terms of system parameters based on the Certainty Equivalence principle. In this regard, the discrepancies and convexity property were used by the proposed adaptive scheme for estimation of weighting vectors. Estimation of the weighting vectors was achieved by either gradient or RLS method. The proposed adaptive schemes provided fast adaptation for even uncertain LTV systems without reinitialisation

and for system states with white noise. Parameter projection was applied to guarantee that the convexity condition was satisfied during adaptation especially for fast transients in system parameters.

Lastly, the proposed adaptive schemes were used to design an LQ based optimal MMAC scheme for polytopic uncertain linear systems. An LQ optimal controller was designed for each identification model to enable the optimal fixed control gains to be off-line computed for all identification models in advance. All LQ controllers utilized the same design parameters Q, R. The adaptive control law was generated by using the proposed either the proposed gradient or the proposed RLS based identification scheme. The stability analysis of the proposed LQ based optimal MMAC has been provided.

In Chapter 4, the proposed LQ based optimal MMAC scheme in Chapter 3 was applied to vehicle motion control. The objective was to improve vehicle handling performance and to maintain stability during cornering manoeuvres, i.e., the vehicle was controlled to track the desired yaw rate while the side-slip angle was close to zero. First, we considered nonlinear vehicle dynamics in Section 2.2. The studied vehicle was equipped with active front steering system and direct yaw control system that uses independent in-wheel motor at corners to generate torque at vehicle CG.

The nonlinear vehicle dynamic model included uncertain time-invariant/varying parameters due to uncertain tire characteristics, tire-road friction coefficient, and combined-slip effect. We lumped all these system uncertainties and readdressed them as the uncertain time varying longitudinal and lateral tire stiffness with their known upper and lower bounds. Since it was assumed that the upper and lower bounds (extreme values) of these uncertain parameters were known, the uncertain nonlinear vehicle dynamic model would have been addressed as a linear MIMO system with polytopic uncertain parameters. These bounds were used to design the multiple fixed models for the system identifier. For each fixed model and given performance matrices, an optimal LQ control gain was computed off-line for the corresponding model in advance. This also saved time for the computation of optimum control input in real-time implementation. The generated control inputs for all fixed models were blended on-line using weighting vector. The weighting vector was continuously estimated by the proposed adaptive schemes in Chapter 3.

The simulation application to uncertain lateral vehicle dynamics in Chapter 4 was presented in Simulink environments. The performances of the proposed LQ based MMAC utilizing the proposed gradient and RLS based schemes have been compared to each other and an LQ controller which was designed using the same performance matrices and fixed nominal values of the uncertain parameters. The results validated the stability and effectiveness of the proposed LQ based MMAC algorithm and demonstrated that the proposed

adaptive LQ control schemes outperformed over an LQ control scheme with fixed parameter values for tracking tasks. Some parts of developed works in Chapter 3 and Chapter 4 have been presented as a conference paper in [83].

Chapter 5 addressed the constraints on actuation systems, including active front steering system and torque vectoring, for an MPC based MMAC design. First, the maximum and minimum bounds were determined in order to generate steering angle and steering angle rate. Second, the maximum and minimum torque and torque rate for each corner (each in-wheel electric motor) were determined. These bound values and vehicle kinematic structure were used to determine the constraints on torque vectoring at vehicle CG. Third, we presented how to estimate the prediction model for each time step using the proposed MMA scheme in Chapter 3. We used the discrete version of the proposed gradient based adaptive scheme in 3. The prediction model and the input constraints were used to define a constrained optimization problem for MPC design. This optimization problem was redefined as a constrained QP problem following the standard steps in Subsection 2.3.2. The QP problem was solved via interior-point algorithm in Optimization Toolbox/MATLAB each time step. The solution of the quadratic programming problem provided MPC inputs, including total steering angle and torque at vehicle CG which was distributed to each corned based on HCC principles.

In order to validate the proposed control scheme, several critical driving scenarios has been simulated using a high-fidelity vehicle simulation environment CarSim/Simulink. The performance of the proposed MPC based MMAC has been compared to an MPC controller which is designed for a wet road condition using the same tuning parameters in objective function design. The results validated the stability and effectiveness of the proposed MPC based MMAC algorithm and demonstrate that the proposed adaptive control scheme outperform over a nonadaptive MPC controller for tracking tasks.

6.2 Future Work

Some future works are made to continue the research that is conducted in this thesis to further improve the performance of overall control structure.

i Longitudinal speed change during manoeuvre has been neglected in the proposed LQ based MMAC scheme since the set of LQ controller gains are computed off-line in advance. Addressing the vehicle's longitudinal speed change in the control design could be necessary for the manoeuvre at high speed for stability concern. At low speed, consideration of the longitudinal speed could enables to take more precise control action, and thus achieve better tracking performance. Thus, longitudinal speed could be considered as a measurable uncertain parameter for LQ based MMAC scheme. However, this approach could increase the number of fixed identification models and LQ controller gains exponentially.

ii Yaw-rate and side-slip angle state were assumed to be either available and perfectly accurate or available with a white noise. In practice, these states contains bias and noise which could adversely affect the performance of the controller. To mitigate bias and noise in these state measurement simultaneously, a state observer could be designed to combine with the proposed blending based multiple-model parameter identifier (i.e., adaptive state observer).

References

[1] M. Abe, Y. Kano, K. Suzuki, Y. Shibahata, and Y. Furukawa. Side-slip control to stabilize vehicle lateral motion by direct yaw moment. *JSAE review*, 22(4):413–419, Oct 2001.

[2] B. Anderson. Exponential stability of linear equations arising in adaptive identification. *IEEE Transactions on Automatic Control*, 22(1):83–88, 1977.

[3] S. Anwar. Yaw stability control of an automotive vehicle via generalized predictive algorithm. In *Proceedings of American Control Conference.*, pages 435–440, 2005.

[4] M. Athans, D. Castanon, K. Dunn, C. Greene, W. Lee, N. Sandell, and A. Willsky. The stochastic control of the f-8c aircraft using a multiple model adaptive control (mmac) method–part i: Equilibrium flight. *IEEE Transactions on Automatic Control*, 22(5): 768–780, Oct 1977.

[5] S. Baldi, P. A. Ioannou, and E. B. Kosmatopoulos. Adaptive mixing control with multiple estimators. *International Journal of Adaptive Control and Signal Processing*, 26(8):800–820, April 2012.

[6] A. Bemporad and M. Morari. Robust model predictive control: A survey. In *Robustness in Identification and Control*, pages 207–226. 1999.

[7] T. K. Bera, K. Bhattacharya, and A. K. Samantaray. Evaluation of antilock braking system with an integrated model of full vehicle system dynamics. *Simulation Modelling Practice and Theory*, 19(10):2131–2150, 2011.

[8] T. Besselmann, J. Lofberg, and M. Morari. Explicit mpc for lpv systems: Stability and optimality. *IEEE Transactions on Automatic Control*, 57(9):2322–2332, 2012.

[9] F. Borrelli, A. Bemporad, and M. Morari. Predictive control for linear and hybrid systems. *preparation, available online at http://www. mpc. berkeley. edu/mpc-course-material*, 2015.

[10] G. Burgio and P. Zegelaar. Integrated vehicle control using steering and brakes. *International Journal of Control*, 79(05):534–541, 2006.

[11] K. Buyukkabasakal, B. Fidan, A. Savran, and N. Koksal. Real-time implementation of mixing adaptive control on quadrotor uavs. In *Control Conference (ECC), 2015 European*, pages 3597–3602. IEEE, 2015.

[12] K. Buyukkabasakal, B. Fidan, and A. Savran. Mixing adaptive fault tolerant control of quadrotor uav. *Asian Journal of Control*, 2017.

[13] M. Canale, L. Fagiano, and M. C. Signorile. A model predictive control approach to vehicle yaw control using identified models. *Proceedings of the Institution of Mechanical Engineers, Part D: Journal of automobile engineering*, 226(5):577–590, Nov 2012.

[14] A. Cezayirli and M. K. Ciliz. Indirect adaptive control of non-linear systems using multiple identification models and switching. *International Journal of Control*, 81(9): 1434–1450, June 2008.

[15] S. Chen, Y. Ghoneim, N. Moshchuk, B. Litkouhi, and V. Pylypchuk. Tire-force based holistic corner control. In *ASME International Mechanical Engineering Congress and Exposition*, pages 133–140, 2012.

[16] W. Cho, J. Yoon, J. Kim, J. Hur, and K. Yi. An investigation into unified chassis control scheme for optimised vehicle stability and manoeuvrability. *Vehicle System Dynamics*, 46(S1):87–105, 2008.

[17] M. Corno, M. Tanelli, I. Boniolo, and S. M. Savaresi. Advanced yaw control of four-wheeled vehicles via rear active differential braking. In *Proceedings of the 48th IEEE Conference onDecision and Control, 2009 held jointly with the 2009 28th Chinese Control Conference.*, pages 5176–5181, 2009.

[18] P. Cortes, J. Rodriguez, C. Silva, and A. Flores. Delay compensation in model predictive current control of a three-phase inverter. *IEEE Transactions on Industrial Electronics*, 59(2):1323–1325, Feb 2012.

[19] F. A. Cuzzola, J. C. Geromel, and M. Morari. An improved approach for constrained robust model predictive control. *Automatica*, 38(7):1183–1189, July 2002.

[20] L. Del R., F. Allgöwer, L. Glielmo, C. Guardiola, and I. Kolmanovsky. *Automotive model predictive control: models, methods and applications*, volume 402. 2010.

[21] J. Deur, M. Hancock, and F. Assadian. Bond graph modeling and analysis of active differential kinematics. In *ASME Dynamic Systems and Control Conference*, pages 1341–1348, 2008.

[22] J. Deur, M. Hancock, and F. Assadian. Modeling of active differential dynamics. In *ASME 2008 International Mechanical Engineering Congress and Exposition*, pages 427–436, 2008.

[23] M. Doumiati, O. Sename, J. Martinez, P. Gáspár, Z. Szabo, L. Dugard, and J. Bokor. Vehicle yaw control via coordinated use of steering/braking systems. *IFAC Proceedings Volumes*, 44(1):644–649, 2011.

[24] P. Falcone, F. Borrelli, J. Asgari, H. E. Tseng, and D. Hrovat. Predictive active steering control for autonomous vehicle systems. *IEEE Transactions on Control Systems Technology*, 15(3):566–580, May 2007.

[25] P. Falcone, F. Borrelli, H. E. Tseng, J. Asgari, and D. Hrovat. Linear time-varying model predictive control and its application to active steering systems: Stability analysis and experimental validation. *International Journal of Robust and Nonlinear Control*, 18(8):862–875, 2008.

[26] L. B. Freidovich and H. K. Khalil. Logic-based switching for robust control of minimum-phase nonlinear systems. *Systems & Control Letters*, 54(8):713–727, Aug 2005.

[27] M. Fu and B. Barmish. Adaptive stabilization of linear systems via switching control. *IEEE Transactions on Automatic Control*, 31(12):1097–1103, Dec 1986.

[28] C. Hamada, K. Fukatani, K. Yamaguchi, and T. Kato. Development of vehicle dynamics integrated management. Technical report, SAE Technical Paper, 2006.

[29] Z. Han and K. S. Narendra. New concepts in adaptive control using multiple models. *IEEE Transactions on Automatic Control*, 57(1):78–89, Jan 2012.

[30] Z. Hao, L. Xian-sheng, S. Shu-ming, L. Hong-fei, G. Rachel, and L. Li. Phase plane analysis for vehicle handling and stability. *International Journal of Computational Intelligence Systems*, 4(6):1179–1186, Nov 2011.

[31] J. Hespanha, D. Liberzon, Stephen M. A., B. D. O. Anderson, T. S. Brinsmead, and F. De Bruyne. Multiple model adaptive control. part 2: switching. *International journal of robust and nonlinear control*, 11(5):479–496, April 2001.

[32] J. P. Hespanha, D. Liberzon, and A. S. Morse. Overcoming the limitations of adaptive control by means of logic-based switching. *Systems & control letters*, 49(1):49–65, 2003.

[33] S. Inagaki, I. Kshiro, and M. Yamamoto. Analysis on vehicle stability in critical cornering using phase-plane method. In *Proceedings of the International Symposium on Advanced Vehicle Control*, 1994.

[34] P. Ioannou and B. Fidan. *Adaptive control tutorial*, volume 11. 2006.

[35] P. Ioannou and J. Sun. *Robust Adaptive Control*. Prentice Hall, Inc., 1996.

[36] J. Kalkkuhl, T. A. Johansen, and J. Ludemann. Improved transient performance of nonlinear adaptive backstepping using estimator resetting based on multiple models. *IEEE Transactions on Automatic Control*, 47(1):136–140, Jan 2002.

[37] T. Keviczky and G. J. Balas. Software-enabled receding horizon control for autonomous unmanned aerial vehicle guidance. *Journal of guidance, control, and dynamics*, 29(3):680–694, 2006.

[38] M. Klomp. *Longitudinal force distribution and road vehicle handling*. PhD thesis, Chalmers University of Technology, 2010.

[39] Y. E. Ko and J. M. Lee. Estimation of the stability region of a vehicle in plane motion using a topological approach. *International Journal of Vehicle Design*, 30(3):181–192, 2002.

[40] P. Koehn and M. Eckrich. Active steering-the bmw approach towards modern steering technology. Technical report, 2004.

[41] M. V. Kothare, V. Balakrishnan, and M. Morari. Robust constrained model predictive control using linear matrix inequalities. *Automatica*, 32(10):1361–1379, Oct 1996.

[42] M. Kuipers and P. Ioannou. Multiple model adaptive control with mixing. *IEEE Transactions on Automatic Control*, 55(8):1822–1836, Aug 2010.

[43] D. G. Lainiotis. Partitioning: A unifying framework for adaptive systems, i: Estimation. *Proceedings of the IEEE*, 64(8):1126–1143, Aug 1976.

[44] R. Lenain, B. Thuilot, C. Cariou, and P. Martinet. Adaptive and predictive path tracking control for off-road mobile robots. *European Journal of Control*, 13(4):419–439, 2007.

[45] H. Li and Y. Shi. Distributed model predictive control of constrained nonlinear systems with communication delays. *Systems & Control Letters*, 62(10):819–826, Oct 2013.

[46] S. Li, K. Li, R. Rajamani, and J. Wang. Model predictive multi-objective vehicular adaptive cruise control. *IEEE Transactions on Control Systems Technology*, 19(3): 556–566, May 2011.

[47] W. Liang, H. Yu, R. McGee, M. Kuang, and J. Medanic. Vehicle pure yaw moment control using differential tire slip. In *American Control Conference*, pages 3331–3336, June 2009.

[48] Daniel Liberzon. Switching in systems and control, ser. systems & control: Foundations & applications. *Birkhauser*, 2003.

[49] Li-hua Luo, Hong Liu, Ping Li, and Hui Wang. Model predictive control for adaptive cruise control with multi-objectives: comfort, fuel-economy, safety and car-following. *Journal of Zhejiang University SCIENCE A*, 11(3):191–201, 2010.

[50] Y. Luo, S. Serrani, A.and Yurkovich, D. B. Doman, and M. W. Oppenheimer. Model predictive dynamic control allocation with actuator dynamics. In *Proceedings of American Control Conference*, volume 2, pages 1695–1700, 2004.

[51] W. J. Manning and D. A. Crolla. A review of yaw rate and sideslip controllers for passenger vehicles. *Transactions of the Institute of Measurement and Control*, 29(2): 117–135, June 2007.

[52] B. Mårtensson. Adaptive stabilization. *PhD Thesis*, 1986.

[53] D. Q. Mayne, M. M. Seron, and S. V. Raković. Robust model predictive control of constrained linear systems with bounded disturbances. *Automatica*, 41(2):219–224, Feb 2005.

[54] R. H. Middleton, G. C. Goodwin, David J. Hill, and D. Q. Mayne. Design issues in adaptive control. *IEEE Transactions on Automatic Control*, 33(1):50–58, Jan 1988.

[55] D. E. Miller and E. J. Davison. An adaptive controller which provides lyapunov stability. *IEEE Transactions on Automatic Control*, 34(6):599–609, June 1989.

[56] H. Mirzaeinejad and M. Mirzaei. Optimization of nonlinear control strategy for anti-lock braking system with improvement of vehicle directional stability on split-μ roads. *Transportation Research Part C: Emerging Technologies*, 46:1–15, 2014.

[57] A. Mori and Y. Shibahata. Drive force control method for four-wheel drive vehicle, 2007. US Patent 7,264,077.

[58] A. S. Morse. Supervisory control of families of linear set-point controllers. In *Proceedings of Decision and Control Conference*, pages 1055–1060, Dec 1993.

[59] A. S. Morse. Supervisory control of families of linear set-point controllers-part i. exact matching. *IEEE Transactions on Automatic Control*, 41(10):1413–1431, 1996.

[60] A Stephen Morse. Supervisory control of families of linear set-point controllers. 2. robustness. *IEEE Transactions on Automatic Control*, 42(11):1500–1515, 1997.

[61] K. S. Narendra. Hierarchical adaptive control of rapidly time-varying systems using multiple models. *Control of Complex Systems: Theory and Applications*, page 33, 2016.

[62] K. S. Narendra and J. Balakrishnan. Improving transient response of adaptive control systems using multiple models and switching. *IEEE Transactions on Automatic Control*, 39(9):1861–1866, Sep 1994.

[63] K. S. Narendra and J. Balakrishnan. Adaptive control using multiple models. *IEEE Transactions on Automatic Control*, 42(2):171–187, Feb 1997.

[64] K. S. Narendra and Z. Han. The changing face of adaptive control: the use of multiple models. *Annual Reviews in Control*, 35(1):1–12, April 2011.

[65] K. S. Narendra and Z. Han. A new approach to adaptive control using multiple models. *International Journal of Adaptive Control and Signal processing*, 26(8):778–799, 2012.

[66] K. S. Narendra, Y. Wang, and W. Chen. The rationale for second level adaptation. *arXiv preprint arXiv:1510.04989*, 2015.

[67] S. B. Noh, Y. H. Kim, Y. I. Lee, and W. H. Kwon. Robust generalised predictive control with terminal output weightings. *Journal of Process Control*, 6(2):137–144, 1996.

[68] E. Ono, S. Hosoe, H. D. Tuan, and S. Doi. Bifurcation in vehicle dynamics and robust front wheel steering control. *IEEE Transactions on Control Systems Technology*, 6(3): 412–420, 1998.

[69] C. Poussot-Vassal, O. Sename, L. Dugard, and S. M. Savaresi. Vehicle dynamic stability improvements through gain-scheduled steering and braking control. *Vehicle System Dynamics*, 49(10):1597–1621, 2011.

[70] V. Pylypchuk, S. Chen, N. Moshchuk, and B. Litkouhi. Slip-based holistic corner control. In *ASME International Mechanical Engineering Congress and Exposition*, pages 337–342, 2011.

[71] J. Samsundar and J. C. Huston. Estimating lateral stability region of a nonlinear 2 degree-of-freedom vehicle. Technical report, SAE Technical Paper, Feb 1998.

[72] K. Sawase, Y.i Ushiroda, and T. Miura. Left-right torque vectoring technology as the core of super all wheel control (s-awc). *Mitsubishi Motors Technical Review*, 18:16–23, 2006.

[73] S. Shen, J. Wang, P. Shi, and G. Premier. Nonlinear dynamics and stability analysis of vehicle plane motions. *Vehicle System Dynamics*, 45(1):15–35, Jan 2007.

[74] Y. Shibahata, K. Shimada, and T. Tomari. Improvement of vehicle maneuverability by direct yaw moment control. *Vehicle System Dynamics*, 22(5-6):465–481, 1993.

[75] S. Solmaz, M. Akar, and R. Shorten. Online center of gravity estimation in automotive vehicles using multiple models and switching. In *International Conference on Control, Automation, Robotics and Vision*, pages 1–7, 2006.

[76] S. Solmaz, M. Akar, R. Shorten, and J. Kalkkuhl. Real-time multiple-model estimation of centre of gravity position in automotive vehicles. *Vehicle System Dynamics*, 46(9): 763–788, July 2008.

[77] J. Tjonnas and T. A. Johansen. Stabilization of automotive vehicles using active steering and adaptive brake control allocation. *IEEE Transactions on Control Systems Technology*, 18(3):545–558, 2010.

[78] R. Wang, H. Zhang, J. Wang, F. Yan, and N. Chen. Robust lateral motion control of four-wheel independently actuated electric vehicles with tire force saturation consideration. *Journal of the Franklin Institute*, 352(2):645–668, 2015.

[79] X. Ye. Nonlinear adaptive control using multiple identification models. *Systems & Control Letters*, 57(7):578–584, July 2008.

[80] S. Yu, C. Bohm, H. Chen, and F. Allgöwer. Stabilizing model predictive control for lpv systems subject to constraints with parameter-dependent control law. In *American Control Conference*, pages 3118–3123, 2009.

[81] S. Yu, C. Böhm, H. Chen, and F. Allgöwer. Model predictive control of constrained lpv systems. *International Journal of Control*, 85(6):671–683, 2012.

[82] E. Zafiriou. Robust model predictive control of processes with hard constraints. *Computers & Chemical Engineering*, 14(4):359–371, May 1990.

[83] H. Zengin, N. Zengin, B. Fidan, and A. Khajepour. Blending based multiple-model adaptive control for multivariable systems and application to lateral vehicle dynamics. In *18th European Control Conference (ECC)*, pages 2957–2962, 2019.

[84] S. Zhang, S. Zhou, and J. Sun. Vehicle dynamics control based on sliding mode control technology. In *Control and Decision Conference*, pages 2435–2439, June 2009.

[85] C. Zhao, W. Xiang, and P. Richardson. Vehicle lateral control and yaw stability control through differential braking. In *2006 IEEE International Symposium on Industrial Electronics*, volume 1, pages 384–389, 2006.

[86] Z. Q. Zheng and M. Morari. Robust stability of constrained model predictive control. In *Proceeding of American Control Conference*, pages 379–383, 1993.